The Detection of Nitric Oxide and its Reactivity with Transition Metal Thiolate Complexes

Andrew Gregory Tennyson

S.B. Honors, Chemistry (2003)
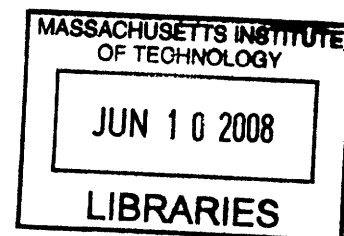S.M., Inorganic Chemistry (2003)
University of Chicago

SUBMITTED TO THE DEPARTMENT OF CHEMISTRY IN PARTIAL FULFILLMENT OF
THE REQUIREMENTS FOR THE DEGREE OF

DOCTOR OF PHILOSOPHY IN INORGANIC CHEMISTRY
at the
MASSACHUSETTS INSTITUTE OF TECHNOLOGY

May 2008
$\mathcal{L}\mathcal{J}u_{v}\mathcal{Q}\; \partial\;\alpha\mathcal{S}$
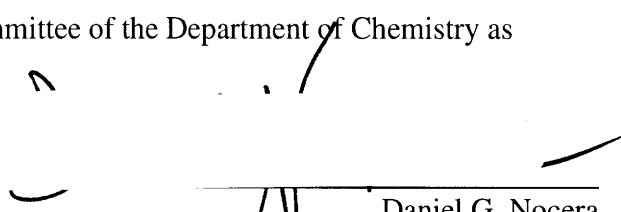
© 2008 Massachusetts Institute of Technology

Signature of Author:_____
Department of Chemistry
May 22, 2008

Certified by:_____
U   Stephen␣J. Lippard
Arthur Amos Noyes Professor of Chemistry
Thesis Supervisor

Accepted by:_____   _____
Robert W. Field
Haslam and Dewey Professor of Chemistry
Chairman, Departmental Committee on Graduate Studies

This doctoral thesis has been examined by a committee of the Department of Chemistry as follows:
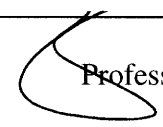
_____

Daniel G. Nocera
Henry Dreyfus Professor of Energy and Chemistry
Committee Chairman

_____

Stephen J. Lippard
Arthur Amos Noyes Professor of Chemistry
Thesis Supervisor

_____

Alice Y. Ting
Professor of Chemistry

The Detection of Nitric Oxide and its Reactivity with Transition Metal Thiolate Complexes

by

Andrew Gregory Tennyson

Submitted to the Department of Chemistry on May 22, 2008
in partial fulfillment of the requirements for the Degree of Doctor of Philosophy

Abstract

Nitric oxide (NO) is a molecule that is essential for life and regulates both beneficial and harmful processes. Because this gaseous radical influences many aspects of health and disease, we wish to explore the relationship between NO and physiology/pathophysiology. To this end, we seek to create tools for the fluorescent imaging of NO *in vivo*. We have adapted an existing small molecule-based sensor for more biologically relevant applications by including it within a polymeric film. We have also developed turn-on fluorescent sensors for NO based on conjugated polymers, which demonstrated good selectivity and sensitivity for this analyte. In addition, we have prepared a related sensor that will detect nitroxyl (HNO) but not NO. These systems demonstrate the versatility and value of the conjugated polymer scaffold for sensing applications.

Many targets of the diatomic radical NO contain redox active units, such as transition metals or thiolate ligands. To gain insight into how NO might regulate biological processes by interacting with these redox active species, we have initiated a fundamental study of the reactivity of NO with transition metal thiolate model complexes. Our explorations in this field have yielded unique nickel and cobalt nitrosyl species with atypical electronic and structural parameters. These studies have suggested intermediates for the more biologically relevant iron nitrosyl complexes that have not yet been observed may exist. Furthermore, the NO chemistry of these small molecule nickel and cobalt thiolate complexes may guide future biological investigations into the regulation of nickel and cobalt metalloproteins by NO.

Thesis Supervisor: Stephen J. Lippard
Title: Arthur Amos Noyes Professor of Chemistry

Dedication

1174

Tomorrow, and tomorrow, and tomorrow,
Creeps in this petty pace from day to day
To the last syllable of recorded time,
And all our yesterdays have lighted fools
The way to dusty death. Out, out, brief candle!
Life's but a walking shadow, a poor player
That struts and frets his hour upon the stage
And then is heard no more: it is a tale
Told by an idiot, full of sound and fury,
Signifying nothing.

Macbeth
Act V, Scene 5

Acknowledgements

Mom, Dad, Ellie, and Glen
For Encouraging, Supporting, and Believing in Me

Rhett C. Smith
A True Friend and Mentor

Professor Stephen J. Lippard
Teacher of Teachers and the Father of Bioinorganic Chemistry

Table of Contents

Chapter 1. The Generation, Translocation and Action of Nitric Oxide in Biology

Chapter 2: Films of Polymer-Shielded Dirhodium Tetracarboxylate–Fluorophore Complexes for the Detection of Nitric Oxide in Aqueous Solution

Chapter 3: Conducting Metallopolymer-Based Sensors for Nitric Oxide and Nitroxyl

Chapter 4. Synthesis of $\{Ni(NO)\}^{10}$ and $\{Co(NO)_2\}^{10}$ Complexes Supported by Thiolate Ligands

List of Tables

List of Schemes

List of Figures

List of Charts

List of Equations

Chapter 1

The Generation, Translocation and Action
of Nitric Oxide in Biology

1.1. Historical Background and Significance

Nitric oxide was first prepared by Jan Baptist van Helmont in the early 17th century, but serious investigations into this gaseous molecule would not be performed until 150 years later by Joseph Priestley,[1] who dubbed it "nitrous air." Although Priestly ardently clung to the phlogiston theory of gases and natural philosophy, he was a thoughtful and honest experimentalist. One of the earliest recorded "uses" of NO(g) was by Priestly as a test of the "purity" of air. He detailed the mixing of "nitrous air" with test gases in a closed volume over mercury or water and measuring the decrease in volume. The greater the partial oxygen pressure in air (*i.e.* of a "higher purity"), the greater the decrease in volume will be upon mixing with NO.

This diatomic molecule has almost no practical industrial use, but is formed as an intermediate in the oxidation of ammonia to nitric acid via the Ostwald process.[2] Recently, NO has found use in the semiconductor industry in the fabrication of semiconductor devices and the number of patents involving these processes have increased dramatically.[3] Historically, this gaseous radical was best known as an industrial and automotive pollutant both environmentally damaging and toxic.[4] Photochemical reaction of NO with ozone causes production of dioxygen and leads to depletion of the ozone layer. Additionally, atmospheric NO can be converted to nitric acid and has been implicated in acid rain. For these reasons, one of the primary functions of a catalytic converter in automobiles is to reduce the amount of NO released into the atmosphere.

The National Institute for Occupational Safety and Health states that the "Immediately Dangerous to Life or Health" (IDLH) concentration of NO is 100 ppm.[5] In comparison, carbon monoxide is a well known toxin produced during incomplete combustion and has an IDLH value of 1200 ppm. A syringe containing 0.5 mL of NO(g) at 1 atm at 25 °C, a volume commonly-

employed in transfers from gas storage bulbs to cuvettes, contains sufficient NO to exceed the IDLH value for one student if the syringe is broken and contents inhaled.[6] Upon exposure to dioxygen, the colorless NO is rapidly oxidized to the brown-orange N_2O_4, which is even more toxic than NO with an IDLH concentration of 20 ppm. The same 0.5 mL volume of NO(g), upon complete oxidation, would exceed the IDLH value for 5 students. A syringe containing 5 mL of NO(g), a volume routinely used in syntheses and reactivity studies, would exceed the IDLH concentration for a research group of 25 students and postdocs twice over.

By the late 1980s, the monolithically negative perception of NO had begun to change as research in various fields, from immunology and oncology to the cardiovascular system, hinted at diverse physiological roles for NO ranging from immune defense to protein regulation. Interest in nitric oxide soon ballooned, with NO being named Molecule of the Year in 1992.[4] Soon thereafter, the 1998 Nobel Prize in Physiology or Medicine was awarded to Furchgott, Ignarro and Murad for their research into the functions of NO as a signaling molecule in the cardiovascular system.[7-9] Nitric oxide is now known to play essential roles in biology, ranging from neuroprotection and immune response to protein regulation to chemotherapeutic resistance.[10-12]

With growing public interest in nitric oxide grows and market share for NO-derived pharmaceuticals, the possibility for scams has increased. For example, noni are plants indigenous to Southeast Asia that have spread throughout much of the Pacific Island region and coastal Asia.[13] Folk medicine remedies involving this plant have been known for centuries, and juice from the fruit of this plant now represents a multibillion dollar industry. This juice is sold as a dietary supplement that will promote good health and vitality, but none of the claims have been supported by peer-reviewed research.

Nitric oxide can be understood in three logically-distinct stages of *in vivo* (**Figure 1.1**). During the first stage, *de novo* synthesis of NO occurs enzymatically by nitric oxide synthase. Next, the NO may diffuse directly to its target or may be converted to a different nitrogen oxide, a nitroso-organic compound, or a metal-nitrosyl complex. Some of these species will be better suited for the delivery of NO and some will be better for long-term storage. Finally, NO or a derivative thereof can exert its physiologic or pathophysiologic function via interaction with or modification of complexes composed of redox active metals and ligands (*e.g.* iron-sulfur clusters), complexes containing only redox active metals (*e.g.* ribonucleotide reductase), complexes of redox inactive metals supported by redox active ligands (*e.g.* zinc finger proteins), or metal-free substrates (*e.g.* thiols, tyrosine, etc).
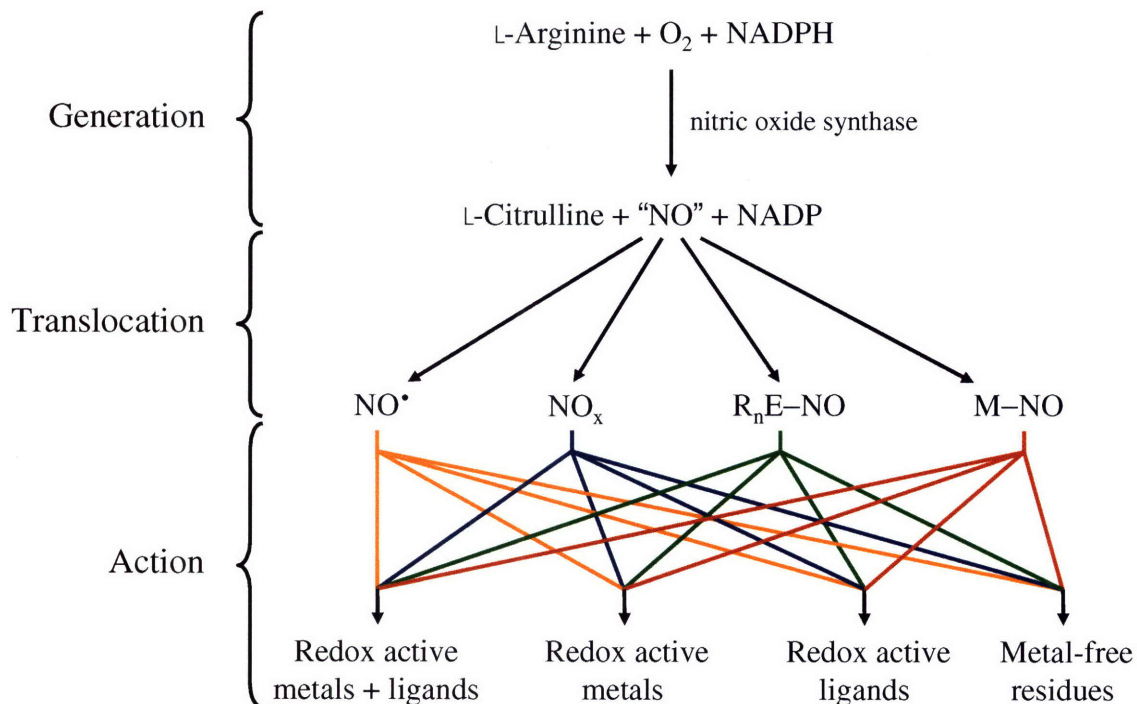
Figure 1.1. Stages of NO *in vivo*.

1.2. Generation

1.2.1. Active Site and Mechanism

Nitric oxide synthases (NOSs) are enzymes that effect the biosynthesis of NO in humans from L-arginine in a dioxygen- and NADPH-dependent manner.[14] During a complete cycle, one molecule of L-arginine and two molecules of dioxygen are converted to one molecule of NO, one molecule of L-citrulline, and two molecules of H_2O in a process that requires three exogenous electrons and protons. Crystallographic studies have revealed the active site in NOS is composed of a cysteine-ligated heme unit, analogous to that found in cytochrome P450, with tetrahydrobiopterin in close proximity to the heme active site as well as a reductase domain farther away.[15]

Conversion of L-arginine into NO and L-citrulline occurs in two discrete mechanistic steps (**Scheme 1.1**). First, L-arginine is hydroxylated to *N*-hydroxy-L-arginine (NHA), which is then converted to L-citrulline with attendant release of NO. Current understanding of this cycle invokes a ferryl intermediate, similar to that observed in cytochrome P450, as the species competent for the hydroxylation of L-arginine.[16] Recent experiments have cast some doubt on this assignment, however, because iodosobenzene-generated ferryl NOS does not result in conversion of L-arginine to NHA.[17] An alternative mechanism for this step has been proposed, whereby a ferric peroxo is formed and deprotonates a guanidinium nitrogen in L-arginine. The lone pair on the neutral imine can then effect nucleophilic attack at the terminal oxygen in the ferric hydroperoxo, leading to the formation of NHA. During the second step, the same ferric peroxo attacks the imine carbon of NHA and subsequent collapse of this intermediate releases NO and L-citrulline.[16]
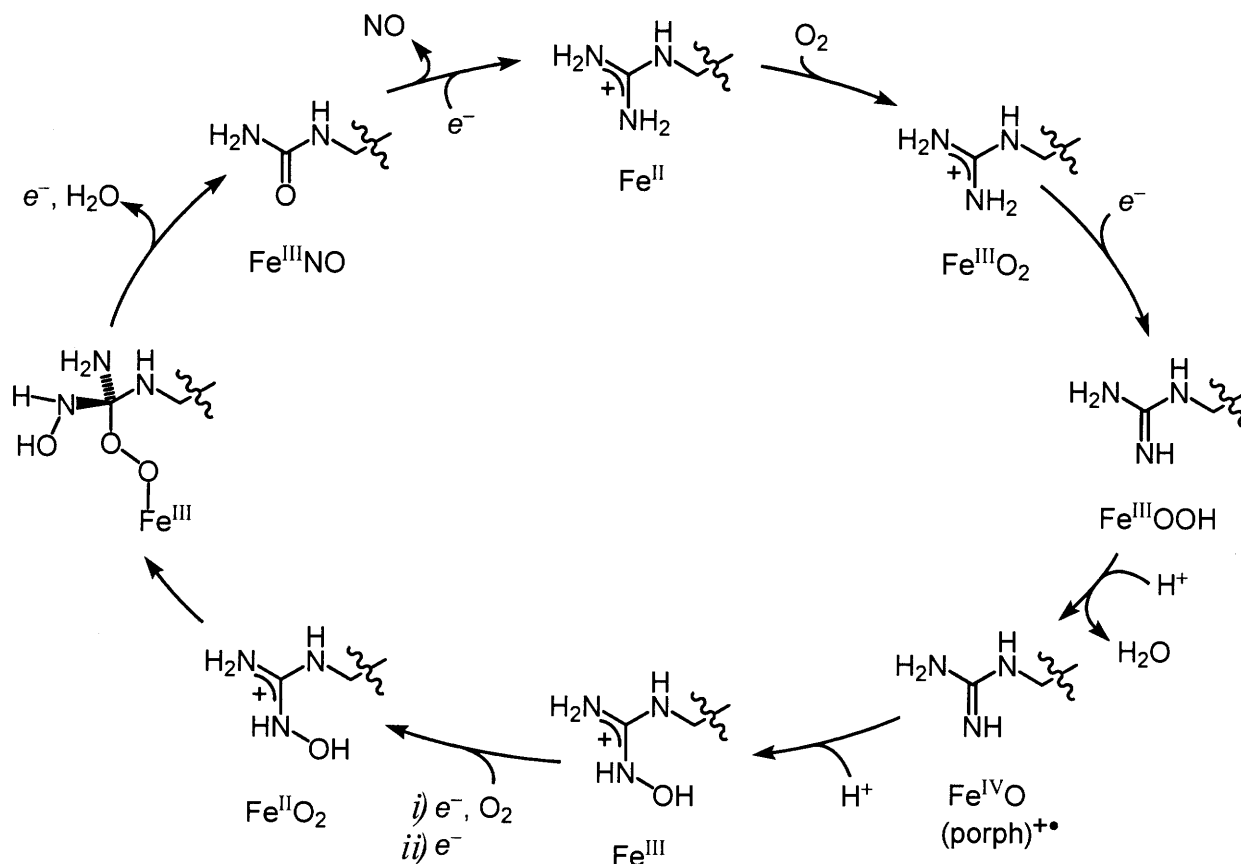
Scheme 1.1. Possible mechanism for the conversion of L-arginine to NO and L-citrulline though an NHA intermediate.

1.2.2. Biochemistry

There are three isoforms of this homodimeric enzyme in humans – endothelial, neuronal and inducible – that share roughly 50% sequence homology.[14] The monomers do not display any NOS activity and are connected by a $[Zn(Cys)_4]$ unit in which each monomer supplies two ligands. Calmodulin binding to NOS is required for enzymatic activity and its affinity for the enzyme may or may not depend on Ca^{2+} concentration.[18] The binding of calmodulin to the inducible isoform is calcium-independent, whereas the other two isoforms display increasing calmodulin affinity with increasing Ca^{2+} concentration. Unsurprisingly, NOS activity for the inducible isoform is independent of Ca^{2+} concentration and the other two exhibit increased

activity with increasing $[Ca^{2+}]$.

Endothelial NOS (eNOS) is an important part of the cardiovascular system, and is essential for vasodilation and maintenance of healthy cardiovascular states.[14] Chemical inhibition of or knocking-down eNOS causes vasoconstriction, hypertension, and may even result in severe aneurisms. This isoform is also responsible for the regulation of vascular-endothelial growth factor and thus plays a role in angiogenesis.

Despite the name, neuronal NOS (nNOS) can be found in nerve endings and muscles.[14] Outside of the brain, nNOS modulates processes ranging from bladder relaxation to respiration. Mice with this enzyme knocked-out demonstrate impaired balance and night vision. Although nNOS has been implicated in long-term potentiation, these mice are still capable of normal learning and memory.

Inducible NOS (iNOS) functions in an immunoprotective capacity, serving to fight off infection from a range of sources, from bacteria to viruses.[14] This isoform is not expressed in healthy somatic cells, but can be rapidly transcribed in response to disease. Unlike the other isoforms, nNOS will produce large concentrations of NO in a short period of time.

Bacterial NOS (bNOS) is the bacterial analog of the enzyme found in humans with a similar heme oxygenase domain.[19] Studies have shown that this enzyme is required for normal bacterial growth, successful infection of a target, and defense against oxidant-based immune response. One notable difference between bNOS and the isoforms found in humans is that the former lacks a reductase domain. Because bacteria expressing this enzyme can produce NO without a dedicated reductase, it is believed that these bacteria can recruit reductants from within the host. Presumably, this redox-dependence could serve as a foundation for the development of a new class of antibiotics.

1.3. Transport and Storage

1.3.1. NO(g), N(2+)

Although nitric oxide is the product of the NOS catalytic cycle, this diatomic radical is unstable in aerobic, aqueous solution, especially in the presence of redox active metals and organic compounds.[20] Under physiological conditions, the half-life for NO can range from minutes to milliseconds. Recent studies have suggested that the intravascular concentrations of NO are too low for observed vasodilative behavior because of limited diffusion range and stability.[21] As a result, consideration must be given to the various nitrogen oxides and other NO-derived species that can be formed from nitric oxide.

1.3.2. NO$_x$

Figure 1 in ref 22 provides an excellent graphical representation of the relationship between nitrogen oxides as a function of oxidation state of nitrogen, Gibbs free energy, and redox potential. For comparison, the oxidation state of the nitrogen(s) is presented along with the chemical formula.

1.3.2.1. ONOO$^-$, N(3+)

Peroxynitrite is formed *in vivo* by the diffusion-limited reaction between NO and superoxide.[22] This molecule is highly oxidizing and can even effect tyrosine nitration, resulting in a variety of pathophysiological effects ranging from inflammation to cancer.[23] Additionally, this molecule can cause oxidation of cysteine to cystine or sulfone formation from methionine.[24] When peroxynitrite is combined with two molecules of NO, N_2O_3 and nitrite are formed.

1.3.2.2. NO_3^-, N(5+)

Nitrate contains a nitrogen atom in the highest possible oxidation state (5+) and has long been considered an inert, thermodynamic sink for reactive nitrogen species.[25,26] The bulk of nitrate in humans (60–80%) is supplied by vegetable consumption. The remainder is produced by the isomerization of peroxynitrite or the reaction of NO with oxygenated heme proteins. Because humans lack the enzymes for which nitrate is a substrate, the majority of nitrate (60%) is excreted in the urine unaltered. Interestingly, nearly 25% of plasma nitrate is directed to the salivary glands and incorporated into saliva at concentrations 10-fold greater than found in plasma. This observation is significant given the fact that there are a number of bacteria inhabiting the human mouth and gastrointestinal system. Whereas nitrate is an inert compound for humans, bacteria employ nitrate reductases in the conversion of nitrate to nitrite. These bacteria can process the nitrate in saliva or elsewhere into nitrite. Although nitrate has been associated with cancer and other diseases, as well as beneficial processes, its 'effects' are due to the action of nitrite or other downstream reactive nitrogen species. For example, ingestion of nitrate caused a large increase in plasma nitrite in test subjects, but if they did not swallow, no such increase was noted. Other studies have shown that nitrate has a protective effect in the gastrointestinal system, such as the prevention of stress-induced injury in rats, accompanied by an increased generation of NO. However, treatment of the rats' oral cavities with topical antibiotics caused death of the resident bacteria and abolished the protective effect of the dietary nitrate. Presumably, the bacteria in the mouth reduce the nitrate to nitrite, which then migrates to the stomach, where the acidic environment can cause formation of a number of reactive nitrogen species through nitrous acid as an intermediate.

1.3.2.3. NO_2^-, N(3+)

Simple autooxidation of NO in aerobic, aqueous solution will give rise to nitrite but not nitrate.[27] As mentioned previously, reduction of nitrate to nitrite is effected by bacteria inhabiting humans.[25,26] Studies of the nitrite anion have revealed it has important biological effects and can even serve as an indicator of infection. Although a majority of nitrate in humans is excreted in the urine, the lack of bacteria therein precludes any formation of nitrite.[28] However, during bacterial infection of the urinary system, nitrite production occurs and its presence can be used as a diagnostic indicator of bacterial infection. Acidification of nitrite-enriched urine below pH 5.5 is lethal to all known urinary infectious bacteria, and both modern treatments and folk remedies for bacterial urinary infections involve the deliberate acidification of urine. Because the physiological and bactericidal functions of nitrite are dependent on acidic conditions, the relevant intermediate is believed to be HNO_2, which disproportionates to the presumed active species N_2O_3 and water. Furthermore, nitrite can be reduced by deoxyhemoglobin or xanthine oxidoreductase to afford NO and hydroxide. Conversely, reaction of nitrite with hemoglobin results in formation of nitrate.

1.3.2.4. N_2O_3, N(2+) and N(4+)

Dinitrogen trioxide can be formed by the disproportionation of nitrous acid or by radical coupling of NO with NO_2.[25,26] This species is too unstable in aqueous solution to exert any direct influence, but can deliver both NO^+ and NO. In the former capacity, N_2O_3 functions as a nitrosating agent and enables the formation of species such as *S*-nitrosothiols and *N*-nitrosamines with concomitant formation of nitrite. In the latter capacity, N_2O_3 serves as a source of NO and NO_2.

1.3.2.5. NO$_2$ and N$_2$O$_4$, N(4+)

Nitrogen dioxide is an unstable species in aqueous solution, and will readily behave as a one-electron oxidant to generate nitrite.[29] Dimerization to N$_2$O$_4$ affords a molecule best viewed as [NO$^+$][NO$_3^-$] and subsequent hydration affords nitrite and nitrate.[30] Because N$_2$O$_4$ formally contains an NO$^+$ unit, it can act as a nitrosating agent in the generation of nitroso-organic compounds.

1.3.2.6. HNO, N(1+)

Nitroxyl (HNO) may play an important role in biology, with a signaling pathway possibly orthogonal to that for NO.[31,32] Although this molecule is toxic at high concentrations and can cause severe depletion of cellular glutathione concentration, it can play a beneficial role in the cardiovascular system and interact with targets that NO cannot (*e.g.* ferric heme). One possible source of nitroxyl *in vivo* is from the reaction of an *S*-nitrosothiol with another thiol to afford a disulfide and HNO. Although one-electron reduction of NO followed by protonation would afford HNO, this process is spin-forbidden.[33] The lowest-energy configuration for NO$^-$ is the triplet state and for HNO is the singlet state, the realization of which led to the revision of the pK_a of HNO from 3.4 to 11.4. However, coordination to a transition metal could favor the singlet state for NO$^-$, and metal-bound nitroxyls have been previously-reported and exhibit much lower pK_a values (~7).[34] The free triatomic molecule can react with thiols to form disulfide and hydroxylamine, and HNO could be a one-electron reductant or a hydrogen-atom source.[32]

1.3.3. R_nENO

Because N_2O_3 can function as a nitrosating agent, it is believed to be the intermediate by which nitrosamines and nitrosothiols are formed. Reaction of morpholine or glutathione with NO under aerobic conditions resulted in the formation of *N*-nitrosomorpholine and *S*-nitroso-glutathione, respectively.[35] In comparison, the same reaction performed under anaerobic conditions afforded no change. Kinetic analysis of this reaction at neutral pH indicated that the responsible intermediate was N_2O_3.

S-Nitrosothiols are commonplace *in vivo* and there is evidence that these molecules are the predominant carriers of NO, but the mechanism of "NO" delivery by these species is disputed.[36-41] Some evidence suggests that RSNOs heterolyzes along the S–N bond, directly transferring a nitrosonium (NO^+) fragment to the target (termed nitrosation). Others experiments imply that homolysis of the S–N bond liberates 0.5 equiv disulfide (RSSR) and 1 equiv NO, which then reacts with the target (termed nitrosylation). The latter pathway is too slow for practical signaling purposes unless accelerated by a transition metal or other redox agent to facilitate homolytic decomposition of the RSNO.[42,43] Most *S*-nitrosothiols decay with first-order kinetics under thermal conditions[44,45] and with second-order kinetics when catalyzed by metals.[46]

N-nitrosamines can function as alkylating agents and are thus potent carcinogens.[47] These RNS can display antibacterial effects as well by a similar mechanism. Although the details for the biological activity of this class of compounds are unclear, loss of dinitrogen occurs, thus excluding possible involvement by derived RNS. Alternatively, nitrosamines have been shown to induce formation of ROS.

1.3.4. MNO

Iron complexes bearing nitrosyl and thiolate ligands have been encountered in biology, and have shown a range of functions from NO donation to antitumroidal function.[48] One intriguing feature of these {FeSNO} complexes is their ability to release NO under photolytic conditions.[49] Roussin black salt $[Fe_4S_3(NO)_7]^-$ (RBS) has been used in vasodilation studies.[48] Roussin red salt $[Fe_2S_2(NO)_4]^{2-}$ (RRS) has been studied as a photolabile source of NO for the sensitization of cancer cells to radiotherapy.[50] Alternatively, Roussin red esters $[Fe_2(NO)_4(\mu–SR)_2]$ (RREs) are attractive substrates for NO photodelivery studies given the precedence for alkylation of the bridging sulfides in RRS. Unfortunately, one limitation of these particular {FeSNO} compounds is that the reverse reaction (NO recapture) is rapid ($\sim10^9$ $M^{-1}s^{-1}$). Adaptation of this scaffold to incorporate longer-wavelength or multiphoton chromophores within the R groups afford RREs with better photophysical properties and quantum yields.[49]

Mononitrosyl iron complexes (MNICs) supported by thiolate ligands have only been recently detailed.[51,52] Measurements of NO transfer from MNICs revealed a quantitative process that was complete within 30 min. Although MNICs have yet to be observed biologically, the properties of small-molecule MNICs suggest these complexes could exert possibly orthogonal influences to those of DNICs or other {FeSNO} complexes. For example, MNICs could function as rapidly releasing donors of NO *in vivo*, whereas DNICs would behave as stores of NO. Chemical modification of the {FeSNO} storage complexes to afford MNIC would thus enable release of NO. Previous studies of other {FeSNO} complexes has shown that photoinduced NO release occurs, but the quantum yields are poor and back reactions are very rapid.[49]

1.4. Targets and Action

1.4.1. Complexes of Redox Active Metals with Redox Active Ligands

1.4.1.1. Cytochrome P450

The active site in this enzyme is the same as that for NOS and effects similar chemical transformations. Reaction of cytochrome P450 with NO results in the reversible inhibition of activity upon formation of an {Fe(NO)} adduct.[53] However, this heme nitrosyl species can cause irreversible suppression of activity upon formation of S-nitrosothiol residues.

1.4.1.2. Iron-Sulfur Clusters

Mitochondrial aconitase contains a [4Fe–4S] cluster in the active state that is reduced to a [3Fe–4S] configuration with nearly identical structural parameters upon inactivation.[54] Treatment of the EPR-silent active enzyme with NO affords an inactive protein with an EPR spectrum consistent with formation of a [3Fe–4S] cluster and a dinitrosyl-iron complex (DNIC).[55] In a similar manner, addition of NO to the redox active transcription factor SoxR, composed of a [2Fe–2S] cluster in its active site, induces activation via DNIC formation.[56]

1.4.2. Complexes of Redox Active Metals with Redox Inactive Ligands

1.4.2.1. Soluble Guanylyl Cyclase

The first-identified target for NO in biology was soluble guanylyl cyclase, in which binding of NO to the heme unit activated the enzyme. In the reduced state, the active site

contains a ferrous heme coordinated by two axial histidine ligands. Reaction of CO with ferrous sGC caused displacement of one of the histidine ligands, but did not induce activity.[57] Reconstitution of this enzyme with non-native metals allowed closer investigation into the dependence of enzymatic activity on the coordination environment of the heme unit (*i.e.* five- vs. six-coordinate).[58] Upon reaction of the manganese analog of sGC with NO, a six-coordinate metal nitrosyl was formed and the enzyme lacked activity. However, treatment of the cobalt-reconstituted sGC with NO yielded a five-coordinate cobalt-nitrosyl porphyrinoid complex and the enzyme was active. Activation of this $[Fe^{II}(P)(His)_2]$ enzyme by NO proceeds by formation of the five-coordinate mononitrosyl $[Fe^{II}(P)(NO)]$.[59]

1.4.2.2. Ribonucleotide Reductase

This enzyme is responsible for the conversion of ribonucleotides to deoxy-ribonucleotides. Binding of NO to the enzyme was studied as an analog for dioxygen binding and two $\{Fe(NO)\}^7$ units were observed.[60] Reaction of this enzyme with NO inhibits activity by quenching of the tyrosine radical. However, adventitious reduction of two molecules of NO yields a diiron(III) state without generating the tyrosyl radical.

This type of binding and reduction occurs with nitric oxide reductases.[61] Although the mechanism is unresolved, two steps that must be involved are iron-nitrosyl bond formation and nitrogen-nitrogen bond formation. For example, the latter could occur on one iron bearing two nitrosyl ligands or between two discrete $\{Fe(NO)\}^7$ units. Related work on the binding of CO to this enzyme suggested that two discrete $\{Fe(CO)\}$ units form that interact with one another, implying a similar configuration could be involved in the nitrogen-nitrogen bond-forming step with NO.[62]

1.4.2.3. Cobalamin

This cobalt(II) unit is essential for methionine synthesis and C_1 metabolism; treatment of cells with NO donors disrupts these functions.[63] Although lacking a cobalt(II)-thiolate bond, cobalamin binds NO very rapidly and tightly.[64]

1.4.3. Complexes of Redox Inactive Metals with Redox Active Ligands

1.4.3.1. Zinc Finger Proteins

Zinc finger domains are encoded by 1–3% of the human genome and are frequently employed in the recognition of specific sequences of DNA or RNA. Nitric oxide can disrupt DNA binding of nuclear zinc finger proteins, and this loss of function may result from cysteine nitrosation followed by zinc release.[44]

The action of NO on zinc thiolate complexes can regulate NOS activity. At the dimer interface of the enzyme is a $[Zn(Cys)_4]$ unit with two residues supplied by each monomer.[65] Introduction of an NO donor under aerobic conditions was discovered to cause *S*-nitrosation at these key residues, displacement of zinc, and subsequent loss of enzymatic activity.[66] Similarly, replacing the exogenous NO donor with an activator of iNOS activity also afforded *S*-nitrosated enzyme. Variants of the enzyme in which a monomer is missing one or two of the key cysteine residues have much lower basal activity and are more sensitive to NO donors. Under aerobic, aqueous conditions, NO is converted to N_2O_3, which can then nitrosate the cysteine residues in the bridging $[Zn(Cys)_4]$ unit.

1.4.3.2. Metallothioneins (MTs)

These enzymes contain multiple zinc cysteine units and are involved in the maintenance of zinc homeostasis. Addition of *S*-nitrosothiols to MTs caused labilization of zinc, presumably by cysteine nitrosation.[38] This observation suggests a role for NO in the regulation of zinc homeostasis.

1.5. Conclusions

From its ignominious beginnings as an industrial pollutant and toxic gas, nitric oxide has become one of the most actively researched signaling and regulatory molecules. The three isoforms of nitric oxide synthase have been implicated in processes ranging from vasodilation to immune response, but the exact mechanism of NO synthesis remains unknown. Furthermore, the belief that NO can freely diffuse over long distances has come under scrutiny, and there is growing evidence that other nitrogen oxides, nitroso-organic compounds and metal-nitrosyl complexes are important in the transportation and storage of NO. Delivery of NO at the target can induce effects ranging from activation of gene transcription to suppression of enzyme function. The fundamental chemistry of NO *in vivo* and the biochemical processes it mediates depend on whether the target contains a complex of a redox active metal and redox active ligands, a complex composed of a redox active metal only, a complex of a redox inactive metal supported by redox active ligands, or organic-only substrates.

1.6. Thesis Goals and Structure

Nitric oxide in biology can be considered in three distinct phases: generation, translocation, and action. These categories provide a logical framework for research in this field.

Investigation into the generation of NO requires detailed kinetic studies of the various isoforms of NOS or the simplified oxygenase domain. Small-molecule biomimetic complexes of the active sites would be unable to incorporate the relevant second- and third-coordination sphere hydrogen-bonding or cofactor-protein interactions that are essential for proper enzyme function. Current understanding of the generation of NO from L-arginine by NOS is incomplete and there is no consensus mechanism. Study into the generation of NO *in vivo* will require exhaustive enzymology and *in situ* analytical techniques.

After synthesis, the NO must diffuse or be transported away from NOS to exert its effects. Recent studies have suggested that the lifetime of NO in aerobic, biological milieu could be too short to account for its observed functions. Other oxides of nitrogen, *S*-nitrosothiols and metal nitrosyl complexes could serve as storage vessels or delivery vectors that retain NO until or transport NO where needed. *S*-Nitrosothiols and metal nitrosyl complexes can release NO by thermal decomposition, metal catalyzed release, or illumination. Because the translocation of NO *in vivo* involves the movement of NO(g) or one of its derivatives, investigations into this behavior under physiologic and pathophysiologic conditions require tools for the detection of NO(g) or related species. To this end, we are interested in developing sensors for the turn-on fluorescent detection of NO(g) selectively over other potentially-interfering RNS. Studies of the spatiotemporal distribution of NO(g) under various healthy or disease states will require a sensor that is selective for NO(g). A sensor that is not selective for NO(g) may afford a false-positive response, reporting the presence of NO that could be derived from HNO, RSNO, $ONOO^-$, etc, and thus obfuscate the relationship between NO(g) and physiology or pathophysiology being studied. Similarly, investigations into the biological effects of other RNS, such as HNO, require sensors that are selective for HNO over NO(g) and other derivatives.

Chapter 2 details the inclusion of a previously-reported solution-based NO sensor, which is water-incompatible, into a polymeric matrix that shields the metal–fluorophore complex. Films of this sensor are unaffected by water or dioxygen and display turn-on responses to NO(g). Other RNS, including the NO donor *S*-nitroso-*N*-acetylpenicillamine, are not interfering analytes for this sensor, indicating that these sensor films could be adapted for use in the selective detection of NO(g) *in vivo*. **Chapter 3** reports the adaptation of an established NO sensing strategy, employing a reductive nitrosylation mechanism, to copper(II)-based conducting metallopolymers (CMPs). These CMPs represent the first examples of turn-on fluorescent sensors for NO based on conjugated polymer (CP) scaffolds. The organic-soluble CPs could be adapted for use in aqueous solution by modification of the spacer side-chains, albeit with diminished performance. One of the CP–Cu(II) complexes investigated was selective for HNO over NO(g) in buffered aqueous solution, representing an important step towards an HNO sensor that could be selective over NO(g) and other RNS *in vivo*. The ease of modification of sensor photoluminescent and solubility properties demonstrated the advantages of constructing a sensor upon a CP-based scaffold.

Whatever the means of NO transport and storage, it exerts its effects through biochemical processes. Given the radical character of NO, it can react with a variety of redox active species including complexes composed of redox active metals and ligands, complexes containing only redox active metals, complexes of redox inactive metals supported by redox active ligands, or metal-free organic species. Nitric oxide can inactivate mitochondrial aconitase by disrupting the [4Fe–4S] active site through loss of a dinitrosyliron complex. Similarly, NO binds tightly to cobalamin and inhibits the activity of methionine synthase. These results suggest regulatory roles for NO in energy production and C_1 metabolism, processes that are essential for life. To gain a

better understanding of the mechanisms by which NO could exert its influence, we have initiated a study of the fundamental NO chemistry of transition metal thiolate complexes. The results for the iron thiolate complexes have been recently reported.

Chapter 4 describes the reactivity of simple nickel and cobalt thiolate complexes with NO and the properties of the resulting nickel and cobalt nitrosyl species. Previous studies with iron suggested intermediates that were not observed or isolated, thus adjacent transition metals were employed in the hopes of stabilizing electronic or geometric configurations that might otherwise be unstable. The first examples of $\{Ni(NO)\}^{10}$ and $\{Co(NO)_2\}^{10}$ units within anionic molecules were obtained. Reaction of the nickel thiolate complex with $NOBF_4$ suggested an intermediate species in the conversion of MNIC to RRE, and a trimetallic $\{Co(NO)_2\}^{10}$ complex bore structural resemblance to RBS. Our strategy of exploring the NO chemistry of adjacent transition metals to iron has yielded unique nickel and cobalt nitrosyl complexes and provided insight into processes by which various iron nitrosyl species might interconvert.

1.7. References

(1)   Greenwood, N. N.; Earnshaw, A., *Chemistry of the Elements*. 2nd ed.; Butterworth-Heinemann: Oxford, 2001.

(2)   Cotton, F. A.; Wilkinson, G.; Murillo, C. A.; Bochmann, M., *Advanced Inorganic Chemistry*. 6th ed.; John Wiley & Sons, Inc.: 1999.

(3)   Yun, Y. B.; Kim, D. J.; Park, S. M.; Lee, N.-E.; Kim, K. S.; Bae, G. H. "Large Etch Rate Enhancement by NO-Induced Surface Chemical Reaction during Chemical Dry Etching of Silicon Oxide in F_2 Remote Plasmas" *J. Electrochem. Soc.* **2007**, *154*, D267–272.

(4)   Culotta, E.; Koshland Jr., D. E. "NO News Is Good News" *Science* **1992**, *258*, 1862–1865.

(5)   *Documentation for Immediately Dangerous to Life or Health Concentrations (IDLH):*
        NIOSH Chemical Listing and Documentation of Revised IDLH Values; PB-94-195047;
        National Institute for Occupational Safety and Health: March 1995.

(6)   assuming the gas is completely inhaled by a person with a typical lung volume of 5 L.

(7)   Furchgott, R. F. "Endothelium-Derived Relaxing Factor: Discovery, Early Studies, and
        Identifcation as Nitric Oxide (Nobel Lecture)" *Angew. Chem. Int. Ed.* **1999**, *38*, 1870–
        1880.

(8)   Ignarro, L. J. "Nitric Oxide: A Unique Endogenous Signaling Molecule in Vascular
        Biology (Nobel Lecture)" *Angew. Chem. Int. Ed.* **1999**, *38*, 1882–1892.

(9)   Murad, F. "Discovery of Some of the Biological Effects of Nitric Oxide and Its Role in
        Cell Signaling (Nobel Lecture)" *Angew. Chem. Int. Ed.* **1999**, *38*, 1856–1868.

(10)   Calabrese, V.; Mancuso, C.; Calvani, M.; Rizzarelli, E.; Butterfield, D. A.; Stella, A. M.
        G. "Nitric oxide in the central nervous system: neuroprotection versus neurotoxicity"
        Nature Rev. Neurosci. **2007**, *8*, 766–775.

(11)   Turchi, J. J. "Nitric oxide and cisplatin resistance: NO easy answers" *Proc. Natl. Acad.*
        Sci. USA **2006**, *103*, 4337–4338.

(12)   Bronte, V.; Zanovello, P. "Regulation of Immune Responses by L-Arginine Metabolism"
        Nature Rev. Immunol. **2005**, *5*, 641–654.

(13)   http://en.wikipedia.org/wiki/Noni (accessed May 2008),

(14)   Vallance, P.; Leiper, J. "Blocking NO Synthesis: How, Where and Why?" *Nature Rev.*
        Drug Disc. **2002**, *1*, 939–950.

(15)   Li, H.; Igarashi, J.; Jamal, J.; Yang, W.; Poulos, T. L. "Structural studies of constitutive
        nitric oxide synthases with diatomic ligands bound" *J. Biol. Inorg. Chem.* **2006**, *11*, 753–
        768.

(16)   Li, D.; Kabir, M.; Stuehr, D. J.; Rousseau, D. L.; Yeh, S.-R. "Substrate- and Isoform-
        Specific Dioxygen Complexes of Nitric Oxide Synthase" *J. Am. Chem. Soc.* **2007**, *129*,
        6943–6951.

(17)   Zhu, Y.; Silverman, R. B. "Revisiting Heme Mechanisms. A Perspective on the
        Mechanisms of Nitric Oxide Synthase (NOS), Heme Oxygenase (HO), and Cytochrome
        P450s (CYP450s)" *Biochemistry* **2008**, *47*, 2231–2243.

(18)   Roman, L. J.; Martásek, P.; Masters, B. S. S. "Intrinsic and Extrinsic Modulation of Nitric Oxide Synthase Activity" *Chem. Rev.* **2002**, *102*, 1179–1189.

(19)   Gusarov, I.; Starodubtseva, M.; Wang, Z.-Q.; McQuade, L.; Lippard, S. J.; Stuehr, D. J.; Nudler, E. "Bacterial Nitric-oxide Synthases Operate without a Dedicated Redox Partner" *J. Biol. Chem.* **2008**, *283*, 13140–13147.

(20)   Nagano, T.; Yoshimura, T. "Bioimaging of Nitric Oxide" *Chem. Rev.* **2002**, *102*, 1235–1269.

(21)   Liu, X.; Yan, Q.; Baskerville, K. L.; Zweier, J. L. "Estimation of Nitric Oxide Concentration in Blood for Different Rates of Generation: Evidence that Intravascular Nitric Oxide Levels are too Low to Exert Physiological Effects" *J. Biol. Chem.* **2007**, *282*, 8831–8836.

(22)   Koppenol, W. H.; Moreno, J. J.; Pryor, W. A.; Ischiropoulos, H.; Beckman, J. S. "Peroxynitrite, a Cloaked Oxidant Formed by Nitric Oxide and Superoxide" *Chem. Res. Toxicol.* **1992**, *5*, 834–842.

(23)   Salvemini, D.; Doyle, T. M.; Cuzzocrea, S. "Superoxide, peroxynitrite and oxidative/nitrative stress in inflammation" *Biochem. Soc. Trans.* **2006**, *34*, 965–970.

(24)   Ullrich, V.; Kissner, R. "Redox signaling: Bioinorganic chemistry at its best" *J. Inorg. Biochem.* **2006**, *100*, 2079–2086.

(25)   Lundberg, J. O.; Weitzberg, E.; Gladwin, M. T. "The nitrate–nitrite–nitric oxide pathway in physiology and therapeutics" *Nature Rev. Drug Disc.* **2008**, *7*, 156–167.

(26)   Lundberg, J. O.; Weitzberg, E.; Cole, J. A.; Benjamin, N. "Nitrate, bacteria and human health" *Nature Rev. Microbiol.* **2004**, *2*, 593–602.

(27)   Lewis, R. S.; Deen, W. M. "Kinetics of the Reaction of Nitric Oxide with Oxygen in Aqueous Solutions" *Chem. Res. Toxicol.* **1994**, *7*, 568–574.

(28)   Carlsson, S.; Wiklund, N. P.; Engstrand, L.; Weitzberg, E.; Lundberg, J. O. N. "Effects of pH, Nitrite, and Ascorbic Acid on Nonenzymatic Nitric Oxide Generation and Bacterial Growth in Urine" *Nitric Oxide* **2001**, *5*, 580–586.

(29)   Hughes, M. N. "Chemistry of Nitric Oxide and Related Species" *Methods Enzymol.* **2008**, *436*, 3–19.

(30)   Addison, C. C. "Dinitrogen Tetroxide, Nitric Acid, and Their Mixtures as Media for Inorganic Reactions" *Chem. Rev.* **1980,** *80*, 21–39.

(31)   Miranda, K. M. "The chemistry of nitroxyl (HNO) and implications in biology" *Coord. Chem. Rev.* **2005,** *249*, 433–455.

(32)   Fukuto, J. M.; Dutton, A. S.; Houk, K. N. "The Chemistry and Biology of Nitroxyl (HNO): A Chemically Unique Species with Novel and Important Biological Activity" *ChemBioChem* **2005,** *6*, 612–619.

(33)   Shafirovich, V.; Lymar, S. V. "Nitroxyl and its anion in aqueous solutions: Spin states, protic equilibria, and reactivities toward oxygen and nitric oxide" *Proc. Natl. Acad. Sci. USA* **2002,** *99*, 7340–7345.

(34)   Southern, J. S.; Green, M. T.; Hillhouse, G. L.; Guzei, I. A.; Rheingold, A. L. "Chemistry of Coordinated Nitroxyl. Reagent-Specific Protonations of *trans*-Re(CO)$_2$(NO)(PR$_3$)$_2$ (R = Ph, Cy) That Give the Neutral Nitroxyl Complexes *cis,trans*-ReCl(CO)$_2$(NH=O)(PR$_3$)$_2$ or the Cationic Hydride Complex [*trans,trans*-ReH(CO)$_2$(NO)(PPh$_3$)$^{2+}$][SO$_3$CF$_3^-$]" *Inorg. Chem.* **2001,** *40*, 6039–6046.

(35)   Keshive, M.; Singh, S.; Wishnok, J. S.; Tannenbaum, S. R.; Deen, W. M. "Kinetics of S-Nitrosation of Thiols in Nitric Oxide Solutions" *Chem. Res. Toxicol.* **1996,** *9*, 988–993.

(36)   Tsikas, D.; Frölich, J. C. "Trouble with the analysis of nitrite, nitrate, *S*-nitrosothiols and 3-nitrotyrosine: freezing-induced artifacts?" *Nitric Oxide* **2004,** *11*, 209–213.

(37)   Vanin, A. F.; Papina, A. A.; Serezhenkov, V. A.; Koppenol, W. H. "The mechanisms of *S*-nitrosothiol decomposition catalyzed by iron" *Nitric Oxide* **2004,** *10*, 60–73.

(38)   Chen, Y.; Irie, Y.; Keung, W. M.; Maret, W. "*S*-Nitrosothiols React Preferentially with Zinc Thiolate Clusters of Metallothionein III through Transnitrosation" *Biochemistry* **2002,** *41*, 8360–8367.

(39)   Kelm, M. "Nitric oxide metabolism and breakdown" *Biochim. Biophys. Acta* **1999,** *1411*, 273–289.

(40)   Dicks, A. P.; Williams, D. L. H. "Generation of nitric oxide from *S*-nitrosothiols using protein-bound Cu^{2+} sources " *Chem. & Biol.* **1996,** *3*, 655–659.

(41)   Singh, S. P.; Wishnok, J. S.; Keshive, M.; Deen, W. M.; Tannenbaum, S. R. "The chemistry of the *S*-nitrosoglutathione/glutathione system" *Proc. Natl. Acad. Sci. USA* **1996,** *93*, 14428–14433.

(42)   Bonner, L.; Stedman, G., The chemistry of nitric oxide and redox-related species. In *Methods in Nitric Oxide Research*, Feelisch, M.; Stamler, J. S., Eds. Wiley: London, 1996; pp 4–18.

(43)   Bazylinski, D. A.; Hollocher, T. C. "Evidence from the Reaction between Trioxodinitrate(II) and ^{15}NO That Trioxodinitrate(II) Decomposes into Nitrosyl Hydride and Nitrite in Neutral Aqueous Solution" *Inorg. Chem.* **1985,** *24*, 4285–4288.

(44)   Kröncke, K.-D.; Kolb-Bachofen, V. "Measurement of Nitric Oxide-Mediated Effects on Zinc Homeostasis and Zinc Finger Transcription Factors " *Methods Enzymol.* **1999,** *301*, 126–135.

(45)   Field, L.; Dilts, R. V.; Ravichandran, R.; Lenhert, P. G.; Carnahan, G. E. "An Unusually Stable Thionitrite from *N*-Acetyl-D,L-penicillamine; X-Ray Crystal and Molecular Structure of 2-(Acetylamino)-2-carboxy-1,1-dimethylethyl Thionitrite" *J. Chem. Soc., Chem. Commun.* **1978,** 249–250.

(46)   Stamler, J. S.; Toone, E. J. "The decomposition of thionitrites" *Curr. Opin. Chem. Biol.* **2002,** *6*, 779–785.

(47)   Lewis, D. F. V.; Brantom, P. G.; Ioannides, C.; Walker, R.; Parke, D. V. "Nitrosamine Carcinogenesis: Rodent Assays, Quantitative Structure-Activity Relationships, and Human Risk Assessment" *Drug Metab. Rev.* **1997,** *29*, 1055–1078.

(48)   Butler, A. R.; Megson, I. L. "Non-Heme Iron Nitrosyls in Biology" *Chem. Rev.* **2002,** *102*, 1155–1165.

(49)   Ford, P. C. "Polychromophoric Metal Complexes for Generating the Bioregulatory Agent Nitric Oxide by Single- and Two-Photon Excitation" *Acc. Chem. Res.* **2008,** *41*, 190–200.

(50)   Bourassa, J.; DeGraff, W.; Kudo, S.; Wink, D. A.; Mitchell, J. B.; Ford, P. C. "Photochemistry of Roussin's Red Salt, $Na_2[Fe_2S_2(NO)_4]$, and of Roussin's Black Salt, $NH_4[Fe_4S_3(NO)_7]$. *In Situ* Nitric Oxide Generation To Sensitize γ-Radiation Induced Cell Death" *J. Am. Chem. Soc.* **1997,** *119*, 2853–2860.

(51)   Harrop, T. C.; Song, D.; Lippard, S. J. "Reactivity pathways for nitric oxide and nitrosonium with iron complexes in biologically relevant sulfur coordination spheres" *J. Inorg. Biochem.* **2007,** *101*, 1730–1738.

(52)   Harrop, T. C.; Song, D.; Lippard, S. J. "Interaction of Nitric Oxide with Tetrathiolato Iron(II) Complexes: Relevance to the Reaction Pathways of Iron Nitrosyls in Sulfur-Rich Biological Coordination Environments" *J. Am. Chem. Soc.* **2006,** *128*, 3528–3529.

(53) Minamiyama, Y.; Takemura, S.; Imaoka, S.; Funae, Y.; Tanimoto, Y.; Inoue, M. "Irreversible Inhibition of Cytochrome P450 by Nitric Oxide" *J. Pharm. Exp. Ther.* **1997,** *283,* 1479–1485.

(54) Robbins, A. H.; Stout, C. D. "Structure of activated aconitase: Formation of the [4Fe–4S] cluster in the crystal" *Proc. Natl. Acad. Sci. USA* **1989,** *86,* 3639–3643.

(55) Kennedy, M. C.; Antholine, W. E.; Beinert, H. "An EPR Investigation of the Products of the Reaction of Cytosolic and Mitochondrial Aconitases with Nitric Oxide" *J. Biol. Chem.* **1997,** *272,* 20340–20347.

(56) Ding, H.; Demple, B. "Direct nitric oxide signal transduction via nitrosylation of iron-sulfur centers in the SoxR transcription activator" *Proc. Natl. Acad. Sci. USA* **2000,** *97,* 5146–5150.

(57) Burstyn, J. N.; Yu, A. E.; Dierks, E. A.; Hawkins, B. K.; Dawson, J. H. "Studies of the Heme Coordination and Ligand Binding Properties of Soluble Guanylyl Cyclase (sGC): Characterization of Fe(II)sGC and Fe(II)sGC(CO) by Electronic Absorption and Magnetic Circular Dichroism Spectroscopies and Failure of CO To Activate the Enzyme" *Biochemistry* **1995,** *34,* 5896–5903.

(58) Dierks, E. A.; Hu, S.; Vogel, K. M.; Yu, A. E.; Spiro, T. G.; Burstyn, J. N. "Demonstration of the Role of Scission of the Proximal Histidine-Iron Bond in the Activation of Soluble Guanylyl Cyclase through Metalloporphyrin Substitution Studies" *J. Am. Chem. Soc.* **1997,** *119,* 7316–7323.

(59) Zhao, Y.; Brandish, P. E.; Ballou, D. P.; Marletta, M. A. "A molecular basis for nitric oxide sensing by soluble guanylate cyclase" *Proc. Natl. Acad. Sci. USA* **1999,** *96,* 14753–14758.

(60) Haskin, C. J.; Ravi, N.; Lynch, J. B.; Munck, E.; Que Jr., L. "Reaction of NO with the Reduced R2 Protein of Ribonucleotide Reductase from *Escherichia coli*" *Biochemistry* **1995,** *34,* 11090–11098.

(61) Kurtz Jr., D. M. "Flavo-diiron enzymes: nitric oxide or dioxygen reductases?" *Dalton Trans.* **2007,** 4115–4121.

(62) Lu, S.; Suharti; Vries, S. d.; Moënne-Loccoz, P. "Two CO Molecules Can Bind Concomitantly at the Diiron Site of NO Reductase from *Bacillus azotoformans*" *J. Am. Chem. Soc.* **2004,** *126,* 15332–15333.

(63)   Danishpajooh, I. O.; Gudi, T.; Chen, Y.; Kharitonov, V. G.; Sharma, V. S.; Boss, G. R. "Nitric Oxide Inhibits Methionine Synthase Activity *in Vivo* and Disrupts Carbon Flow through the Folate Pathway" *J. Biol. Chem.* **2001**, *276*, 27296–27303.

(64)   Wolak, M.; Zahl, A.; Schneppensieper, T.; Stochel, G.; Eldik, R. v. "Kinetics and Mechanism of the Reversible Binding of Nitric Oxide to Reduced Cobalamin B_{12r} (Cob(II)alamin)" *J. Am. Chem. Soc.* **2001**, *123*, 9780–9791.

(65)   Raman, C. S.; Li, H.; Martásek, P.; Král, V.; Masters, B. S. S.; Poulos, T. L. "Crystal Structure of Constitutive Endothelial Nitric Oxide Synthase: A Paradigm for Pterin Function Involving a Novel Metal Center" *Cell* **1998**, *95*, 939–950.

(66)   Mitchell, D. A.; Erwin, P. A.; Michel, T.; Marletta, M. A. "S-Nitrosation and Regulation of Inducible Nitric Oxide Synthase" *Biochemistry* **2005**, *44*, 4636–4647.

Chapter 2

Films of Polymer-Shielded
Dirhodium Tetracarboxylate–Fluorophore Complexes
for the Detection of Nitric Oxide in Aqueous Solution

2.1. Introduction

One of the simplest available NO sensing strategies involves NO-induced fluorophore displacement. In this strategy, a fluorophore (Fl) is coordinated to a metal complex $[M^{n+}(L_m)]$ that quenches its fluorescence (**Scheme 2.1**).[1] Upon reaction of the complex with NO, the fluorophore is displaced from the metal and emission is restored. Because the fluorophore undergoes no chemical changes and no change in metal oxidation state occurs, such a system should be readily reversible. Upon loss of NO from the metal, the fluorophore will re-coordinate and be quenched again. This strategy has served as the basis for a number of NO sensors.[2-4]
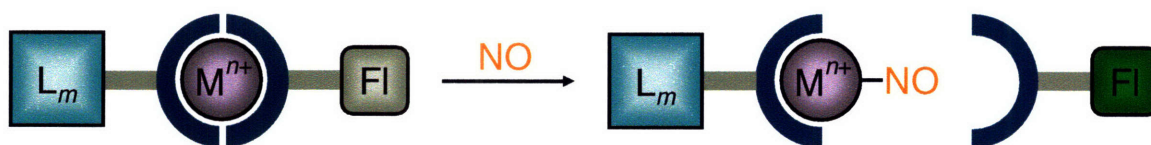
Scheme 2.1. Fluorophore displacement strategy for the fluorescent turn-on detection of NO.

One of the most promising early NO sensors prepared by our lab utilized the fluorophore-displacement strategy. Upon axial coordination to $[Rh_2(O_2CCH_3)_4]$, the fluorescence of *N*-dansylimidazole (Ds–im) or *N*-dansylpiperazine (Ds–pip) is quenched (**Scheme 2.2**).[5] Because $[Rh_2(O_2CCH_3)_4]$ must be added in excess, quenching is believed to occur via formation of a 1:1 dirhodium–dye complex. Addition of excess NO(g) to $[Rh_2(O_2CCH_3)_4(Ds–pip)]$ in non-coordinating solvents yielded an immediate 26-fold increase in integrated emission. Subsequent purging with argon restored the quenched state, and multiple cycles of NO(g)/Ar(g) showed reversible on-off behavior. Sensitivity measurements indicated that the related Ds–im complex could detect concentrations of NO as low as 4 μM. Although dioxygen does not affect the fluorescence of the dirhodium–dye complexes and the components themselves are water-soluble,

these complexes are incompatible with aqueous solutions. Exposure of the sensor to water results in immediate, irreversible turn-on due to displacement of the fluorophore by water.
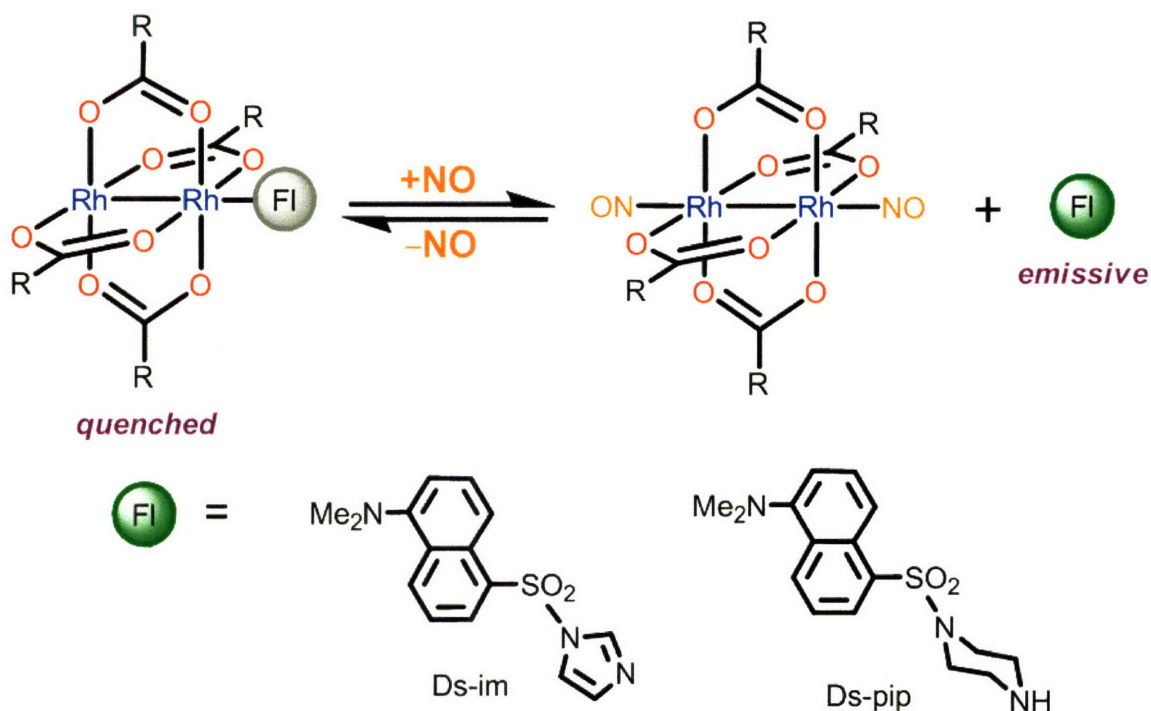
Scheme 2.2. Previous fluorophore-displacement NO sensors based on a dirhodium–dye scaffold.

Fundamentally, the problem with water-induced dye displacement arises from the radically different concentrations of fluorophore vs. water (*e.g.* 10 μM vs. 50 M). Thus, the equilibrium shown in Equation 2.1 will lie to the right. Two chemical methods to overcome this

$$[Rh_2(O_2CCH_3)_4(Fl)] \; + \; H_2O \; \rightleftharpoons \; [Rh_2(O_2CCH_3)_4(H_2O)] \; + \; Fl \quad (2.1)$$

driving force would be to 1) increase the affinity of the dye for the metal or 2) decrease the affinity of the metal for water. Unfortunately, the first method would make NO-induced

displacement of the dye more difficult and thus decrease the sensitivity of the sensor. The second method would require selection of an entirely different quenching construct. Alternatively, *physical* exclusion of water from the dirhodium–dye complex while permitting access by NO(g) would accomplish the same goal.

Many gas-permeable, water-impermeable materials are known and have been used in a range of applications from analyte sensing to separation and purification of mixtures of gases.[6–9] When a vial filled with [$Rh_2(O_2CCH_3)_4(Ds–pip)$] in CH_2Cl_2 solution and covered with a Silastic® membrane was submerged in water, no increase in fluorescence was observed.[5] However, submersion of a similarly-sequestered CH_2Cl_2 solution of this complex in saturated NO(aq) afforded a visible restoration of emission that allowed detection down to 100 μM NO. These results suggest that *existing* dirhodium–dye complexes can be adapted for NO biosensing applications via water-exclusion strategies. Unfortunately, a major limitation to the physical exclusion strategy is that the sensor must be dissolved in non-coordinating solvent to detect and report NO properly. Any biomedical devices based on this strategy would require careful handling to prevent leakage of carcinogenic solvent into the specimen and would be extremely sensitive to membrane tears or leaks.

A simpler and more effective approach would be to include a dirhodium–dye complex *chemically* within a water-impermeable polymer matrix that permits NO(g) diffusion (**Scheme 2.3**). This polymer could then be readily fabricated into a material suited for biosensing applications that would remain functional even if the film were physically damaged. Inclusion of small-molecule complexes into polymers has been used in a wide variety of applications, ranging from sensing to catalysis.[10–13] Sensors have been successfully incorporated into polymeric matrices designed to exclude interfering substances, thus enhancing the biosensing abilities of

the sensors. Here we report the preparation of a polymer-bound dirhodium-dye complex designed to detect NO(g) while excluding water and other potentially interfering analytes.
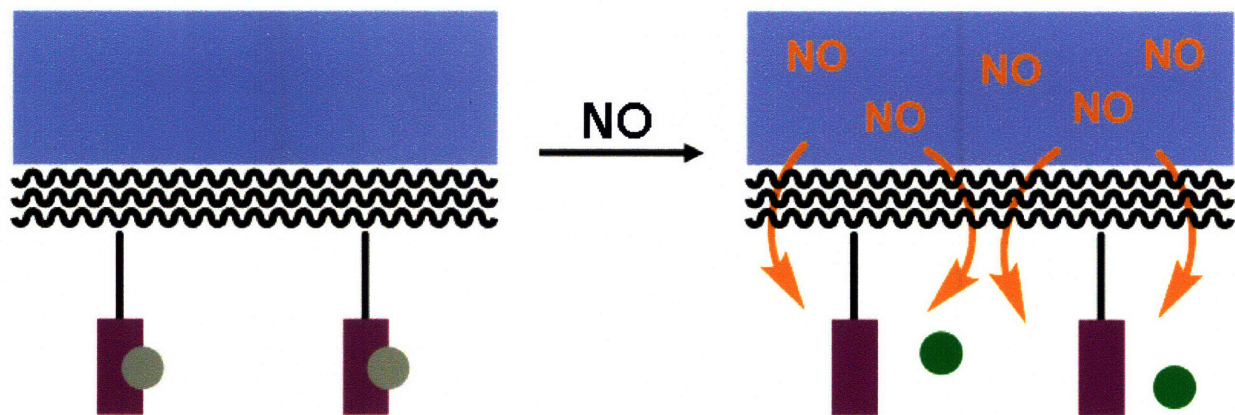
Scheme 2.3. Illustration of the polymer-shielding strategy. The polymeric material (black wavy lines) prevents water from interacting with the dirhodium complexes (purple rectangles) bound by quenched fluorophores (grey circles). After addition to the water, NO can diffuse through the polymer, react with the dirhodium–dye complexes, and cause fluorophore release with attendant restoration of emission (green circles).

2.2. Experimental Section

2.2.1. Materials and Methods

The synthesis, characterization and preparation of films of the polymer-bound dirhodium-dye complex [{Rh$_2$(O$_2$CCH$_3$)$_3$(Ds-pip)}$_n$(O$_2$C−**P**)] (**1**) were performed by Prof. Rhett Smith and are described elsewhere.[14] Gaseous nitric oxide was purified following a reported procedure[15] via passage first through a 2 m stainless steel coil packed with silica and cooled to −78 °C, then through an Ascarite column. Manipulations and transfers of purified NO(g) were performed under an inert atmosphere via gas-tight syringe. The reactive nitrogen species *S*-nitroso-*N*-acetyl-penicillamine (SNAP, an NO donor), 5-amino-3-(4-morpholino)-1,2,3-oxadiazolium chloride

(SIN-1-Cl, an ONOO⁻ donor, **Chart 2.1**), peroxynitrite (in 0.3 M NaOH) and $Na_2N_2O_3$ (an HNO

donor) were purchased from Cayman Chemical Company. Stocks of SNAP (in water), $Na_2N_2O_3$

(in 1.0 M KOH) and peroxynitrite were kept frozen at −80 °C until needed. Immediately prior to

use, these solutions were thawed and the concentrations of reactive nitrogen species (RNS) were

quantified by UV-vis spectroscopy.[16-18] Potassium superoxide was purchased from Strem

Chemicals and stock solutions of 10 mM KO_2 in DMSO were prepared using 18-crown-6 as a

stabilizer.[19,20] Potassium chloride (Puratronic®, 99.997%) was purchased from Alfa Aesar and 4-

(2-hydroxyethyl)-1-piperazineethane sulfonic acid (HEPES, free acid, Ultrapure Bioreagent) was

purchased from J. T. Baker. All other reagents and chemicals were used as received. Buffer (50

mM HEPES, 100 mM KCl, pH 7.4) was prepared in freshly collected Millipore water (≥18.2

MΩ). Subsequent passage through a column of Chelex® 100 resin removed all transition metal

contaminants.
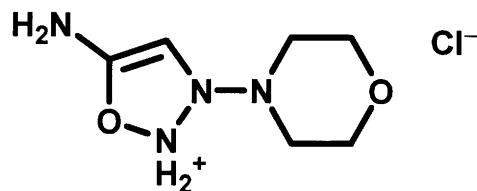
Chart 2.1. Structure of SIN-1-Cl.

2.2.2. General Spectrophotometric Considerations

Absorption spectra were recorded on a Cary 1E or 50 spectrophotometer. Fluorescence

spectra were acquired on a Photon Technology International Quanta Master 4L fluorimeter. Slit

widths, excitation wavelength, and integration time were kept constant for all experiments.

Circulating water baths were used to maintain all samples at 25 ± 1 °C. Samples for fluorescence

had a path length of 1 cm in Spectrosil quartz (6Q), polymethyl-methacrylate (PMMA) or polystyrene (PS) cuvettes from Starna, with optical densities <0.05 and 3.0 mL sample solution volumes. Each film of **1** contained 57.1 nmol of $\{Rh_2(O_2CCH_3)_3(Ds-pip)\}$ in total and was drop-cast from a CH_2Cl_2 solution onto the inner wall of a cuvette. Excitation on the film-coated face of the cuvette was provided at 395 nm and the 90° emission was integrated from 405 nm to 705 nm (**Figure 2.1**) and a representative spectrum of **1** is presented in **Figure 2.2** (red trace). Final concentrations and equivalents of analyte, along with the corresponding response of **1**, are presented in **Table 2.1**.
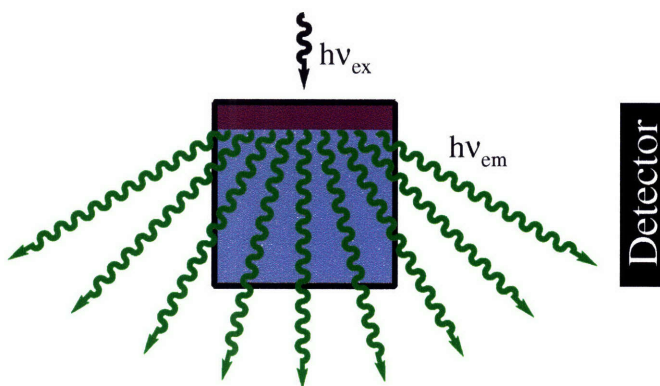
Figure 2.1. Experimental setup for measuring emission from a film of **1**.

2.2.3. Water and Dioxygen Compatibility

To a gastight quartz cuvette containing a film of **1** on one face was added 3 mL of degassed buffer in an inert-atmosphere wetbox. The cuvette was equipped with a septum cap and sealed, removed from the wetbox, and a basal fluorescence scan was acquired. No changes in the absorption or emission spectra were observed after time periods ranging up to 4 h, but after 24 h the integrated emission began to increase.

2.2.4. Response to NO(g) and Reversibility

To a gastight quartz cuvette containing a film of **1** on one face was added 3 mL of degassed buffer in an inert-atmosphere wetbox. The cuvette was equipped with a septum cap and sealed, removed from the wetbox, and a basal fluorescence scan was acquired (**Figure 2.2A**, red trace). Immediately afterwards, 250 μL of NO(g) (10.2 μmol, 179 equiv per Rh_2) were added to this solution and a fluorescence scan was acquired (**Figure 2.2B**, blue trace). The integrated emission increased by a factor of 2.2 ± 0.09 (average of 3 measurements). Purging the cuvette with argon for 30 min afforded an incomplete (50–77%) restoration of initial fluorescence.
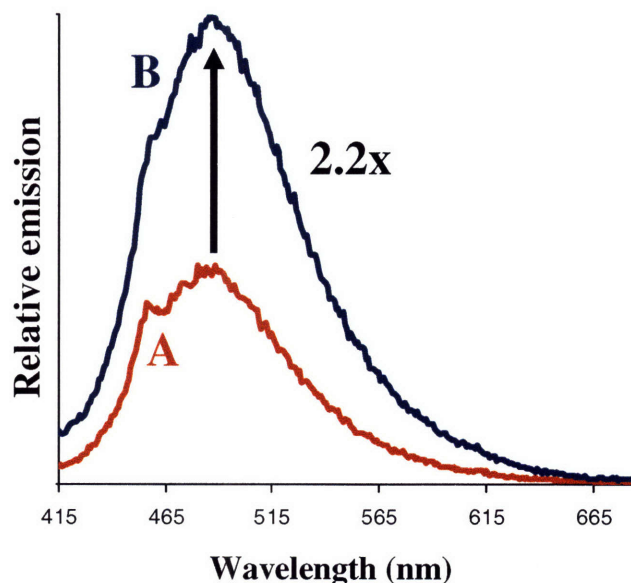
Figure 2.2. Response of a film of **1** to NO(aq). The emission of **1** (**A**, red trace) increased 2.2-fold upon addition of excess NO(g) to the solution (**B**, blue trace).

*2.2.5. Selectivity Studies (see **Figure 2.3** and **Table 2.1** for summarized results)*

2.2.5.1. Response to SNAP

To a gastight PMMA cuvette containing a film of **1** on one face was added solid SNAP (1.0 mg, 4.5 μmol, 79 equiv per Rh_2) in an inert-atmosphere drybox. The cuvette was equipped with a septum cap and sealed, removed from the drybox, and a basal fluorescence scan was acquired. Under a positive nitrogen purge was added 3 mL of degassed buffer to afford a homogeneous solution ([SNAP]$_f$ = 1.5 mM) and a fluorescence scan was immediately acquired. No change in integrated emission occurred upon addition and only a 30% increase was observed after 2 h. After 24 h, the emission had increased by 2.2-fold.

2.2.5.2. Response to $Na_2N_2O_3$

To a gastight PMMA cuvette containing a film of **1** on one face was added solid $Na_2N_2O_3$ (0.5 mg, 4.1 μmol, 72 equiv per Rh_2) in an inert-atmosphere drybox. The cuvette was equipped with a septum cap and sealed, the cuvette was cycled out of the drybox, and a basal fluorescence scan was acquired. Under a positive nitrogen purge was added 3 mL of degassed buffer to afford a homogeneous solution ([$Na_2N_2O_3$]$_f$ = 1.4 mM) and a fluorescence scan was immediately acquired. No change in integrated emission occurred upon addition and a 12% *decrease* was observed after 2 h.

2.2.5.3. Response to SIN-1-Cl

To a gastight PMMA cuvette containing a film of **1** on one face was added solid SIN-1-Cl (1.5 mg, 7.3 μmol, 128 equiv per Rh_2) in an inert-atmosphere drybox. The cuvette was

equipped with a septum cap and sealed, cycled out of the drybox, and a basal fluorescence scan was acquired. Under a positive nitrogen purge was added 3 mL of degassed buffer to afford a homogeneous solution ([SIN-1-Cl]$_f$ = 2.4 mM) and a fluorescence scan was immediately acquired. No change in integrated emission occurred upon addition and none was observed after 2 h.

2.2.5.4. Response to Peroxynitrite

To a gastight quartz cuvette containing a film of **1** on one face and 3 mL of buffer was added 75 µL of 3.76 mM peroxynitrite solution (0.28 µmol, 4.9 equiv per Rh$_2$, [ONOO$^-$]$_f$ = 94 µM) was added and a fluorescence scan was immediately acquired. No change in integrated emission occurred upon addition and a 13% *decrease* was observed after 2 h.

2.2.5.5. Response to Nitrate and Nitrite

To a gastight quartz cuvette containing a film of **1** on one face was added 3 mL of buffer and a basal fluorescence scan was acquired. The buffer was removed via syringe and replaced with 3 mL of buffer containing 10 mM NaNO$_3$ or 10 mM NaNO$_2$ (30 µmol, 525 equiv per Rh$_2$) and a fluorescence scan was acquired. No change in integrated emission occurred upon addition and none was observed after 2 h.

2.2.5.6. Response to Hydrogen Peroxide

To a gastight quartz cuvette containing a film of **1** on one face and 3 mL of buffer was added 3.5 µL of 30% H$_2$O$_2$(aq) (34.3 µmol, 600 equiv per Rh$_2$, [H$_2$O$_2$]$_f$ = 11.4 mM) was added and a fluorescence scan was immediately acquired. No change in integrated emission occurred

upon addition and a 15% *decrease* was observed after 2 h.

2.2.5.7. Response to Superoxide

To a gastight quartz cuvette containing a film of **1** on one face and 3 mL of buffer was added 30 μL of a 10 mM KO_2 solution in DMSO (0.30 μmol, 5.3 equiv per Rh_2, $[KO_2]_f = 0.10$ mM) and a fluorescence scan was immediately acquired. No change in integrated emission occurred upon addition and an 8% *decrease* was observed after 2 h.

2.3. Results and Discussion

2.3.1. Design and Synthesis

Two sites are available on $[Rh_2(O_2CCH_3)_4]$ for attachment to a polymer: the axial positions and the carboxylates. Although coordination of ligands to the axial sites of dirhodium complexes is well-established,[21] this type of linkage is susceptible to disruption by water and NO. Alternatively, a covalent bond between one of the carboxylates and a polymer chain would be kinetically inert. Carboxylate exchange with $[Rh_2(O_2CCH_3)_4]$ is known[21-23] and a number of polymer-bound dirhodium tetracarboxylates have been investigated.[24,25] Thus, we sought to perform carboxylate exchange between $[Rh_2(O_2CCH_3)_4]$ and a polymer bearing carboxylate side-chains.

For use in biosensing applications, a sensor material must be biocompatible and have good photoluminescent properties. Furthermore, our dirhodium inclusion strategy requires a polymer with available carboxylate side-chains. Polymerization of methyl methacrylate (MMA) with methacrylic acid (MAA) affords a copolymer (PMMA) that is transparent from 285–800

nm and can be cast into uniform films.[26] This type of copolymer has also been used extensively in sensing applications ranging from the selective detection of arene vapors to quantitative measurements of partial oxygen pressure in gas mixtures.[27–29] Furthermore, PMMA membranes are permeable to NO(g) and have been incorporated into commercially-available NO detection devices.[30]
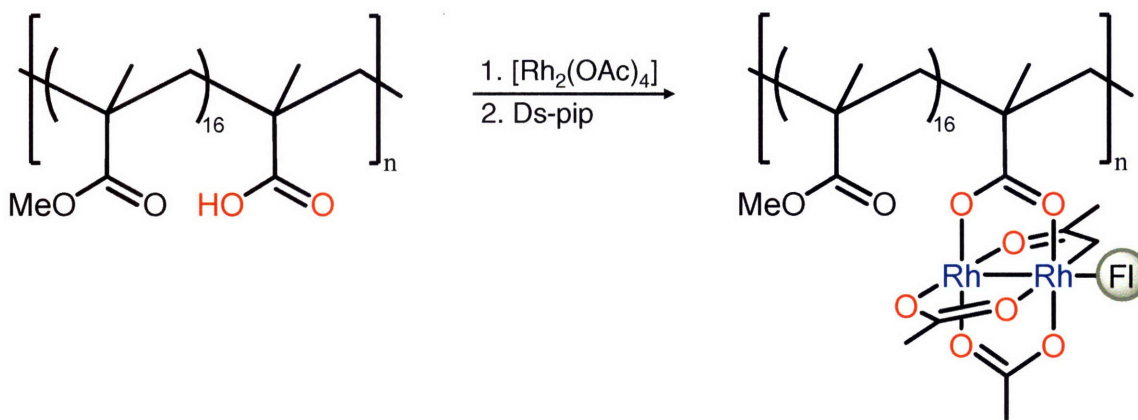
Scheme 2.4. Synthesis of **1** (Fl = Ds−pip)

Given the precedence for carboxylate exchange with $[Rh_2(O_2CCH_3)_4]$ and the established permeability of PMMA to NO(g), we sought to prepare a polymer-bound dirhodium complex via exchange of one acetate with one of the carboxylate side chains of PMMA. A 16:1 MMA/MAA copolymer ($O_2C–$**P**) was prepared as previously described.[26] Subsequent 1:1 MAA/$CH_3CO_2^-$ carboxylate exchange between the copolymer and $[Rh_2(O_2CCH_3)_4]$ was accomplished by refluxing in THF. Incorporation of axial fluorophore into the resultant polymer-bound dirhodium tetracarboxylate complex was effected by stirring with Ds−pip (1 equiv per Rh_2) followed by precipitation of **1** with diethyl ether.

2.3.2. Film Casting and Stability

Films of **1** were drop-cast in 250 μL portions from a solution of **1** in CH_2Cl_2 (228 μM in Rh_2) onto 10 mm × 43 mm PMMA substrates, then cured in the dark for 24 h. Reproducibility of film casting was measured by comparing the emission spectra of nine independently-cast films. The variation in the emission from these films (± 8%) was similar to the instrument error (± 6%). Film homogeneity was determined by comparing the integrated emission spectra from eleven points within a representative film. The standard deviation of these measurements (± 6%) matched instrument error. Because these films were not brittle, we believe they may have retained some amount of CH_2Cl_2, as has been observed for other PMMA films.[31]

Films of **1** display good photostability, with no change in integrated emission even after 90 min of continuous irradiation at 395 nm. These films successfully exclude water: no change in fluorescence was observed after 4 h of immersion in water. Because the fluorescence began to increase after 24 h, all aqueous analyte response measurements were limited to 2 h for a large safety margin. No change in the emission from a film of **1** was observed upon saturating the buffer with O_2 or air, indicating that the fluorescence is not adversely affected by exposure to conditions that would be found in living specimens.

2.3.3. Response to NO(g)

When films of **1** immersed in 3 mL buffer were treated with NO(g), an immediate 2.2-fold increase (σ = 0.09) in integrated emission was observed (**Figure 2.2**). Purging with Ar(g) to remove NO could partially reverse the turn-on, with only a 50–77% return to the initial fluorescence observed. The incompleteness of reversal could be due to the fact that re-coordination of Ds–pip requires diffusion through a solid material instead of a solution.

Variability of restoration may be due to irregular morphology at the molecular level, which would result from the amount of trapped CH_2Cl_2 varying from film to film.[31] The rapidity of response to NO(g) might be a consequence of the films being swollen by encapsulated CH_2Cl_2 and therefore more permeable to NO(g) than a totally desolvated film.

2.3.4. Response to Reactive Nitrogen Species (RNS)

Many studies have been performed to elucidate the biological roles of NO, but the fundamental mechanism of NO transport *in vivo* is unclear.[32-34] Because NO(g) is extremely toxic and difficult to purify,[35] many labs prefer to use nitrosothiols (RSNOs) instead. However, the mechanism of "NO" delivery by these species is disputed.[36-41] Some researchers claim that RSNOs heterolyzes along the S–N bond, directly transferring a nitrosonium (NO$^+$) fragment to the target (termed nitrosation). Others contend that homolysis of the S–N bond liberates 0.5 equiv disulfide (RSSR) and 1 equiv NO, which then reacts with the target (termed nitrosylation). The latter pathway requires a transition metal or other redox agent to facilitate homolytic decomposition of the RSNO.[42,43] A metal center embedded in a polymer matrix should be inaccessible for direct nitrosation and not promote RSNO homolysis. Consequently, we expected that exposure of a polymer-shielded NO sensor to a solution of RSNO would not affect the fluorescence. As our RSNO, we chose SNAP because it exhibits slow first-order thermal[44,45] and second-order metal-induced decomposition.[46] Treatment of a film of **1** with excess SNAP in rigorously metal-free buffer afforded no statistically significant change in integrated emission. After 2 h, a 30% increase in fluorescence indicated some generation of NO, presumably due to slow thermal decomposition of SNAP. The full 2.2-fold restoration of emission was not observed until 24 h after addition. This result indicates that SNAP is unable to access the metal centers.

Our film-based sensor therefore has the capacity to distinguish NO(g) from RSNO, a decided advantage for deconvoluting their respective biological functions.
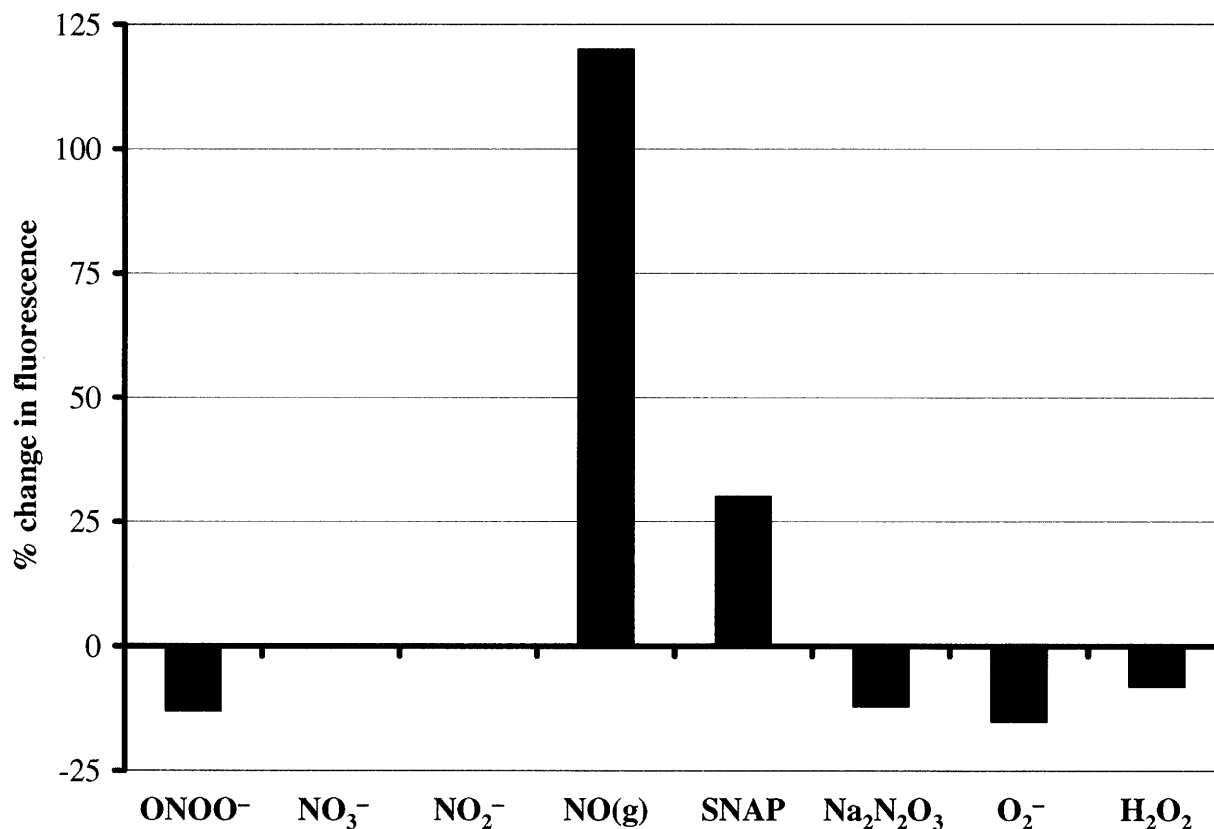
Figure 2.3. Response of **1** to NO(g), RNS and ROS depicted in absolute change in integrated emission. Values for RNS and ROS are 2 h after addition.

Peroxynitrite is one of the most oxidizing RNS and is often produced *in vivo* by rapid reaction of NO with superoxide. This RNS can sometimes produce false positives and is generally considered an interfering analyte for NO sensing.[47] Because peroxynitrite itself must be stored at low concentrations and is unstable at room temperature, we employed SIN-1-Cl as the source. This peroxynitrite donor is readily soluble in organic solvents, can be prepared at higher concentrations, and has been previously used in studies of the biological effects of

peroxynitrite.[48,49] Treatment of a film of **1** with excess SIN-1-Cl yielded no change in fluorescence. Exposure to 4.9 equiv of peroxynitrite itself caused a 13% decrease in integrated emission. These experiments demonstrate that our film-encapsulated sensor will not produce a false turn-on response when peroxynitrite, rather than NO, is being generated.

Nitroxyl (HNO) may play an important role in biology, with a signaling pathway possibly orthogonal to that for NO.[50,51] Surprisingly, few NO sensors have been screened for selectivity over or interference from HNO. To probe the proposed orthogonality of the NO/HNO signaling pathways, sensors that are selective for one over the other are required. We chose $Na_2N_2O_3$ as our donor because the kinetics of HNO release have been thoroughly investigated[18] and other HNO donors produce a mixture of species.[52] Exposure of a film of **1** to excess $Na_2N_2O_3$ induced no immediate change in integrated emission. Even after 1 h, only a 12% *decrease* was observed. Thus, films of **1** respond to HNO far more slowly than and in a way opposite to NO(g).

Table 2.1. Response of **1** to NO(g), RNS and ROS by final concentration of analyte and equiv per Rh_2, reported in absolute change in integrated emission. Numbers in parentheses represent the response after 2 h.

	SIN-1-Cl	ONOO⁻	NO_3^-	NO_2^-	NO(g)	SNAP	$Na_2N_2O_3$	O_2^-	H_2O_2
Final conc. (mM)	2.4	0.094	10	10	1.6	1.5	1.4	0.10	9.2
Equiv per Rh_2	128	4.9	525	525	179	79	72	5.3	480
% change in emission	0	(−13)	0	0	+120	(+30)	(−12)	(−8)	(−15)

Although nitrite and nitrate are considered to be 'inert' oxidized byproducts of NO, recent studies have shown that these species have important biological functions.[53] There is evidence that under conditions of oxygen deprivation, nitrite and nitrate are used in the NOS-

independent synthesis of NO *in vivo*. Because these species are present in biological systems and can deliver NO, we sought to determine the response of **1** to nitrite and nitrate. Treatment of films of **1** with excess $NaNO_2$ or $NaNO_3$ afforded no statistically significant changes in film fluorescence. Thus, films of **1** can discriminate for NO(g) over nitrite and nitrate.

2.3.5. Response to Reactive Oxygen Species (ROS)

Reactive oxygen species such as O_2^- and H_2O_2 are formed as byproducts of the respiratory pathway and are involved in a range of processes from DNA damage to signal transduction.[54,55] Because there is significant overlap between ROS and RNS signaling pathways, these highly oxidizing molecules could potentially interfere with fluorescent NO sensors employing the fluorophore displacement strategy. However, exposure of films of **1** to hydrogen peroxide or superoxide in buffer yielded slight decreases in integrated emission (15% and 8%, respectively) after 2 h. As observed with peroxynitrite, **1** responds to ROS in a manner opposite to NO(g) and can thus distinguish between the two.

2.4. Conclusions

To the best of our knowledge, **1** is the first example of a polymer-bound metal complex that can detect NO(g) under physiologically-relevant conditions by a turn-on fluorescence response. We believe the rapid response, irregular reversibility, and non-brittle character of these films may be due to CH_2Cl_2 being trapped within the polymer matrix and might even be necessary for proper sensor functioning. Shielding the dirhodium-dye complex prevents interference of sensor function by restricting access of a range of potentially interfering analytes, such as RNS other than NO(g), ROS and water. Furthermore, **1** can distinguish NO(g) from other

commonly used NO donors. Our experiments strongly suggest that **1** can selectively sense gaseous NO over other oxides of nitrogen and its functionally orthogonal analog HNO, permitting highly detailed studies into the mechanisms of generation, translocation, and action of NO(g) *in vivo*, without interference by other species. Furthermore, functional films such as those described here are promising candidates for incorporation into fiber optic-based sensing devices for monitoring real-time NO(g) distribution in living organisms.

2.5. References

(1)   Bergonzi, R.; Fabbrizzi, L.; Licchelli, M.; Mangano, C. "Molecular switches of fluorescence operating through metal centered redox couples" *Coord. Chem. Rev.* **1998,** *170,* 31–46.

(2)   Lim, M. H.; Lippard, S. J. "Metal-Based Turn-On Fluorescent Probes for Sensing Nitric Oxide" *Acc. Chem. Res.* **2007,** *40,* 41–51.

(3)   Lim, M. H.; Lippard, S. J. "Fluorescence-Based Nitric Oxide Detection by Ruthenium Porphyrin Fluorophore Complexes" *Inorg. Chem.* **2004,** *43,* 6366–6370.

(4)   Hilderbrand, S. A.; Lim, M. H.; Lippard, S. J., Fluorescence-Based Nitric Oxide Detection. In *Topics in Fluorescence Spectroscopy*, Geddes, C. D.; Lakowicz, J. R., Eds. Springer: 2005; Vol. 9, pp 163–180.

(5)   Hilderbrand, S. A.; Lim, M. H.; Lippard, S. J. "Dirhodium Tetracarboxylate Scaffolds as Reversible Fluorescence-Based Nitric Oxide Sensors" *J. Am. Chem. Soc.* **2004,** *126,* 4972–4978.

(6)   Sairam, M.; Nataraj, S. K.; Aminabhavi, T. M.; Roy, S.; Madhusoodana, C. D. "Polyaniline Membranes for Separation and Purification of Gases, Liquids, and Electrolyte Solutions" *Separ. & Purif. Rev.* **2006,** *35,* 249–283.

(7)   Lin, H.; Freeman, B. D. "Materials selection guidelines for membranes that remove CO_2 from gas mixtures" *J. Mol. Struct.* **2005,** *739,* 57–74.

(8)   Nagai, K.; Masuda, T.; Nakagawa, T.; Freeman, B. D.; Pinnau, I. "Poly[1-(trimethylsilyl)-1-propyne] and related polymers: synthesis, properties and functions" *Prog. Polym. Sci.* **2001,** *26,* 721–798.

(9)   Flaconnèche, B.; Martin, J.; Klopffer, M. H. "Transport Properties of Gases in Polymers: Experimental Methods" *Oil & Gas Sci. Tech.* **2001**, *56*, 245–259.

(10)   Adhikari, B.; Sen, A. K., Utilization of Polymers in Sensor Devices. In *Macromolecular Engineering: Applications*, Matyjaszewski, K.; Gnanou, Y.; Leibler, L., Eds. Wiley: 2007; Vol. 4, pp 2493–2540.

(11)   Mukherjee, D. K.; Saha, C. R. "Soluble and Polymer-Anchored Rhodium Catalyst for Carbonylation Reaction: Kinetics and Mechanism of Diphenylurea Formation" *J. Catal.* **2002**, *210*, 255–262.

(12)   Haupt, K. "Molecularly imprinted polymers in analytical chemistry" *Analyst* **2001**, *126*, 747–756.

(13)   Lindner, E.; Schneller, T.; Auer, F.; Mayer, H. A. "Chemistry in Interphases—A New Approach to Organometallic Syntheses and Catalysis" *Angew. Chem. Int. Ed.* **1999**, *38*, 2154–2174.

(14)   Smith, R. C.; Tennyson, A. G.; Lippard, S. J. "Polymer-Bound Dirhodium Tetracarboxylate Films for Fluorescent Detection of Nitric Oxide" *Inorg. Chem.* **2006**, *45*, 6222–6226.

(15)   Tran, D.; Skelton, B. W.; White, A. H.; Laverman, L. E.; Ford, P. C. "Investigation of the Nitric Oxide Reduction of the Bis(2,9-Dimethyl-1,10-phenanthroline) Complex of Copper(II) and the Structure of [Cu(dmp)$_2$(H$_2$O)](CF$_3$SO$_3$)$_2$" *Inorg. Chem.* **1998**, *37*, 2505–2511.

(16)   Chipinda, I.; Simoyi, R. H. "Formation and Stability of a Nitric Oxide Donor: *S*-Nitroso-*N*-acetylpenicillamine" *J. Phys. Chem. B* **2006**, *110*, 5052–5061.

(17)   Nauser, T.; Merkofer, M.; Kissner, R.; Koppenol, W. H. "Gibbs Energy of Formation of Peroxynitrite" *Chem. Res. Toxicol.* **2001**, *14*, 348–350.

(18)   Bonner, F. T.; Ravid, B. "Thermal Decomposition of Oxyhyponitrite (Sodium Trioxodinitrate(II)) in Aqueous Solution" *Inorg. Chem.* **1975**, *14*, 558–563.

(19)   Bielski, B. H. J.; Allen, A. O. "Mechanism of the Disproportionation of Superoxide Radicals" *J. Phys. Chem.* **1977**, *81*, 1048–1050.

(20)   Valentine, J. S.; Curtis, B. "A Convenient Preparation of Solutions of Superoxide Anion and the Reaction of Superoxide Anion with a Copper(II) Complex" *J. Am. Chem. Soc.* **1975**, *97*, 224–226.

(21)   Boyar, E. B.; Robinson, S. D. "Rhodium(II) carboxylates" *Coord. Chem. Rev.* **1983,** *50,* 109–208.

(22)   Felthouse, T. R., The Chemistry, Structure, and Metal–Metal Bonding in Compounds of Rhodium(II). In *Prog. Inorg. Chem.*, Lippard, S. J., Ed. 1982; Vol. 29, pp 73–166.

(23)   Cotton, F. A.; Murillo, C. A.; Walton, R. A., *Multiple Bonds between Metal Atoms.* 3rd ed.; Springer Science and Business Media: New York, 2005.

(24)   Nagashima, T.; Davies, H. M. L. "Catalytic Asymmetric Cyclopropanation Using Bridged Dirhodium Tetraprolinates on Solid Support" *Org. Lett.* **2002,** *4,* 1989–1992.

(25)   Davies, H. M. L.; Walji, A. M.; Nagashima, T. "Simple Strategy for the Immobilization of Dirhodium Tetraprolinate Catalysts Using a Pyridine-Linked Solid Support" *J. Am. Chem. Soc.* **2004,** *126,* 4271–4280.

(26)   Shonaike, G. O.; Simon, G. P., *Polymer Blends and Alloys.* Marcel Dekker, Inc.: New York, 1999.

(27)   Mills, A.; Lepre, A. "Controlling the Response Characteristics of Luminescent Porphyrin Plastic Film Sensors for Oxygen" *Anal. Chem.* **1997,** *69,* 4653–4659.

(28)   Capan, R.; Ray, A. K.; Hassan, A. K.; Tanrisever, T. "Poly(methyl methacrylate) films for organic vapour sensing" *J. Phys. D.: Appl. Phys.* **2003,** *36,* 1115–1119.

(29)   Aspée, A.; García, O.; Maretti, L.; Sastre, R.; Scaiano, J. C. "Free Radical Reactions in Poly(methyl methacrylate) Films Monitored Using a Prefluorescent Quinoline–TEMPO Sensor" *Macromolecules* **2003,** *36,* 3550–3556.

(30)   Lai, C.-S. Methods for the detection of nitric oxide in fluid media. US 5,885,842, March 23, 1999.

(31)   Nocera, D. G. personal communication.

(32)   Weichsel, A.; Maes, E. M.; Andersen, J. F.; Valenzuela, J. G.; Shokhireva, T. K.; Walker, F. A.; Montfort, W. R. "Heme-assisted S-nitrosation of a proximal thiolate in a nitric oxide transport protein" *Proc. Natl. Acad. Sci. USA* **2005,** *102,* 594–599.

(33)   Butler, A. R.; Megson, I. L. "Non-Heme Iron Nitrosyls in Biology" *Chem. Rev.* **2002,** *102,* 1155–1165.

(34)   Vedernikov, Y. P.; Mordvintcev, P. I.; Malenkova, I. V.; Vanin, A. F. "Similarity between the vasorelaxing activity of dinitrosyl iron cysteine complexes and endothelium-derived relaxing factor" *Eur. J. Pharmacol.* **1992**, *211*, 313–317.

(35)   Lorković, I. M.; Ford, P. C. "Reactivity of the Iron Porphyrin Fe(TPP)(NO) with Excess NO. Formation of Fe(TPP)(NO)(NO$_2$) Occurs via Reaction with Trace NO$_2$" *Inorg. Chem.* **2002**, *39*, 632–633.

(36)   Tsikas, D.; Frölich, J. C. "Trouble with the analysis of nitrite, nitrate, *S*-nitrosothiols and 3-nitrotyrosine: freezing-induced artifacts?" *Nitric Oxide* **2004**, *11*, 209–213.

(37)   Vanin, A. F.; Papina, A. A.; Serezhenkov, V. A.; Koppenol, W. H. "The mechanisms of *S*-nitrosothiol decomposition catalyzed by iron" *Nitric Oxide* **2004**, *10*, 60–73.

(38)   Chen, Y.; Irie, Y.; Keung, W. M.; Maret, W. "*S*-Nitrosothiols React Preferentially with Zinc Thiolate Clusters of Metallothionein III through Transnitrosation" *Biochemistry* **2002**, *41*, 8360–8367.

(39)   Kelm, M. "Nitric oxide metabolism and breakdown" *Biochim. Biophys. Acta* **1999**, *1411*, 273–289.

(40)   Dicks, A. P.; Williams, D. L. H. "Generation of nitric oxide from *S*-nitrosothiols using protein-bound Cu^{2+} sources " *Chem. & Biol.* **1996**, *3*, 655–659.

(41)   Singh, S. P.; Wishnok, J. S.; Keshive, M.; Deen, W. M.; Tannenbaum, S. R. "The chemistry of the *S*-nitrosoglutathione/glutathione system" *Proc. Natl. Acad. Sci. USA* **1996**, *93*, 14428–14433.

(42)   Bonner, L.; Stedman, G., The chemistry of nitric oxide and redox-related species. In *Methods in Nitric Oxide Research*, Feelisch, M.; Stamler, J. S., Eds. Wiley: London, 1996; pp 4–18.

(43)   Bazylinski, D. A.; Hollocher, T. C. "Evidence from the Reaction between Trioxodinitrate(II) and [15]NO That Trioxodinitrate(II) Decomposes into Nitrosyl Hydride and Nitrite in Neutral Aqueous Solution" *Inorg. Chem.* **1985**, *24*, 4285–4288.

(44)   Kröncke, K.-D.; Kolb-Bachofen, V. "Measurement of Nitric Oxide-Mediated Effects on Zinc Homeostasis and Zinc Finger Transcription Factors " *Methods Enzymol.* **1999**, *301*, 126–135.

(45)   Field, L.; Dilts, R. V.; Ravichandran, R.; Lenhert, P. G.; Carnahan, G. E. "An Unusually Stable Thionitrite from *N*-Acetyl-D,L-penicillamine; X-Ray Crystal and Molecular

Structure of 2-(Acetylamino)-2-carboxy-1,1-dimethylethyl Thionitrite" *J. Chem. Soc., Chem. Commun.* **1978**, 249–250.

(46)   Stamler, J. S.; Toone, E. J. "The decomposition of thionitrites" *Curr. Opin. Chem. Biol.* **2002**, *6*, 779–785.

(47)   Crow, J. P. "Dichlorodihydrofluorescein and Dihydrorhodamine 123 Are Sensitive Indicators of Peroxynitrite in Vitro: Implications for Intracellular Measurement of Reactive Nitrogen and Oxygen Species" *Nitric Oxide* **1997**, *1*, 145–157.

(48)   Lomonosova, E. E.; Kirsch, M.; Rauen, U.; de Groot, H. "The Critical Role of HEPES in SIN-1 Cytotoxicity, Peroxynitrite versus Hydrogen Peroxide" *Free Radic. Biol. Med.* **1998**, *24*, 522–528.

(49)   Brunelli, L.; Crow, J. P.; Beckman, J. B. "The Comparative Toxicity of Nitric Oxide and Peroxynitrite to *Escherichia Coli*" *Arch. Biochem. Biophys.* **1995**, *316*, 327–344.

(50)   Miranda, K. M. "The chemistry of nitroxyl (HNO) and implications in biology" *Coord. Chem. Rev.* **2005**, *249*, 433–455.

(51)   Fukuto, J. M.; Dutton, A. S.; Houk, K. N. "The Chemistry and Biology of Nitroxyl (HNO): A Chemically Unique Species with Novel and Important Biological Activity" *ChemBioChem* **2005**, *6*, 612–619.

(52)   Hughes, M. N.; Cammack, R. "Synthesis, Chemistry, and Applications of Nitroxyl Ion Releasers Sodium Trioxodinitrate or Angeli's Salt and Piloty's Acid" *Methods Enzymol.* **1999**, *301*, 279–287.

(53)   Lundberg, J. O.; Weitzberg, E.; Gladwin, M. T. "The nitrate–nitrite–nitric oxide pathway in physiology and therapeutics" *Nature Rev. Drug Disc.* **2008**, *7*, 156–167.

(54)   Hoye, A. T.; Davoren, J. E.; Wipf, P.; Fink, M. P.; Kagan, V. E. "Targeting Mitochondria" *Acc. Chem. Res.* **2008**, *41*, 87–97.

(55)   D'Autréaux, B.; Toledano, M. B. "ROS as signalling molecules: mechanisms that generate specificity in ROS homeostasis" *Nature Rev. Mol. Cell Biol.* **2007**, *8*, 813–824.

Chapter 3

Conducting Metallopolymer-Based Sensors for Nitric Oxide and Nitroxyl

3.1. Introduction

A. Solvent traps NO⁺ fragment

B. Fluorophore traps NO⁺ fragment

C. Metal traps NO⁺ fragment
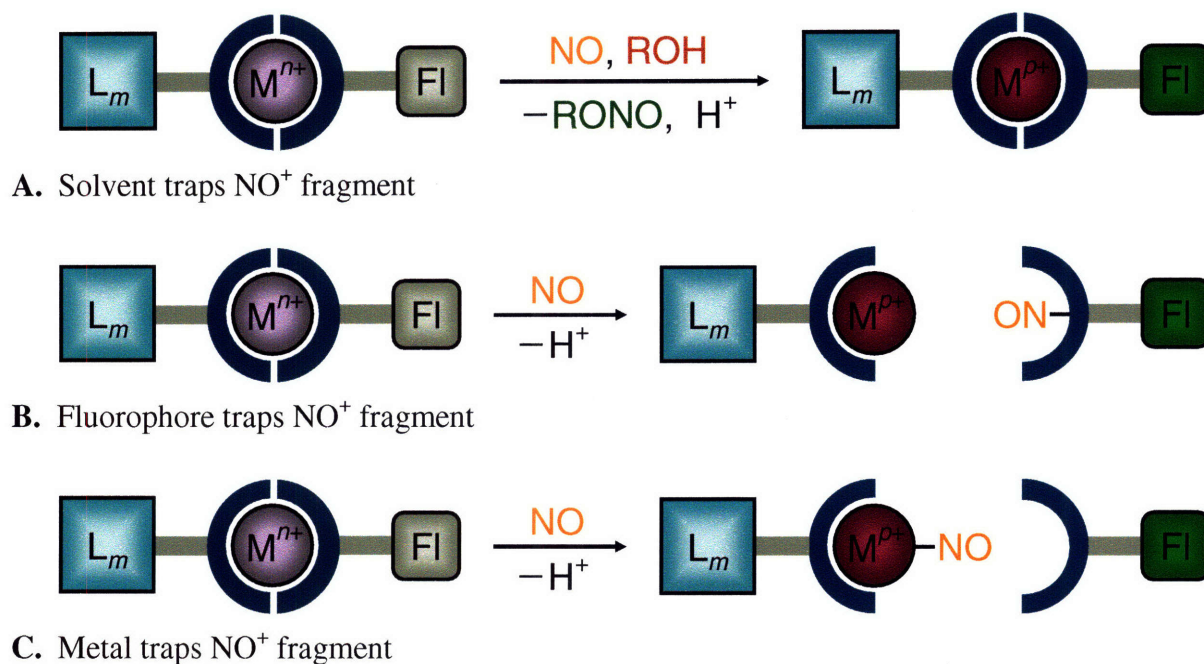
Scheme 3.1. Possible mechanisms of reductive nitrosylation of a metal–fluorophore complex.

Most of the nitric oxide sensors used in bioimaging take advantage of the redox active nature of this diatomic radical[1–6] or higher oxides thereof produced under physiological conditions.[7–13] Some of the earliest examples of inorganic complex-based fluorescent NO sensors function via reductive nitrosylation,[14,15] whereby NO acts as a reducing agent. As with the fluorophore displacement strategy, a fluorophore (Fl) is coordinated to a metal complex [$M^{n+}(L_m)$] that quenches its fluorescence (**Scheme 3.1**).[16] However, exposure to NO can result in a restoration of emission by three mechanisms. In the simplest case, reaction of [$M^{n+}(L_m)(Fl)$] with NO causes reduction of the metal without changing the nature or number of ligands. The resulting NO⁺ fragment is trapped by protic solvent ROH to afford H⁺ and RONO (**Scheme 3.1A**). However, if the fluorophore has relatively acidic protons (*e.g.* N–H, O–H, etc), NO⁺ may

react with it instead of solvent, yielding H^+ and Fl–NO (**Scheme 3.1B**). Alternatively, one or more equiv of NO may bind to and reduce the metal with concomitant displacement of fluorophore (**Scheme 3.1C**). These three cases are merely limiting examples: it is possible for a sensor to respond to NO by a combination of these mechanisms, such as nitrosylation of metal *and* fluorophore.

For the reductive nitrosylation mechanism to be applied to fluorescent NO sensing by inorganic complexes, the metal must have a quenching, open-shell electronic configuration in its oxidized state and a non-quenching, closed-shell configuration in its reduced state. To maximize sensitivity of the sensor, the complex should be able to react with stoichiometric NO and not require higher equivalents, thus the oxidized and reduced states must be separated by a one-electron redox couple. The only reductions that satisfy these criteria are (i) $d^3 \rightarrow$ low-spin tetrahedral or trigonal bipyramidal d^4, (ii) $d^5 \rightarrow$ low-spin, octahedral or square-planar d^6, (iii) $d^7 \rightarrow$ low-spin, square-planar or trigonal bipyriamidal d^8, (iv) or $d^9 \rightarrow d^{10}$. Excluding zero-valent metals and oxidation states higher than +5, the redox pairs that satisfy (i) are V(II/I), Cr(III/II), Mn(IV/III), and Fe(V/IV). However, none of these oxidation states would be compatible with aerobic, aqueous conditions. For (ii), the available pairs are Mn(II/I), Fe(III/II), Co(IV/III), and Ni(V/IV). Of these four possibilities, only Fe(III/II) is suitable for use in bioimaging. To be diamagnetic, the resulting Fe(II) complex must be low-spin octahedral, square-planar or trigonal bipyramidal. However, the iron-based, turn-on fluorescent NO sensors that have been reported to date function by fluorophore displacement with[3,17] or without reductive nitrosylation.[18] For (iii), the suitable pairs are Co(II/I), Ni(III/II), and Cr(IV/III), but only Co(II/I) would be feasible for use in aqueous, aerobic environments. However, Co(II) tends to be unstable under aerobic conditions and the reported cobalt-based fluorescent NO sensors employ a Co(III/I) two-electron

couple.[14,15,19] For (iv), Cu(II/I) is the only available redox pairing. Because, Cu(II) is d^9 and Cu(I) is d^{10}, neither the quenching ability of the former nor diamagnetic character of the latter will be dependent on geometry.

During reductive nitrosylation of copper, NO and Cu(II) are converted to NO^+ and Cu(I) (**Equation 3.1**). Because NO^+ is a much stronger oxidant that Cu(II), the equilibrium will lie to the left. Consequently, reaction of a Cu(II)–dye complex with NO will yield no restoration in emission. If the NO^+ fragment can be irreversibly consumed (*e.g.* conversion to RONO), the reaction will go to completion and emission will be restored. For this reason, measurements of NO response should be performed in protic solvent or with a sensor bearing a functional group that can be nitrosated (*e.g.* N–H).

$$Cu(II) \quad + \quad NO \quad \rightleftharpoons \quad Cu(I) \quad + \quad NO^+ \qquad (3.1)$$

Because we ultimately wish to image NO *in vivo* in real-time, we are interested in preparing NO sensors that are reversible. Unfortunately, two of the three possible reductive nitrosylation pathways involve fluorophore displacement and are inherently irreversible. The only viable mechanism for sensing NO via reductive nitrosylation is the one that causes reduction of the metal without fluorophore dissociation and the resulting NO^+ is trapped by solvent or a pendant ligand that does not dissociate. For this process to be reversible, the amount of reorganization within the metal complex must be minimal: ligands cannot be coordinating and dissociating to accommodate the changes in redox state. Complexes of Cu(II) are most commonly square-planar geometries whereas those of Cu(I) prefer pseudotetrahedral con-figurations. In both cases, the coordination number at the metal is four and the primary

coordination spheres are related by a simple geometric rearrangement. Thus, a Cu(II)–dye complex satisfies both the electronic and geometric requirements for a reversible, reductive nitrosylation-based NO sensor. Successful turn-on fluorescent sensors for NO employing this strategy have been reported by us[1,20–23] and others.[24–26]

3.2. Experimental Section

3.2.1. Materials and Methods

The syntheses and characterization of polymers **1–6** were performed by Prof. Rhett Smith and are described elsewhere.[27–30] Gaseous nitric oxide was purified following a reported procedure[31] via passage first through a 2 m stainless steel coil packed with silica and cooled to −78 °C, then through an Ascarite column. Manipulations and transfers of purified NO(g) were performed under an inert atmosphere via gas-tight syringe. The reactive nitrogen species *S*-nitroso-*N*-acetyl-penicillamine (SNAP, an NO donor), 5-amino-3-(4-morpholino)-1,2,3-oxa-diazolium chloride (SIN-1-Cl, an $ONOO^-$ donor), peroxynitrite (in 0.3 M NaOH) and $Na_2N_2O_3$ (an HNO donor) were purchased from Cayman Chemical Company. Stocks of SNAP (in water), $Na_2N_2O_3$ (in 1.0 M KOH) and peroxynitrite were kept frozen at −80 °C until needed. Immediately prior to use, these solutions were thawed and the concentrations of reactive nitrogen species (RNS) were quantified by UV-vis spectroscopy.[32–34] Potassium superoxide was purchased from Strem Chemicals and stock solutions of 10 mM KO_2 in DMSO were prepared using 18-crown-6 as a stabilizer.[35,36] Potassium chloride (Puratronic®, 99.997%) was purchased from Alfa Aesar and 4-(2-hydroxyethyl)-1-piperazineethane sulfonic acid (HEPES, free acid, Ultrapure Bioreagent) was purchased from J. T. Baker. All other reagents and chemicals were

used as received. Buffer (50 mM HEPES, 100 mM KCl, pH 7.4) was prepared in freshly collected Millipore water ($\geq$18.2 MΩ). Subsequent passage through a column of Chelex® 100 resin removed all transition metal contaminants.

3.2.2. General Spectrophotometric Considerations

Absorption spectra were recorded on a Cary 1E or 50 spectrophotometer. Fluorescence spectra were acquired on a Photon Technology International Quanta Master 4L fluorimeter. Slit widths, excitation wavelength, and integration time were kept constant for all experiments. Circulating water baths were used to maintain all samples at 25 $\pm$ 1 °C. Samples for fluorescence had a path length of 1 cm in Spectrosil quartz (6Q), polymethyl-methacrylate (PMMA) or polystyrene (PS) cuvettes from Starna, with optical densities <0.05 and 3.0 mL sample solution volumes. Quantum yields (Φ) were determined by averaging the results of at least three trials. Values were referenced both to fluorescein (0.100 M NaOH, Φ = 0.92) and to NIST-issued quinine bisulfate (in 0.105 M perchloric acid in Millipore water, Φ = 0.546). X-band EPR spectra were recorded by Dr. Mi Hee Lim on a Bruker EMX EPR spectrometer (9.37 GHz) running WinEPR software. The temperature was maintained at 5 K for these measurements with an Oxford Instruments ESR900 liquid-helium cryostat and an ITC503 controller.

3.2.3. Response of Organic-Soluble CPs to Metal Ions

See **Table 3.1** for summarized results.

3.2.3.1. Titration of 1-3 with Cu(OTf)$_2$

A 3.0 mL aliquot of a 2.0 μM solution of CP in 4:1 CH$_2$Cl$_2$/EtOH was added to a quartz

cuvette, which was sealed with a gas-tight Teflon-lined screw cap equipped with a septum, and a basal fluorescence spectrum was acquired. Small (5–75 µL) aliquots of a 60 µM solution of Cu(OTf)$_2$ in 4:1 CH$_2$Cl$_2$/EtOH, where 5 µL represents 0.05 equiv of Cu(II) per binding unit, were then added through the septum. The cuvette was shaken for 3 s and a fluorescence scan was acquired after each aliquot addition. Characteristic spectra are given for **1a** (**Figure 3.1**).

3.2.3.2. *Response of 1a to Excess Cu(OAc)*

A 3.0 mL aliquot of a 2.0 µM solution of **1a** in 4:1 CH$_2$Cl$_2$/EtOH was added to a quartz cuvette, which was sealed with a gas-tight Teflon-lined screw cap equipped with a septum, and a basal fluorescence spectrum was acquired. A 200 µL aliquot of a 0.30 mM solution of Cu(OAc) in CH$_3$CN, corresponding to 10 equiv of Cu(I) per binding unit, was then added through the septum. The cuvette was shaken for 3 s and a fluorescence scan was acquired (**Figure 3.2**).

3.2.4. *Response of Water-Soluble CPs to Metal Ions*

See **Table 3.2** and **Table 3.3** for summarized results.

3.2.4.1. *Titration of 4 with CuSO₄·5H₂O*

A 3.0 mL aliquot of a 2.1 µM solution of **4** (in 95:5 CH$_3$CN/H$_2$O or H$_2$O) was added to a quartz or PMMA cuvette and a basal fluorescence spectrum was acquired. Small aliquots (1.8–18 µL) of 3.45 mM or 34.5 mM CuSO$_4$·5H$_2$O(aq) were added to the cuvette, where 1.8 µL corresponds to 1.0 or 10 equiv of Cu(II) per mol binding unit, respectively. The cuvette was shaken for 3 s and a fluorescence scan was acquired after each aliquot addition.

3.2.4.2. Titration of 5 with $CuSO_4 \cdot 5H_2O$

A 3.0 mL aliquot of a 14 μM solution of **5** (in 95:5 CH_3CN/H_2O, H_2O, or 10 mM SDS) was added to a quartz or PMMA cuvette and a basal fluorescence spectrum was acquired. Small aliquots (1.2 μL) of 3.45 mM or 34.5 mM $CuSO_4 \cdot 5H_2O$(aq) were added to the cuvette, where 1.2 μL corresponds to 1.0 or 10 equiv of Cu(II) per mol binding unit, respectively. The cuvette was shaken for 3 s and a fluorescence scan was acquired after each aliquot addition.

3.2.4.3. Titration of 6 with $CuSO_4 \cdot 5H_2O$

A 3.0 mL aliquot of a 7.9 μM solution of **6** (in 90:10 CH_3CN/H_2O, H_2O, or buffer) was added to a quartz or PS cuvette and a basal fluorescence spectrum was acquired. Small aliquots (4.0–20 μL) of 0.60 mM or 6.0 mM $CuSO_4 \cdot 5H_2O$(aq) were added to the cuvette, where 4.0 μL corresponds to 1.0 or 10 equiv of Cu(II) per bithiophene unit in the polymer backbone, respectively. The cuvette was shaken for 3 s and a fluorescence scan was acquired after each aliquot addition.

3.2.4.4. Metal Ion Selectivity for 4b and 6

A 3.0 mL aliquot of a solution of CP ([**4b**] = 2.1 μM, [**6**] = 7.9 μM) in H_2O was added to each of 17 PMMA or PS cuvettes and basal fluorescence spectra were acquired for each sample. Aliquots (10 μL) of various 6.0 mM aqueous stock solutions of metal salts were added to each cuvette, where 10 μL corresponds to 10 or 2.5 equiv of metal ion per binding unit in **4b** or **6**, respectively. The salts used were NaCl, KNO_3, $MgSO_4$, $CaCl_2$, $BaCl_2$, $EuCl_3$, Mn(OAc)$_2$, Co(acac)$_2$, $CoSO_4 \cdot 6H_2O$, $NiSO_4 \cdot 6H_2O$, K_2PtCl_4, $CuCl_2$, Cu(NO$_3$)$_2 \cdot 5H_2O$, $CuSO_4 \cdot 5H_2O$, $ZnCl_2$, $CdCl_2$, $CdSO_4$, Hg(OAc)$_2$, Ag(O$_2$CCF$_3$), Al$_2$(SO$_4$)$_3$, and Pb(OAc)$_2 \cdot 3H_2O$. Fluorescent spectra

were recorded within 1 min following addition and again after 10 min. No differences were observed between spectra acquired after 1 or 10 min (**Figure 3.6** and **3.9**)

3.2.5. Response of Organic-Soluble CMPs to NO(g)

See **Table 3.1** for summarized results.

3.2.5.1. Response of CP–Cu(II) Complex to Excess NO(g) (CP = 1–3)

A 3.0 mL aliquot of a 2.0 μM solution of CP in 4:1 CH_2Cl_2/EtOH was added to each of two quartz cuvettes, which were sealed with gas-tight Teflon-lined screw caps equipped with septa, and basal fluorescence spectra was acquired. An aliquot (50 or 100 μL) of a 60 μM solution of $Cu(OTf)_2$ in 4:1 CH_2Cl_2/EtOH, corresponding to 0.5 equiv per bipyridyl (for **1**) or 1 equiv per terpyridyl (for **2** and **3**), was added through the septum in each sample cell to form the CP–Cu(II) complex and the fluorescence spectra were acquired. To one of the cuvettes containing CP–Cu(II) was added 50 μL of NO(g) (680 or 340 equiv per Cu(II) added for **1** or **2–3**, respectively) via a gas-tight syringe through the septum in the cell cap, the solution was shaken for 3 s, and the fluorescence spectrum was acquired. Characteristic spectra are given for **1a** (**Figure 3.2**).

3.2.6. Response of Water-Soluble CMPs to NO(g)

See **Table 3.2** and **Table 3.3** for summarized results.

3.2.6.1. Response of 4a–Cu(II) to Excess NO(g) in Unbuffered Solution

A 3.0 mL aliquot of a 2.1 μM solution of **4a** (in 95:5 CH_3CN/H_2O or H_2O) was added to

a quartz cuvette followed by a 36 μL aliquot of 3.45 mM CuSO$_4$·5H$_2$O(aq) to form the **4a**–Cu(II) complex. The cuvette was sealed with a gas-tight Teflon-lined screw cap equipped with a septum and the fluorescence spectrum was acquired. A 250 μL aliquot of NO(g) (83 equiv per total Cu(II) added) was bubbled through the solution via a gastight syringe inserted through the septum, the solution was vigorously shaken for 3 s, and the fluorescence response was measured. Characteristic spectra are given for **4a** in 95:5 CH$_3$CN/H$_2$O (**Figure 3.8**).

3.2.6.2. Response of 5–Cu(II) to Excess NO(g) in Unbuffered Solution

A 3.0 mL aliquot of a 14 μM solution of **5** (in 95:5 CH$_3$CN/H$_2$O, H$_2$O, or 10 mM SDS) was added to a quartz cuvette followed by an 84 or 840 μL aliquot of 3.45 mM CuSO$_4$·5H$_2$O(aq) to form the **5**–Cu(II) complex, in non-SDS and SDS(aq), respectively. The cuvette was sealed with gas-tight Teflon-lined screw cap equipped with a septum and the fluorescence spectrum was acquired. A 250 μL aliquot of NO(g) (34 or 3.4 equiv per total Cu(II) added, in non-SDS and SDS solution, respectively) was bubbled through the solution via a gastight syringe inserted through the septum, the solution was vigorously shaken for 3 s, and the fluorescence response was measured.

3.2.6.3. Response of 6–Cu(II) to Excess NO(g) in Unbuffered Solution

A 3.0 mL aliquot of a 7.9 μM solution of **6** (in 90:10 CH$_3$CN/H$_2$O or H$_2$O) was added to a quartz cuvette followed by a 20 μL aliquot of 6.0 mM CuSO$_4$·5H$_2$O(aq) to form the **6**–Cu(II) complex. The cuvette was sealed with gas-tight Teflon-lined screw cap equipped with a septum and the fluorescence spectrum was acquired. A 250 μL aliquot of NO(g) (83 equiv per total Cu(II) added) was bubbled through the solution via a gastight syringe inserted through the

septum, the solution was vigorously shaken for 3 s, and the fluorescence response was measured.

3.2.6.4. Response of 6–Cu(II) to Excess NO(g) in Buffered Solution

A 3.0 mL aliquot of a 7.9 μM solution of **6** in buffer was added to a quartz cuvette followed by a 100 μL aliquot of 6.0 mM $CuSO_4 \cdot 5H_2O$(aq) to form the **6**–Cu(II) complex. The cuvette was sealed with gas-tight Teflon-lined screw cap equipped with a septum and the fluorescence spectrum was acquired. A 250 μL aliquot of NO(g) (17 equiv per total Cu(II) added) was bubbled through the solution via a gastight syringe inserted through the septum, the solution was vigorously shaken for 3 s, and the fluorescence response was measured (**Figure 3.10**).

3.2.7. Selectivity Studies of Organic-Soluble CMPs

3.2.7.1. Response of 1a–Cu(II) to SNAP

A 3.0 mL aliquot of a 0.63 μM solution of **1a** in 1:1:3 CH_2Cl_2/EtOH/CH_3CN was added to a quartz cuvette, which was sealed with a gas-tight Teflon-lined screw cap equipped with a septum, and the basal fluorescence spectrum was acquired. The high relative percentage of CH_3CN was selected to ensure miscibility with aqueous SNAP solution. A 16 μL aliquot of a 60 μM solution of Cu(OTf)$_2$ in 1:1:3 CH_2Cl_2/EtOH/CH_3CN, corresponding to 0.5 equiv of Cu(II) per binding unit, was added to the cuvette to form **1a**–Cu(II) and the fluorescence spectrum was acquired. To this solution was added a 30 μL aliquot of 3.15 mM SNAP(aq) (50 equiv per total Cu(II) added) via a syringe inserted through the septum, the solution was vigorously shaken for 3 s, and the fluorescence response was measured. Immediately after addition, a statistically

insignificant increase in integrated emission was observed that, after two hours, represented a 1.5-fold increase over the fluorescence of **1a**–Cu(I). When the experiment was repeated with [Cu(CH$_3$CN)$_4$]BF$_4$ in place of Cu(OTf)$_2$, no fluorescence change was observed in the presence of 50 equiv of SNAP, even after 24 h. Addition of SNAP before Cu(OTf)$_2$ yields the same 1.5-fold increase in integrated emission.

3.2.7.2. Detection Limit of 1a–Cu(II) for SNAP

A 3.0 mL aliquot of a 0.63 µM solution of **1a** in 1:1:3 CH$_2$Cl$_2$/EtOH/CH$_3$CN was added to each of two quartz cuvettes, which were sealed with gas-tight Teflon-lined screw caps equipped with septa, and the basal fluorescence spectra were acquired. A 16 µL aliquot of a 60 µM solution of Cu(OTf)$_2$ in 1:1:3 CH$_2$Cl$_2$/EtOH/CH$_3$CN, corresponding to 0.5 equiv of Cu(II) per binding unit, was added to each cuvette to form **1a**–Cu(II) and the fluorescence spectra were acquired. Addition of 0.1 equiv of SNAP to one cuvette and 0.01 equiv of SNAP to the other, ([SNAP]$_f$ = 63 and 6.3 nM, respectively) caused an increase in integrated emission by 42% and 14%, respectively.

3.2.7.3. Response of CP–Cu(II) and CP–Cu(I) to NOBF$_4$ (CP = 1–3)

A 3.0 mL aliquot of a 2.0 µM solution of CP in 1:1:3 CH$_2$Cl$_2$/EtOH/CH$_3$CN was added to each of three matched quartz cuvettes, which were sealed with gas-tight Teflon-lined screw caps equipped with septa, and the basal fluorescence spectra were acquired. One equiv of [Cu(CH$_3$CN)$_4$]BF$_4$ was added to one cuvette and 0.5 equiv of Cu(OTf)$_2$ was added to another to form the CP–Cu(I) and CP–Cu(II) complexes, respectively. A 30 µL aliquot of a 3.15 mM CH$_3$CN solution of NOBF$_4$ (25 or 50 equiv per total Cu(I) or Cu(II) added, respectively) was

subsequently added to each cuvette. None of the CP, CP–Cu(I) or CP–Cu(II) solutions exhibited a significant change in the emission spectrum. Addition of 1 equiv of $Cu(OTf)_2$ to a solution containing CP and $NOBF_4$ yielded a spectrum similar to that for CP-Cu(II), indicating that nitrosonium does not interfere with metal binding if it is present prior to metal addition.

3.2.7.4. *Response of CP–Cu(II) and CP–Cu(I) to $Na_2N_2O_3$ (CP = 1–3)*

A 3.0 mL aliquot of a 2.0 μM solution of CP in 1:1:3 CH_2Cl_2/EtOH/CH_3CN was added to each of three matched quartz cuvettes, which were sealed with gas-tight Teflon-lined screw caps equipped with septa, and the basal fluorescence spectra were acquired. One equiv of $[Cu(CH_3CN)_4]BF_4$ was added to one cuvette and 0.5 equiv of $Cu(OTf)_2$ was added to another to form the CP–Cu(I) and CP–Cu(II) complexes, respectively. A 3.0 μL aliquot of a solution of 32 mM $Na_2N_2O_3$ in 1.0 M KOH (16 or 32 equiv per total Cu(I) or Cu(II) added, respectively) followed by 30 μL of buffer (to induce decomposition of $Na_2N_2O_3$ to HNO) were added to each cuvette. The fluorescent response of each sample was then measured within 60 s of addition. No additional changes in integrated emission were noted up to 20 min.

3.2.8. *Selectivity studies of Water-Soluble CMPs*

3.2.8.1. *Response of 4a–Cu(II) to Excess $Na_2N_2O_3$ in 95:5 CH_3CN/H_2O*

A 3.0 mL aliquot of a 2.1 μM solution of 4 in 95:5 CH_3CN/H_2O was added to a quartz cuvette, which was sealed with a gas-tight Teflon-lined cap equipped with a septum, and the basal fluorescence spectrum was acquired. An 18 μL aliquot of 3.45 mM $CuSO_4 \cdot 5H_2O$(aq) was added to form the 4a–Cu(II) complex and the fluorescence spectrum was acquired. A 30 μL

aliquot of 32 mM $Na_2N_2O_3$ in 1 M KOH(aq) (15 equiv per total Cu(II) ion) was then added to the cuvette, followed by 60 μL of buffer to induce decomposition to HNO. The fluorescent response of the sample was measured within 60 s of addition and no change was observed up to 1 h (**Figure 3.8**).

3.2.8.2. *Response of 6–Cu(II) to Excess SIN-1-Cl in H₂O*

A 3.0 mL aliquot of a 7.9 μM solution of **6** in H_2O was added to a polystyrene cuvette followed by a 20 μL aliquot of 6.0 mM $CuSO_4·5H_2O$(aq) to form the **6–Cu(II)** complex. The cuvette was sealed with a gas-tight Teflon-lined cap equipped with a septum and the fluorescence spectrum was acquired. This solution was transferred to a polystyrene cuvette containing SIN-1-Cl (1.5 mg, 7.2 μmol, 60 equiv per total Cu(II) ion), the cuvette was shaken for 3 s, and the fluorescence was measured. No change in integrated emission was observed.

3.2.8.3. *Response of 6–Cu(II) to Excess Na₂N₂O₃ in Unbuffered Solution*

A 3.0 mL aliquot of a 7.9 μM solution of **6** (in 90:10 MeCN/H_2O or H_2O) was added to a polystyrene cuvette followed by a 20 μL aliquot of 6.0 mM $CuSO_4·5H_2O$(aq) to form the **6–Cu(II)** complex. The cuvette was sealed with a gas-tight Teflon-lined cap equipped with a septum and the fluorescence spectrum was acquired. This solution was transferred to a polystyrene cuvette containing $Na_2N_2O_3$ (2.4 mg, 20 μmol, 170 equiv per total Cu(II) ion), the cuvette was vigorously shaken for 3 s, and the fluorescence was measured.

3.2.8.4. *Response of 6–Cu(II) to Excess Na₂N₂O₃ in Buffered Solution*

A 3.0 mL aliquot of a 7.9 μM solution of **6** in buffer was added to a polystyrene cuvette

followed by a 100 μL aliquot of 6.0 mM $CuSO_4 \cdot 5H_2O$(aq) to form the **6–Cu(II)** complex. The cuvette was sealed with a gas-tight Teflon-lined cap equipped with a septum and the fluorescence spectrum was acquired. This solution was transferred to a polystyrene cuvette containing $Na_2N_2O_3$ (2.4 mg, 20 μmol, 33 equiv per total Cu(II) ion), the cuvette was vigorously shaken for 3 s, and the fluorescence was measured (**Figure 3.10**).

3.3. Results and Discussion

3.3.1. Design and Synthesis of 1a

To employ copper-based CMPs for the detection of NO via reductive nitrosylation, the fluorescence of the CPs must be quenched by Cu(II) with little or no quenching by Cu(I). Additionally, the metal binding unit should be able to chelate the copper in both oxidation states and the CP should be biocompatible and have good photoluminescent properties (*e.g.* high quantum yield and long emission wavelengths). Fluorescent CPs are widely known and have been applied to diverse fields ranging from sensing[37,38] to electronics.[39–41] Sensors built upon CP-based scaffolds have been used in the detection of a variety of analytes, from explosives[37,42] to prion aggregates.[43–45]

Bipyridyl-type ligands can chelate both Cu(I) and Cu(II), and the resultant complexes can be highly kinetically inert. There are several examples of CPs incorporating bipyridyls as metal binding units and these have been successfully used as sensors.[46–51] One of the CP scaffolds previously investigated matched our criteria perfectly: these polymers were composed of 2,2'-bipyridyl units embedded within a poly(*p*-phenylene vinylene) (PPV) chain and exhibited emission wavelengths above 500 nm.[52] For enhanced solubility in organic solvents, *n*-

dodecyloxy side-chains were emplaced on the PPV spacers.

Furthermore, these CPs showed the desired fluorescence response to Cu(I) and Cu(II) ions. Addition of Cu(OAc)$_2$ to a solution of this CP in CHCl$_3$ afforded near-total quenching of fluorescence, whereas addition of Cu(OAc) yielded only a moderate decrease in the integrated emission. Detailed mechanistic studies of a related poly(p-phenylene ethynylene) (PPE) CP revealed that formation of 2:1 bipyridyl-copper(I) linkages caused quenching of emission via formation of coordinative cross-links.[48] Studies of related CPs have shown that bipyridyl-based systems are maximally quenched with 0.5 equiv of Cu(II) or Cu(I). The ability of open-shell metal ions to quench fluorescence is well-known, but Cu(I) is a d^{10} ion with no unpaired electrons. Instead, coordinatively cross-linked polymer chains may increase the nonradiative decay rate by promoting the self-annihilation of singlet excitons.[53] Because the coordination chemistry and photoluminescent properties of the CP–Cu(I) and CP–Cu(II) complexes were known, we selected this scaffold as the foundation for our CMP-based NO sensors.
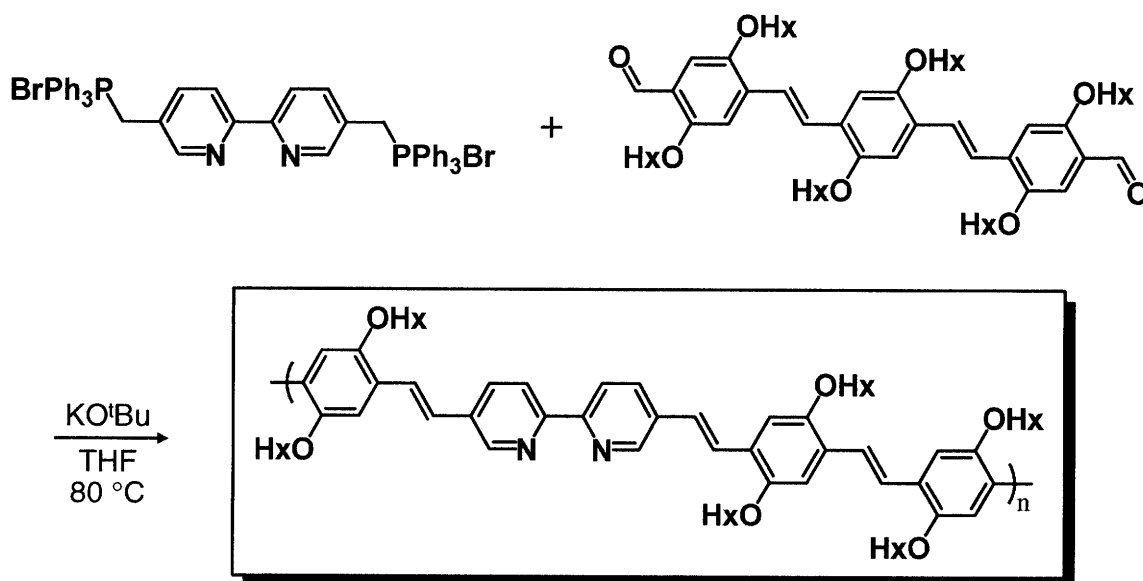
Scheme 3.2. Synthesis of **1a**.

Because reductive nitrosylation requires an NO^+ acceptor and the bipyridyl-PPV scaffold has no functional groups suited to this purpose, all measurements would need to be performed in protic solution. For the proton source, we desired the least polar alcohol possible that would still provide a kinetic driving force for the reaction. Both MeONO and EtONO are gases at room temperature, but EtOH is less polar than MeOH. Consequently, we selected 4:1 CH_2Cl_2/EtOH as the solvent for our fluorescence measurements.

By minor modification of the monomer syntheses and subsequent copolymerization conditions for the previously reported bipyridyl-PPV system, we could prepare the *n*-hexyloxy variant **1a** in excellent yield via Wittig condensation (**Scheme 3.2**). This CP exhibited desirable photoluminescent properties, where $\lambda_{max} = 462$ nm ($\varepsilon = 4.4 \times 10^4$ $M^{-1}cm^{-1}$) and $\lambda_{em} = 540$ nm ($\Phi = 0.30 \pm 0.05$, **Table 3.1**). Both excitation and emission occur at suitably long wavelengths, and the quantum yield for **1a** was reasonably high. Other CPs based on the bipyridyl-PPV scaffold have quantum yields ranging from 0.47 to 0.57.[54,55] For PPV-type CPs in general, the observed range widens appreciably ($\Phi = 0.0019 - 1.00$).[37,56–61]
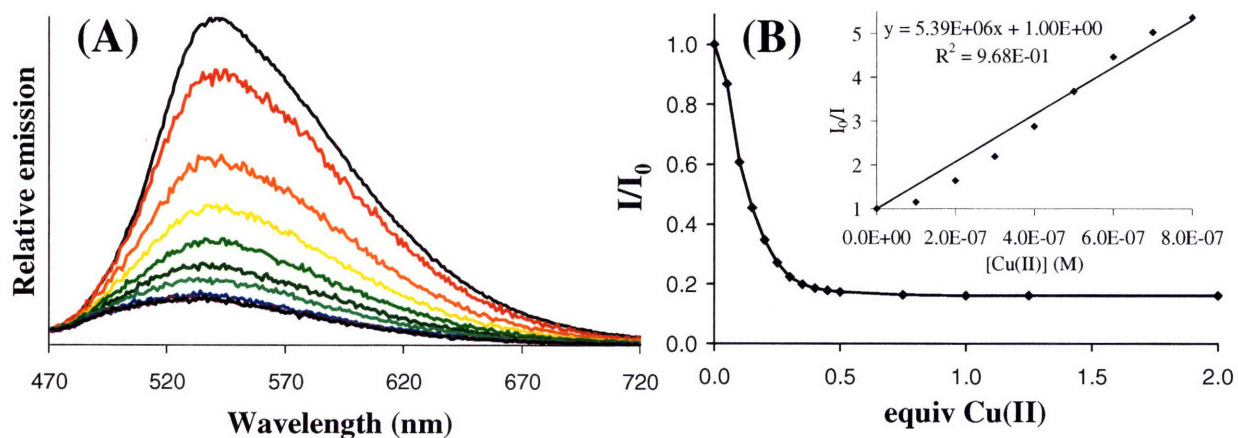
Figure 3.1. Titration of **1a** with Cu(OTf)$_2$ in 4:1 CH$_2$Cl$_2$. (**A**) Fluorescence traces from the titration of **1a** (top to bottom, 0 to 0.50 equiv of Cu(II) in increments of 0.05 equiv). (**B**) Plot of integrated emission vs. equiv of Cu(II) and Stern-Volmer plot (inset).

79

3.3.2. Response of 1a to Metal Ions

Titration of **1a** with $Cu(OTf)_2$ revealed a linear decrease in fluorescence (K_{SV} = 5.39 ×

10^6) that maximized with 0.5 equiv of Cu(II) per bipyridyl unit (**Figure 3.1** and **Table 3.1**).

Addition of Cu(II) beyond this stoichiometry afforded no change in the integrated emission,

consistent with the photoluminescent response of other main-chain bipyridyl-based CPs to

Cu(II).[46] Although there are several studies of the quenching effects of metal ions on main-chain

bipyridyl-based CPs, few report the Stern-Volmer quenching constants. For a main-chain

bipyridyl-fluorene copolymer, the K_{SV} for Cu(II) is 1.22 × 10^7, whereby the greater quenching

efficiency reflects a different electronic interaction between spacer and metal binding unit.[49] A

related CP with a side-chain bipyridyl unit instead of main-chain displayed comparable

quenching efficiency (K_{SV} = 7.67 × 10^6). Similarly, titration of **1a** with Cu(OAc) showed a

maximum 30% quenching of emission from 0.5 equiv to 10 equiv. A PPE-based analog of **1a**

showed more dramatic quenching (> 10-fold) with $[Cu(CH_3CN)_4](PF_6)$ but still maximized with

0.5 equiv of Cu(I) per bipyridyl unit.[48]

Table 3.1. Photoluminescent properties and analyte response of organic-soluble CPs in 4:1 $CH_2Cl_2/EtOH$.

	$\lambda_{\pi\rightarrow\pi^*}$ (nm)	$\varepsilon \times 10^{-4}$ $(M^{-1}cm^{-1})$	λ_{em} (nm)	Φ_{eff}	$K_{SV} \times 10^{-5}$ (M^{-1})	$\int_{Cu(II)} \div \int_0$ [a]	$\int_{NO} \div \int_{Cu(II)}$ [b]
1a	462	4.25	540	0.30	53.9	16 %	2.8
1b	379	3.72	435	0.41	3.54	1.7 %	2.8
1c	400	2.34	481	0.44	51.1	0.32 %	2.8
2b	329	9.55	415	0.17	9.51	25 %	1.9
2c	389	4.27	460	0.27	1.53	3.6 %	0.5
3a	328	2.16	462	0.018	38.4	24 %	1.3
3b	331	1.97	416	0.055	6.07	11 %	1.9
3c	329	1.14	474	0.058	23.2	4.5 %	1.4

[a] Ratio of integrated emission from CP–Cu(II) to that from CP alone. [b] Ratio of integrated emission from CP–Cu(II) + NO(g) reaction to that from CP–Cu(II).
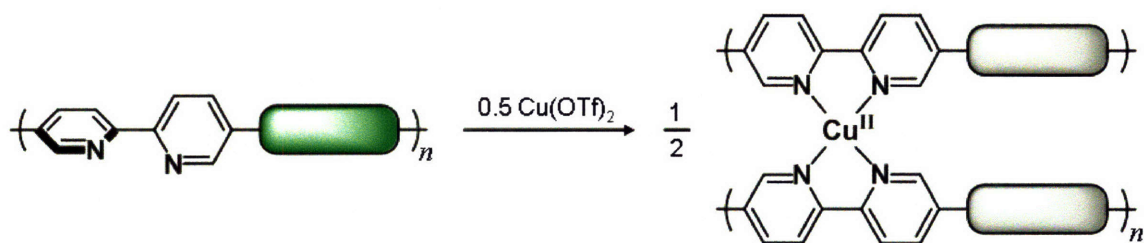
Scheme 3.3. Proposed mechanism of copper(II)-induced quenching of **1a**.

3.3.3. Response of **1a**–Cu(II) to NO(g)

Addition of 300 equiv of NO(g) to **1a**–Cu(II) yielded an immediate 2.8-fold increase in integrated emission and the resultant spectrum was indistinguishable from that of **1a**–Cu(I) (**Figure 3.2**). When this reaction was performed in pure CH_2Cl_2 or with **1a** or **1a**–Cu(I) in 4:1 CH_2Cl_2/EtOH, no change in the fluorescence spectra were observed. These results suggest that the fluorescence increase can only occur in the presence of an electron acceptor and a protic solvent.
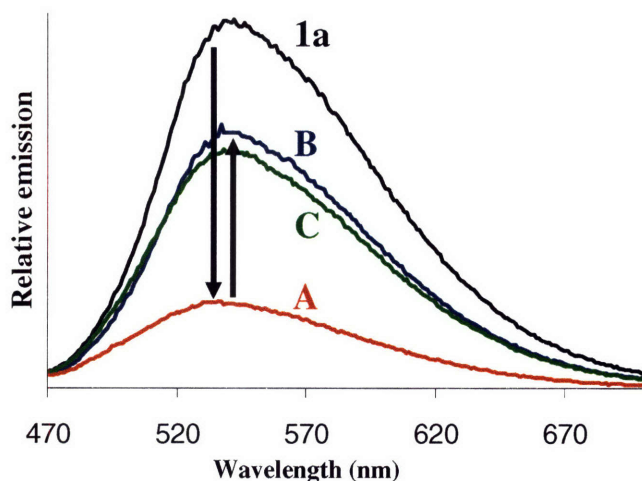
Figure 3.2. Response of **1a**–Cu(II) to NO(g) in 4:1 CH_2Cl_2. Upon treatment of **1a** (black trace) with 0.5 equiv of Cu(OTf)$_2$, **1a**–Cu(II) is formed and an 85% decrease in integrated emission occurs (**A**, red trace). Reaction with NO affords a 2.8-fold restoration of fluorescence (**B**, blue trace). This fluorescence spectrum is nearly identical to that for **1a**–Cu(I) (**C**, green trace)

3.3.4. Mechanistic Insight for 1a

To probe the mechanism giving rise to this fluorescence increase in greater detail, we performed a series of controls. Because NO transfers an electron to Cu(II) to form NO^+ and Cu(I) during reductive nitrosylation, the emission spectrum for the reaction of 1a–Cu(II) + NO(g) should match the spectrum for the reaction of 1a–Cu(I) with $NOBF_4$. Addition of $NOBF_4$ to a solution of 1a–Cu(I) yielded no change in integrated emission and the resultant spectrum was identical to the spectrum obtained for the reaction of 1a–Cu(II) with NO(g).

To complement the fluorescence measurements, we monitored the reaction of 1a–Cu(II) + NO(g) by EPR spectroscopy. To a solution of 1a in 4:1 CH_2Cl_2/EtOH was added 1.0 equiv of $Cu(OTf)_2$, rather than the typical 0.5 equiv; this modified procedure was adopted so that 50% of the Cu(II) would be bound to 1a and the other 50% would be free in solution. Addition of 1 equiv of NO(g) (relative to total Cu(II) added) caused a decrease in the integrated EPR signal intensity by 45%. Because the total Cu(II)-based EPR signal decreased by only one-half in the presence of sufficient NO(g) to reduce all the Cu(II), we concluded that only the Cu(II) bound to 1a is reduced. Furthermore, this result demonstrates that the resultant Cu(I) remains bound to 1a. If the Cu(I) were released, the remaining 0.5 equiv of Cu(II) would bind to 1a, then the remaining 0.5 equiv of NO(g) would reduce that to Cu(I), yielding a net 100% decrease in integrated EPR signal.

An intermediate/transition state that has been invoked in previous studies of copper(II)-based NO sensors is a copper nitrosyl. Our attempts to observe metal nitrosyl species via solution IR have failed because 1a is insufficiently soluble at the necessary concentrations (> 20 mM). Kinetic analysis of the reaction of copper(II) with a similar primary coordination sphere, $[Cu(dmp)_2]^{2+}$ (dmp = 2,9-dimethyl-1,10-phenanthroline), with NO(g) suggests that the first step

in its reductive nitrosylation is formation of $[Cu(NO)(dmp)_2]^{2+}$.[62] Additionally, $[Cu(Me_2bpy)_2]^{2+}$

(Me_2bpy = 5,5'-dimethyl-2,2'-bipyridine) complexes can readily bind additional small ligands,

such as halide or formate, without displacement of a bipyridyl ligand.[63] Furthermore, copper-

nitrosyl complexes supported by tris(pyrazolyl)borate-type ligands have been structurally

characterized.[64-67] These other studies suggest that it would be possible for NO to coordinate to

one of the $[Cu(bpy)_2]^{2+}$ units in **1a–Cu(II)**, then reduce the metal to Cu(I) with the NO^+ fragment

being trapped by ethanol (**Scheme 3.4**).

Although the combination of the fluorescence and EPR measurements offer compelling

evidence that **1a–Cu(II)** detects NO via reductive nitrosylation, detailed mechanistic studies

require non-macromolecular substrates. Subsequent work on small-molecule copper complexes

by us[22,23] and others[62] have demonstrated the validity of the proposed mechanism.
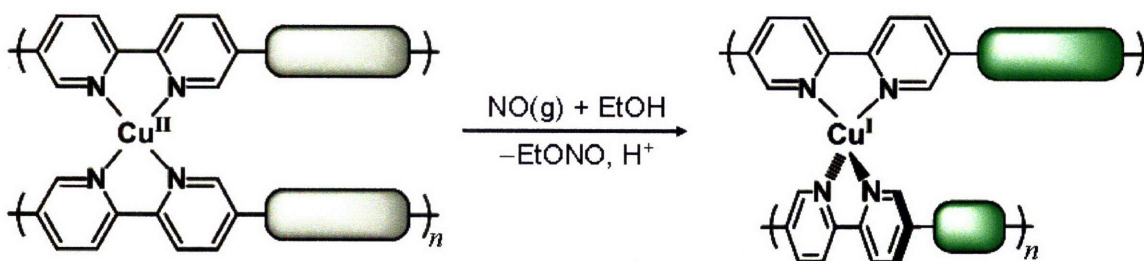
Scheme 3.4. Proposed mechanism for NO-induced restoration of emission from **1a–Cu(II)** in 4:1 CH_2Cl_2/EtOH

3.3.5. Selectivity Studies for **1a** and **1a–Cu(II)**

3.3.5.1. Response to SNAP

Biological systems contain a variety of reactive nitrogen and oxygen species in addition

to NO, thus a sensor for the detection of NO *in vivo* should be selective for NO(g) over

potentially-interfering analytes. Nitrosothiols are believed to be the major carriers and donors of NO in biology, performing a range of functions from simple NO release to protein and gene regulation.[68–73] We selected SNAP as our NO donor because it is commercially available, it is frequently used in biological NO experiments, it is minimally toxic, and its optical characteristics are well-studied.

Addition of 50 equiv of SNAP to 1a–Cu(II) in 1:1:3 CH_2Cl_2/EtOH/CH_3CN caused a gradual 1.5-fold increase in integrated emission over 2 h. This new solvent system was selected to ensure solubility of SNAP and to meet the necessary conditions for reductive nitrosylation. Presumably, the delayed response to SNAP is a result of NO release from RSNO by thermal decomposition that is very slow in the absence of transition metals in solution.[74–77] Addition of SNAP to 1a alone or 1a–Cu(I) did not affect the emission spectrum; however, subsequent addition of Cu(II) caused an immediate quenching to the same level as 1a–Cu(II) followed by a gradual increase to a 1.5-fold restoration. These observations demonstrate that the turn-on response by SNAP is not the result of CMP demetallation. For both the 1a + Cu(II) + SNAP and 1a + SNAP + Cu(II) experiments, the full NO-induced turn-on (2.1-fold) was not observed until 24 h after addition. Because the response of 1a–Cu(II) to SNAP is much slower than to NO(g), this CMP-based sensor should be able to distinguish between these two analytes on sufficiently short timescales.

One advantage to using SNAP as the source of NO instead of NO(g) is that stoichiometry is much easier to control. Although the nitrosothiol experiments will take longer than the NO(g) experiments and must be performed in a different solvent, the ability to weigh out SNAP, prepare serial dilutions, and add aliquots allow for the quantitative determination of the CMP sensitivity threshold for NO. Numerous measurements of NIST-issued quinine bisulfate as our

emission standard have shown that our instrumental error is ± 5%. Thus, for a response to be statistically significant, the difference between the pre- and post-addition integrated emission values must be greater than 10%. Exposure of **1a**–Cu(II) in 1:1:3 CH_2Cl_2/EtOH/CH_3CN to successively more dilute solutions of SNAP revealed the sensitivity limit for this CMP was 6.3 nM SNAP (corresponding to a 12% increase).

The mechanism of NO donation from nitrosothiols, delivered as NO or NO^+, remains unclear and is disputed.[78–83] Because the NO(g) measurements already demonstrated the response of the CMP to NO, we sought to determine the response of our system to $NOBF_4$. Addition of 50 equiv of $NOBF_4$ to **1a**, **1a**–Cu(II) and **1a**–Cu(I) afforded no change in the fluorescence spectra. Similarly, the spectrum for **1a** + $NOBF_4$ + Cu(II) was indistinguishable from the spectrum for **1a** + Cu(II) + $NOBF_4$, indicating that NO^+ does not interfere with copper binding.

3.3.5.2. Response to $Na_2N_2O_3$

Nitroxyl is related to NO by one-electron reduction followed by protonation, and HNO has been implicated in several biological processes ranging from regulation of vassal tone to DNA damage.[84,85] Furthermore, HNO may even have functions orthogonal to those of NO. Because these two species may have discrete roles, a sensor for NO must be able to distinguish between the two. Unfortunately, addition of 50 equiv of $Na_2N_2O_3$ to **1a**–Cu(II) afforded an emission spectrum nearly identical to the spectra for **1a**–Cu(I) and the reaction of **1a**–Cu(II) + NO(g). Presumably, this response to $Na_2N_2O_3$ also occurs via reduction of Cu(II) to Cu(I). Because there is no change in the fluorescence of **1a**–Cu(I) upon addition of $Na_2N_2O_3$, we can exclude formation of Cu(0). Furthermore, Cu(0) would precipitate and the resultant spectrum

would resemble that of **1a** alone with markedly increased Rayleigh scattering. The integrated emission of **1a** is unchanged upon treatment with $Na_2N_2O_3$, demonstrating that the fluorescence response is not an artifact of chemical modification of the CP.

3.3.6. Summary of Results for 1a

To the best of our knowledge, **1a** represented the first example of a fluorescent NO sensor employing a CP-based scaffold. This system was able to detect concentrations of NO as low as 6.3 nM and could distinguish between NO(g) and SNAP. Unfortunately, $Na_2N_2O_3$ also afforded a turn-on fluorescence response, indicating that this CMP would be unable to distinguish between HNO and NO. Having demonstrated the utility of a CMP scaffold as the foundation for an NO sensor, we sought a better understanding of how the chemical nature of the polymer (*i.e.* metal binding unit, spacers, side-chains) influences photoluminescence, copper quenching efficiency, and NO response and set out to prepare a family of CPs for this purpose.

3.3.7. Design and Synthesis of Organic-Soluble CPs

A CMP is composed of two monomer types: those containing metals and those that do not. As the redox potentials of these monomers become more similar, the effective conjugation length within the polymer will be greater.[86] The photoluminescent properties of such a CP will be more sensitive to metal binding than a CP with poor redox matching and will thus exhibit better copper(II)-induced quenching. Because the mechanism of NO sensing by a copper(II)-based CMP involves restoration from this quenched state by reductive nitrosylation, the more-efficiently quenched CP will offer better contrast between the 'off' and 'on' states. Thus, we were interested in probing the interaction between the metal binding units and the spacers to

determine the optimum combination for maximum quenching efficiency and best contrast.
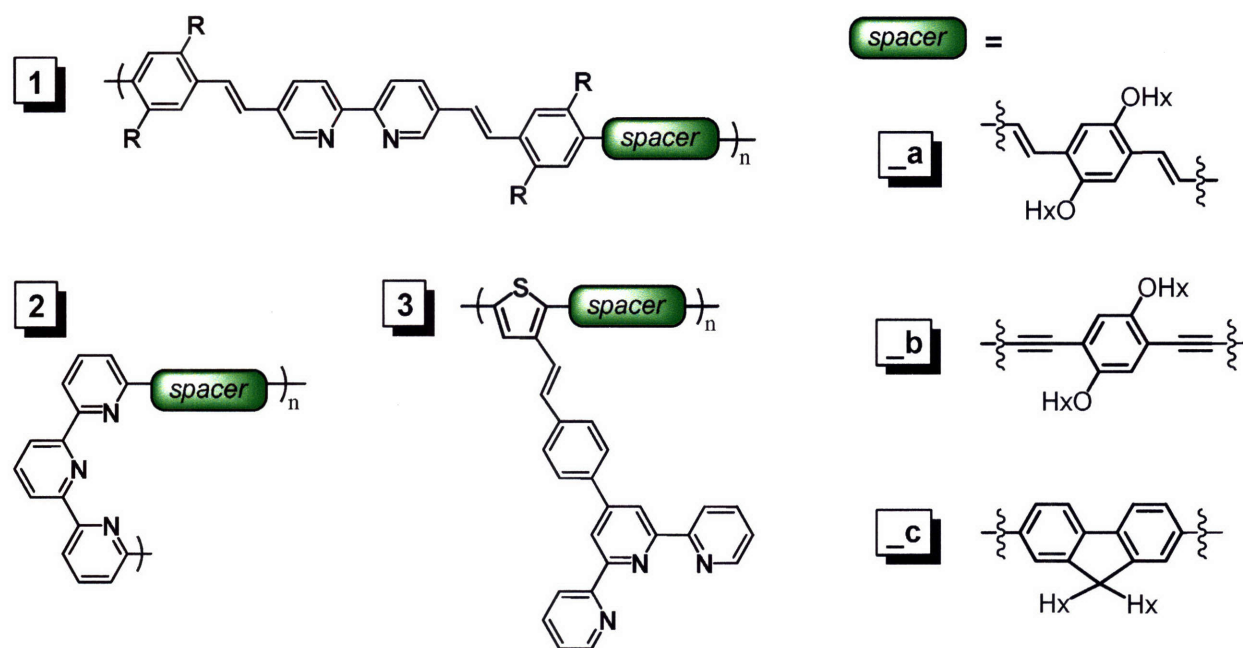
Chart 3.1. Organic-soluble CPs. For **1a**, R = OHx. For all other organic-soluble CPs, R = H.

To this end, we sought to prepare a family of CPs comprising 2,2'-bipyridyl units connected to the main-chain in the 5,5' positions (**1**), 6,6''-terpyridyl units connected to the main-chain in the 2,2''-positions (**2**), and 6,6'-terpyridyl units as side-chains of the main-chain (**3**) along with *p*-phenylene vinylene (PPV, **_a**), *p*-phenylene ethynylene (PPE, **_b**) and fluorene (**_c**) spacers (**Chart 3.1**). Studies of polymers containing pyridyl- or oligopyridyl-units in the main chains have revealed these CPs are efficiently quenched by a variety of metal ions.[48–50,52,87–89] Systems featuring bipyridyl- and terpyridyl-type side-chains attached to main-chain thiophene units also exhibit fluorescence quenching by metal ions, including Cu(II).[90] Because metal ion binding and redox changes thereof will cause perturbations in the inter/intrachain interactions,[91] CPs based on bipyridyl and terpyridyl scaffolds should display a rich variety of emissive

responses to metal ions and redox active analytes, two characteristics necessary for an NO sensor. Furthermore, CPs incorporating PPE-, polyfluorene-, and polythiophene-type spacers have been used in a variety of biosensing applications: PPE-based CPs have been used to detect protease activity,[92] fluorene-based CPs have been used for sensing DNA,[93] and thiophene-based CPs can selectively report amyloid fibrilliar insulin over native-folded protein.[94]
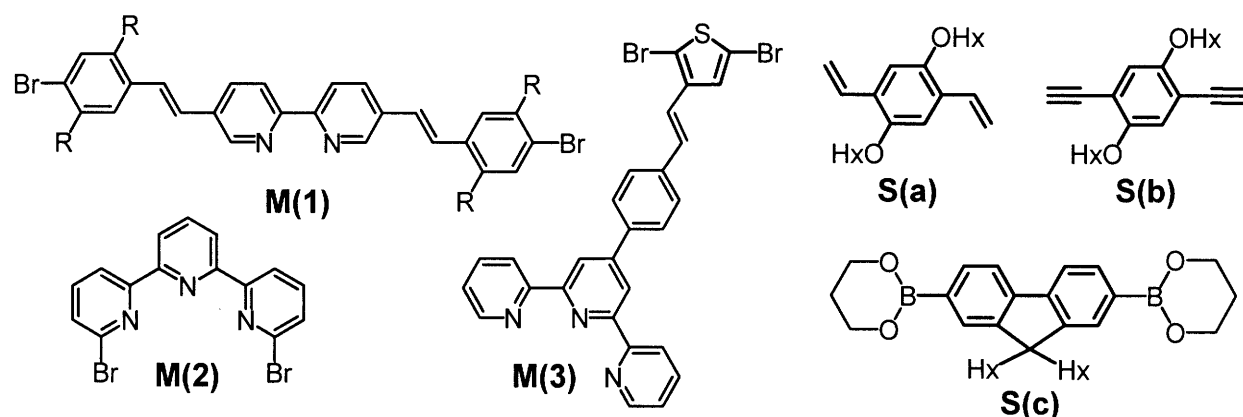
Chart 3.2. Monomers used in the syntheses of organic-soluble CPs.

Conjugated polymer **3a** was prepared via Heck coupling of **M(3)** and **S(a)**, but attempts to prepare **2a** by this route failed to produce sufficiently high molecular weight material for subsequent investigations, one of the limitations inherent to Heck coupling-based CP synthesis (**Chart 3.2**).[95,96] Sonogashira coupling of **M(1)**–**M(3)** with **S(b)** afforded the PPE-based CPs **1b**, **2b** and **3b**. Alternatively, reaction of **S(c)** with the same metal binding unit precursors via Suzuki coupling yielded the polyfluorene-based CPs **1c**, **2c** and **3c**. Unfortunately, few of these CPs showed suitable photoluminescent properties (**Table 3.1**). For example, **2b** and the side-chain terpyridyl-based **3** had excitation wavelengths at 330 nm or less; because biological milieu contains many absorbing species below 350 nm,[97] these CPs cannot be adapted for use *in vivo*.

Worse yet, **3** exhibited quantum yields < 6%. Presumably, the poor photoluminescent properties or **2b** and **3** are due to short conjugation lengths (*e.g.* the fluorescence of **3** arises mainly from the terpyridyl-thiophene unit). Overall, the quantum yields measured for **1–3** are in the middle to low-end of the range of those reported for similar systems. Quantum yields range from 0.0006 to 1.00 for CPs with *p*-phenylene ethynylene-based spacers,[60,92,98–105] from 0.01 to 1.00 for CPs with fluorene-based spacers,[93,106–110] and from 0.04 to 0.70 for CPs with thiophene-based spacers.[98,106,111,112]

3.3.8. Quenching of Organic-Soluble CPs by Cu(II)

3.3.8.1. Dependence on Metal Binding Unit

All CPs investigated were quenched efficiently by Cu(II), with Stern-Volmer constants ranging from 1.5×10^5 to 5.4×10^6 M^{-1} (**Table 3.1**). The main-chain terpyridyl-based **2** displayed the least efficient average quenching (5.52×10^5) that was incomplete even in the presence of 1 equiv of Cu(II). Because κ^3 binding to one metal center would introduce a horseshoe kink in the polymer chain and cause significant intrachain steric congestion, we believe a mixture of κ^1 and κ^2 terpyridyl conformations is preferred, with the remainder of the Cu(II) coordination sphere filled by the formation of interchain cross-links. This mixture of Cu(II) coordination environments would give rise to the poor quenching efficiency and the need for > 1 equiv of Cu(II) per terpyridyl unit for maximum quenching. Conjugated polymers **1** and **3** exhibited much better quenching efficiencies, whereby the average K_{SV} for **1** was greater than that for **3** (3.62×10^6 vs. 2.26×10^6), consistent with the 2:1 and 1:1 ligand/metal binding ratios, respectively. As has been previously demonstrated, the 2:1 bipyridyl/copper(II) binding mode

involves interchain cross-links.[48] Terpyridyl-copper(II) binding modes can include 1:1 and 2:1 metal-ligand complexes,[113] as well as 2:2 complexes in which each metal is coordinated by one κ^2 and one κ^1 terpyridyl ligand in the same manner as is proposed for 2–Cu(II).[114]

Additionally, the difference *between* CP classes (*e.g.* main-chain bipyridyl vs. main-chain terpyridyl) can be explained by redox matching. The metal binding units in **1** are embedded within the CP main-chain, whereas the metal binding units in **3** are attached as side-chains to the CP main-chain. Thus, there will be better electronic communication between the metal binding units and the CP main-chain in **1** than the metal binding units and the CP main-chain in **3**. As a result, coordination of Cu(II) to the metal binding units in **1** will perturb the main-chain emission more significantly than it would for **3**. The observed average K_{SV} value for **1** is greater than for **3**.

3.3.8.2. Dependence on Spacer

Within each polymer type, a correlation between spacer type and quenching efficiency was noted. For example, **1b** and **3b** had the worst quenching efficiencies of main-chain bipyridyl-based **1** and side-chain terpyridyl-based **3**, respectively. Similarly, these PPE-based CPs display the shortest emission wavelengths of their classes by nearly 50 nm. We believe this inefficient quenching and relatively blue fluorescence can be explained by a poor redox match between the metal binding units and PPE-type spacers. A poor match would give rise to a short effective conjugation length and thus shorter emission wavelengths. Furthermore, because these CPs would be composed of multiple discrete fluorescent subunits, interaction with Cu(II) at one site would only cause quenching locally, with minimal or no quenching at distant sites. Alternating copolymers of electron-rich and -deficient monomers exhibit energy mismatches at the interfacial regions and attendant short conjugation lengths.[115] Of the three types within each

class of CP, the PPE-type spacers are the most electron releasing to the π-conjugated main-chain.

For the main-chain bipyridyl **1** and side-chain terpyridyl **3**, the PPV-type (**a**) was quenched more efficiently by than the polyfluorene-type (**c**) These trends can also be understood in the context of redox matching: a fluorene-based spacer is less electron-releasing than a divinyl-bisalkoxyarene-based spacer and a metal binding unit is more electron-releasing than its copper(II) complex. Thus, the bipyridyl- and thiophene-PPV combinations in **1a** and **3a** will exhibit better matching redox potentials. As the redox match between the metal binding unit and spacer improves, the increased conjugation length will correlate to a greater sensitivity to metal binding and, thus, greater quenching efficiency. This hypothesis is borne out by the measured quenching efficiencies, with **1a** > **1c** and **3a** > **3c**.

3.3.9. Response of Organic-Soluble CMPs to NO(g)

Addition of excess NO(g) to CP–Cu(II) in 4:1 CH_2Cl_2/EtOH yielded an increase in integrated emission of 30% to 180% for all CPs except **2c**, which showed a 50% *decrease* (**Table 3.1**). Because this decrease is accompanied by an increase in Rayleigh scattering, we believe that the resultant **2c**–Cu(I) complex precipitates upon formation. If demetallation were occurring, the Rayleigh scattering could increase, but the resulting emission spectrum would match that of **2c**.

Although the different spacer types of **1** exhibited varied Cu(II) quenching efficiencies of **1**, all the **1**–Cu(II) complexes displayed the same relative NO-induced fluorescence response. The CP–Cu(II) complexes of **2b** and **3** exhibited intermediate restoration of fluorescence upon reaction with NO, with increases ranging from 30% to 90%. Presumably, the similarity of the **1**–Cu(II) response arises from the similar quenching efficiencies of Cu(I) relative to Cu(II) for

each spacer type within **1**. Although we were surprised by these results, such similarities are possible if the interchain reorganizations upon reduction of the CMP are similar for the three spacer types. Because bipyridyl-based ligands can form stable 2:1 complexes with both Cu(II) and Cu(I), the interchain interactions for CMPs based on **1** will be dominated by the preferred coordination geometry of the bridging metal, which, in turn, will be controlled by its oxidation state. Consequently, the reduction of **1**–Cu(II) to **1**–Cu(I) will cause the same type of rearrangement and thus the same *relative* change in emission. As was previously observed for **1a**–Cu(II), the spectra for the reaction of **1**–Cu(II) with NO(g) matched the spectra for **1**–Cu(I).

3.3.10. Selectivity studies for Organic-Soluble CMPs

None of the CPs or complexes thereof with Cu(II) or Cu(I) exhibited a change in integrated emission in 4:1 CH_2Cl_2/EtOH upon addition of $NOBF_4$. Conversely, addition of Cu(II) to a solution of CP and $NOBF_4$ afforded a fluorescence spectrum identical to that for CP–Cu(II), indicating that NO^+ does not interfere with metal binding. As observed for **1a**–Cu(II), addition of $Na_2N_2O_3$ to solutions of **1b**–Cu(II) and **1c**–Cu(II) resulted in restorations of emission that matched those observed in the NO(g) reactions.

3.3.11. Summary of Results for Organic-Soluble CPs

Our investigations into the dependence of CP photoluminescence and analyte response on the nature of the metal binding unit and spacers have provided valuable insights. We determined that the most efficient Cu(II)-induced quenching occurred with CPs containing main-chain bipyridyls (*i.e.* **1**). Furthermore, this class of polymer displayed the best NO-induced restoration of emission. Interestingly, PPV-type **1a** exhibited the most efficient Cu(II)-induced quenching

and the CP–Cu(II) complexes of **1** displayed the greatest NO-induced restoration of emission. Although the side-chain terpyridyl-based **3** demonstrated good quenching with Cu(II) and response to NO(g), its quantum yields and short excitation wavelengths preclude use in biosensing applications. Ironically, our systematic study revealed that **1a**, our *first* choice of CP, was the best suited for adaptation to NO biosensing applications.
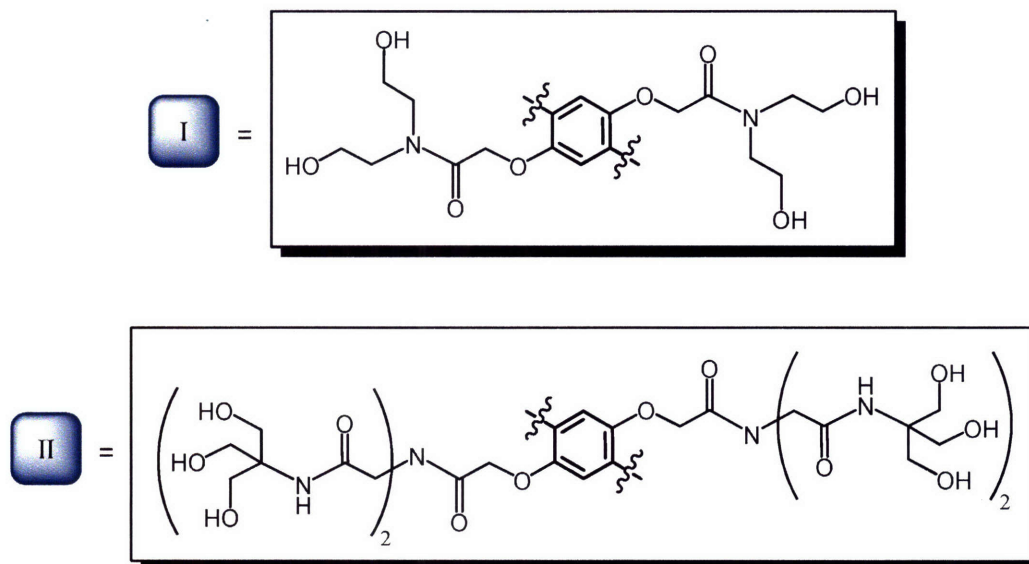
Chart 3.3. Polyol-based water-solubilizing side-chain functionalized PPE-type spacers.

3.3.12. *Design and Synthesis of Water-Soluble CPs*

An enormous advantage to constructing a sensor on a CP-based scaffold is the inherent structural modularity. A previously reported and characterized CP can be adapted to various applications by simply changing the combination of monomers used in the polymerization step. In our case, we sought to prepare a water-soluble analog of **1a** that could be used for the detection of NO in aqueous solution.

Because CPs are modular in nature, one of the easiest ways to alter the solubility

properties of the polymer is to incorporate side-chains that will enhance solubility in the solvent of interest. For aqueous solubility, some of the most commonly employed side-chains have been those containing sulfonate and alkylammonium groups. However, ionic side-chains such as these can lead to nonspecific biological interactions[116] that can cause polymer aggregation and obfuscate analyte detection.

To avoid these limitations, there has been interest in the development of non-ionic, water-solubilizing side-chains. Another advantage is that CPs bearing these side-chains will be exhibit photoluminescent properties that are less dependent on solution pH and ionic strength.[117] Polyols have been successfully employed to confer water solubility on CPs for a range of biological applications (**Chart 3.3**).[38,117–120] Using similar side-chains, a CP-based NO sensor could be able to enter a cell and image the subcellular distribution of NO under normal and disease states.

	MBU	x	y	z
4a	1	0.40	0.50	0.10
4b	1	0.20	0.50	0.30
5	5	0.25	0.50	0.25
6	6	0.25	0.50	0.25
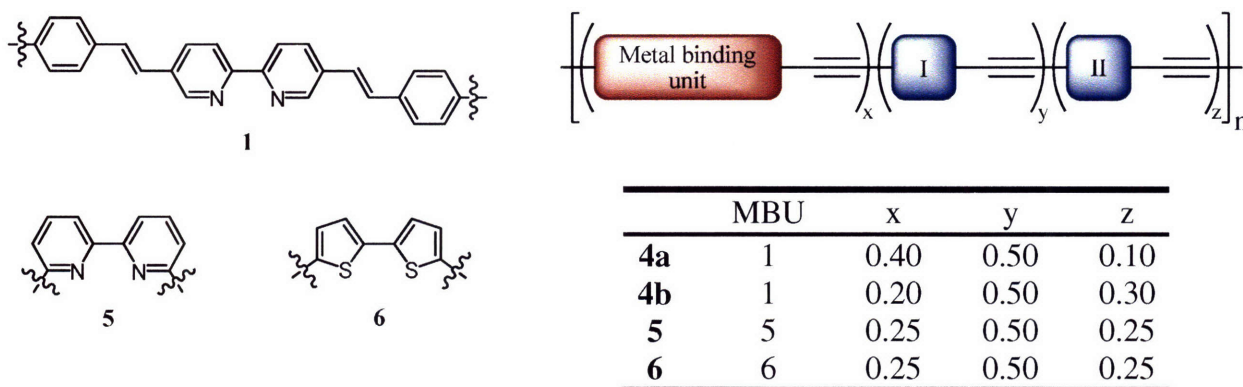
Chart 3.4. Water-soluble CPs and relative composition by metal binding unit (MBU) and water-solubilizing spacers I and II (see **Chart 3.3**).

We have demonstrated that a CP comprising bipyridyl-based metal binding units in the main-chain and PPV-type spacers has the best combination of emission wavelength, quantum yield, copper(II) quenching efficiency and response to NO(g). Unfortunately, variants of the

PPV-type spacer with polyol groups would be incompatible with the Wittig coupling conditions used in the polymerization of **1a**, and Heck coupling does not afford sufficiently high molecular weight CPs. However, PPE-type spacers bearing polyol side-chains are known and have been successfully included in CPs,[117] but emplacing spacers with polyol side-chains close to the metal binding units could diminish their binding affinities and thus quenching efficiencies. As a compromise solution, we opted to employ a mixed PPV-PPE system, whereby each metal binding unit would be flanked by unfunctionalized PPV-type spacers and the remainder of the CP main-chain would incorporate PPE-type spacers bearing the polyol-based water-solubilizing side-chains (*i.e.* a water-soluble analog of **1b**). To test our concerns about polyol side-chain proximity to metal binding unit, we also sought to prepare a CP incorporating the same 2,2'-bipyridyl metal binding unit, but with the main-chain attached to the 6,6'-positions and composed entirely of PPE-type spacers: this configuration should cause maximum interference between the polyol side-chains and the metal binding unit.
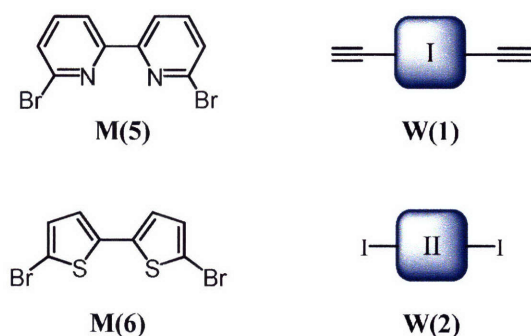
Chart 3.5. Monomers used in the syntheses of water-soluble CPs.

The water-soluble analog of **1b** (**4**) or 6,6'-bipyridyl-functionalized **5** could be prepared via Sonogashira-type coupling of polyol-functionalized diethynylarene **W(1)** and diiodoarene **W(2)** with metal binding units **M(1)** or **M(5)**, respectively (**Chart 3.4** and **3.5**). These CPs were

readily soluble in polar solvents such as 95:5 CH_3CN/H_2O or pure water and exhibited reasonable emission wavelengths (455 nm) and absorptivities (1.4×10^4 to 3.9×10^4 $M^{-1}cm^{-1}$, (**Table 3.2** and **3.3**). Unfortunately, the excitation wavelengths were at the low end of the desirable region (415 nm for **4** and 381 nm for **5**) and the quantum yields were less than 3% for **4** and less than 1% for **5**.
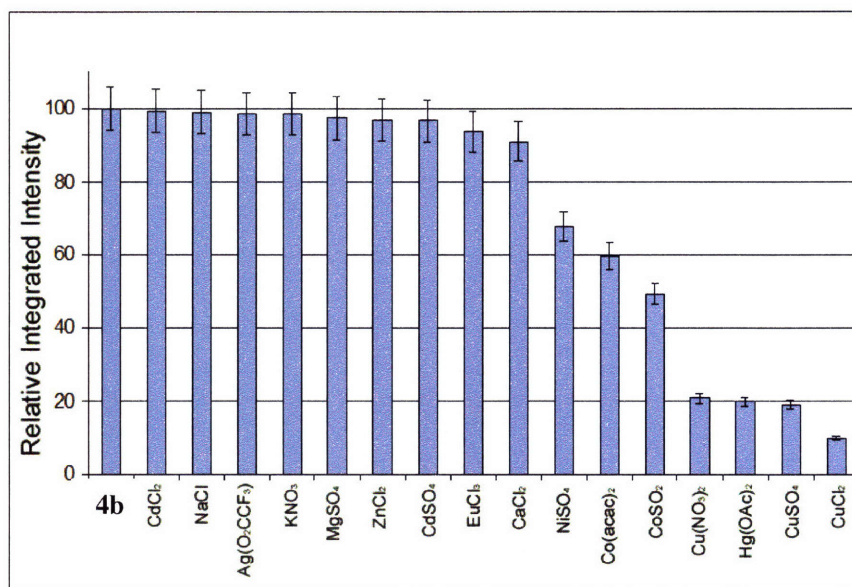
Figure 3.3. Response of **4b** to metal ions in pure water.

3.3.13. Response of Water-Soluble CPs to Metal Ions

To determine whether other metals could interfere with the emissive response of the water-soluble CPs, we screened a variety of inorganic compounds with **4b** (**Figure 3.3**). No statistically significant changes in emission were observed for the Group 1, 2 and 12 metals, as well as Ag(I) and Eu(III). Moderate quenching (30–50%) by Ni(II) and Co(II) and substantial quenching (>80%) by Hg(II) and Cu(II) were observed. Based on these results, we continued to use Cu(II) as the quenching metal for our CMP-based sensors.

After determining the relative quenching efficiency of Cu(II) compared to other metal ions, we sought to quantify it via Stern-Volmer plots (for **4b** see **Figure 3.4**). Although **4** is derived from **1**, its average quenching efficiency by Cu(II) in pure water was nearly two orders of magnitude worse (8.1×104 vs. 3.2×10^6, **Table 3.3**). The observed ratio of the K_{SV} values for **4a** and **4b** (2.1:1) matched the relative loading of metal binding units within these CPs (0.4:0.2). As expected, **5** containing water-solubilizing spacers immediately adjacent to the metal binding unit exhibited the worst Cu(II) quenching efficiency of the polymers investigated. Performing the quencher titrations of **4** and **5** in 95:5 CH_3CN/H_2O instead of water afforded Stern-Volmer constants that were, on average, nearly three times greater (1.6×10^5 vs. 6.0×10^4, **Table 3.2**).
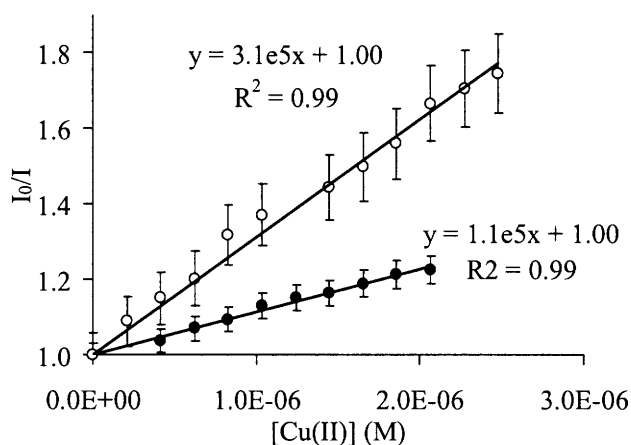
Figure 3.4. Titration of **4b** with $CuSO_4$ in 95:5 CH_3CN/H_2O ($\circ$) and pure water ($\bullet$).

Although photoluminescent properties can be highly solvatochromic, we believe the greatly diminished Cu(II) quenching efficiency of the water-soluble vs. the organic-soluble CPs is a result of interference by the polyol functionalities. One possible cause of this interference is competitive chelation of Cu(II) by the water-solubilizing side-chains. Alternatively, the polyols

could adversely affect the interchain interactions that give rise to quenching, ranging from steric hindrance of interchain approach to formation of aggregates. Because **5** displayed the worst quenching efficiency in water, we believed this CP would display the most dramatic response to an aggregation-disruption strategy. When the titration of **5** with Cu(II) was performed in 10 mM SDS(aq) instead of pure water, the quenching efficiency was over five times greater (**Table 3.3**). Related studies have demonstrated that the use of this surfactant similarly disrupts other CP aggregates.[121] Unfortunately, we have been unable to perform any measurements in buffer due to precipitation of the resulting CP–Cu(II) complexes.

Table 3.2. Photoluminescent properties and analyte response of water-soluble CPs in 95:5 CH_3CN/H_2O.

	$\lambda_{\pi\to\pi*}$ (nm)	$\varepsilon \times 10^{-4}$ $(M^{-1}cm^{-1})$	λ_{em} (nm)	Φ_{eff}	$K_{SV} \times 10^{-4}$ (M^{-1})	$\int_{Cu(II)} \div \int_0$ [a]	$\int_{NO} \div \int_{Cu(II)}$ [b]
4a	415	3.9	455	0.027	31	14 %	3.2
4b	415	3.3	455	0.020	11	25 %	3.1
5	400	1.4	455	0.0047	5.0	9.1 %	3.5
6 [c]	425	0.28	490	0.019	43	10 %	4.9

[a] Ratio of integrated emission from CP–Cu(II) to that from CP alone. [b] Ratio of integrated emission from CP–Cu(II) + NO reaction to that from CP–Cu(II). [c] Measurements were performed in 90:10 CH_3CN/H_2O.

Table 3.3. Photoluminescent properties and analyte response of water-soluble CPs in aqueous solutions.

	$K_{SV} \times 10^{-4}$ (M^{-1}) [d]	$\int_{Cu(II)} \div \int_0$ [a,c]	$\int_{NO} \div \int_{Cu(II)}$ [b,c]	$K_{SV} \times 10^{-4}$ (M^{-1})	$\int_{Cu(II)} \div \int_0$	$\int_{NO} \div \int_{Cu(II)}$
4a	11	63 %	0.67	—	—	—
4b	5.2	7.7 %	0.85	—	—	—
5	1.7	36 %	0.90	9.2 [d]	24 % [d]	1.3 [d]
6	6.1	24 %	2.1	1.4 [e]	10 % [e]	0.88 [e]

[a] Ratio of integrated emission from CP–Cu(II) to that from CP alone. [b] Ratio of integrated emission from CP–Cu(II) + NO reaction to that from CP–Cu(II). [c] Measurements were performed in pure water. [d] Measurements were performed in 10 mM SDS(aq). [e] Measurements were performed in buffer.

3.3.14. Response of Water-Soluble CMPs to NO(g) and RNS

The CP–Cu(II) complexes displayed 3.2- to 3.5-fold increases in integrated emission upon treatment with NO(g) in 95:5 CH_3CN/H_2O (**Table 3.2**, for **4a** see **Figure 3.5**). However, when these measurements were performed in pure water, the CP–Cu(II) complexes exhibited 10% to 30% quenching (**Table 3.3**). Because these decreases in fluorescence are *not* accompanied by increases in Rayleigh scattering, we believe the resultant CP–Cu(I) complexes are aggregating but *not* precipitating. Addition of NO(g) to **5**–Cu(II) in 10 mM SDS(aq) afforded a 30% increase in fluorescence, indicating that aggregation in the absence of surfactant could be the cause of emission quenching. This modest response to NO is not surprising given the poor Cu(II) quenching efficiency of **5**. Because the fluorescence of **5** is poorly quenched by Cu(II), there is less quenched emission to restore upon reaction with NO(g). Surprisingly, treatment of **4**–Cu(II) and **5**–Cu(II) with $Na_2N_2O_3$ displayed no changes in fluorescence, suggesting these CMP-based NO sensors could be selective over HNO.
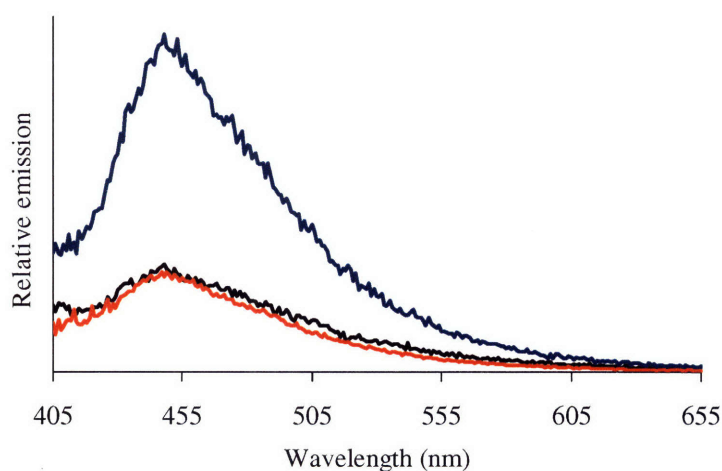
Figure 3.5. Response of **4a**–Cu(II) in 95:5 CH_3CN/H_2O (black trace) to NO(g) (blue trace) or $Na_2N_2O_3$ (red trace).

3.3.15. Summary of Results for Water-Soluble CPs

Our attempts to prepare fluorescent, water-soluble, bipyridyl-based NO sensors have yielded mixed results. All the CPs investigated showed poor Cu(II) quenching efficiency due to aggregation as well as competition between the metal binding units and the polyol side-chains. Furthermore, the CP–Cu(II) complexes exhibited *diminished* fluorescence upon treatment with NO(g) due to the formation of CP–Cu(I) aggregates. Addition of NO(g) to **5**–Cu(II) in 10 mM SDS(aq), to disrupt aggregation, afforded a modest increase in fluorescence. These CP–Cu(II) complexes were unresponsive to $Na_2N_2O_3$, suggesting that sensors derived from these CPs could be suitable for the selective detection of NO over HNO. Although these CMPs cannot be used for NO detection in buffer or other solutions without a surfactant, **4** and **5** represent the first examples of fluorescent, water-soluble NO sensors based on copper(II) CMPs.

3.3.16. Design and Synthesis of 6

The poor Cu(II) quenching efficiency in **4** and **5** precludes any biosensing applications: an excess of toxic Cu(II) ions must be added to biological samples to achieve sufficient quenching of CP emission. This inefficiency results from competition between the metal binding units and water-solubilizing side-chains for Cu(II). To increase the Cu(II) quenching efficiency of a CP, there are two strategies available: perturb the balance of binding affinities more towards the metal binding unit or more towards the side-chains. The former strategy involves increasing the affinity of the metal binding unit or decreasing the competition from the side-chains. Alteration of the water-solubilizing side-chains to facilitate this effect would be synthetically challenging and could negatively affect the solubility and biocompatibility of the CP, perhaps even eliminating the conferred solubility in water. Because bis(bipyridyl) complexes of Cu(I)

and Cu(II) are kinetically very stable, the only way to enhance the affinity of the metal binding unit would be by increasing its chelation number, replacing the bidentate bipyridyl unit with a ligand such as the tetradentate cyclam. Unfortunately, ligands for Cu(II) of higher denticity are less able to reorganize to accommodate Cu(I) and NO sensors based on these types of ligands would operate by a different type of reductive nitrosylation mechanism.

An alternative strategy would be to decrease the affinity of the metal binding unit, or eliminate it entirely, and rely on the water-solubilizing side-chains for Cu(II) binding. Although this strategy would seem to preclude Cu(II)-induced quenching of emission, a transition metal can perturb the photoluminescent properties of a CP without forming substitutionally inert bonds to atoms in the main chain. In this spirit, we sought to prepare a water-soluble CP lacking a metal binding unit that could still be quenched by Cu(II). Such a system requires a copolymer of spacers bearing water-solubilizing side-chains and spacers containing donor atoms with weak metal affinities.

Thiophene is a poor ligand for metal ions, and the few structurally characterized complexes that exhibit direct M–S(thiophene) bonds reveal that the thiophene can be displaced by coordinating solvents such as CH_3CN or even weakly-coordinating solvents such as CH_2Cl_2.[122,123] Presumably, this kinetic lability can be attenuated via inclusion of the thiophene moiety into a multidentate ligand framework or by supramolecular preorganization that holds the thiophene in proximity to the metal. Although a thiophene–Cu(II) bond will be readily disrupted in aqueous solution, a fast kinetic exchange rate will allow a transition metal to quench the main-chain emission through transient coordination. Furthermore, the red-shifted emission of thiophene relative to simple arenes confers upon CPs incorporating it emission profiles more amenable for biological sensing applications.

Because of the poor metal affinity and redshifted emission of thiophene, we selected bithiophene as the replacement for the bipyridyl metal binding unit used in **1–5** (**Chart 3.4**). Synthesis of **6** was performed via Sonogashira-type coupling of dibromobithiophene **M(5)** with polyol-functionalized diethynyl- and diiodoarenes **W(1)** and **W(2)** (**Chart 3.5**) Polymer **6** was readily soluble in 90:10 CH_3CN/H_2O, pure water, and even 0.1 M ionic strength buffer. Although this CP exhibited good emission wavelengths (nearly 500 nm), the absorptivities were poor ($<10^4$), and the quantum yields were similar to those observed for **4** and **5** (**Table 3.2** and **3.3**).
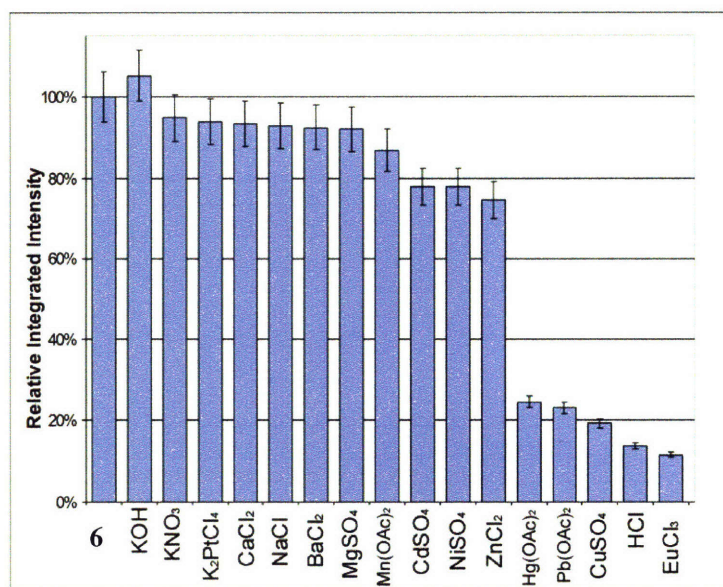
Figure 3.6. Response of **6** to metal ions in pure water.

3.3.17. Response of 6 to Metal Ions

Because alteration of the metal binding unit would inherently alter the metal affinity of **6**, we first explored the relative quenching abilities of a variety of metals (**Figure 3.6**). No statistically significant changes in integrated emission were observed upon treatment of **6** in

buffer with Group 1 metals, Group 2 metals, Pt(II) or base. Modest fluorescence quenching (10–25%) was observed with Mn(II), Cd(II), Ni(II) and Zn(II). Near-total loss of emission (>80%) resulted from addition of Cu(II), Hg(II), Eu(III) and acid.

For consistency with the preceding studies and greatest biocompatibility, we chose to continue working with copper(II)-based CMPs. Titration of **6** with Cu(II) revealed quenching efficiencies in CH_3CN/H_2O and pure water that were as good as or better than those of **4** and **5** (Table **3.2** and **3.3**). These results indicated that our strategy for increasing quenching efficiency by eliminating competing metal binding units was successful. In 90:10 CH_3CN/H_2O and pure water, the Stern-Volmer plots are linear at low Cu(II) concentrations and level off after 0.5 equiv of Cu(II) per bithiophene unit, suggesting that each Cu(II) center can only access *one* thiophene moiety, consistent with a mixed side-chain/main-chain coordination environment for copper (**Table 3.2–3**). Fortuitously, **6** could be dissolved in buffer and the resultant **6**–Cu(II) complex did not precipitate. Unfortunately, the Cu(II) quenching efficiency of **6** in buffer was extremely poor, presumably due to the high chloride concentration causing $[CuCl_4]^{2-}$ to be the dominant Cu(II) species in solution.

3.3.18. Response of 6–Cu(II) to NO(g)

Addition of NO(g) to **6**–Cu(II) in 90:10 CH_3CN/H_2O or pure water induced a 2.1- or 4.9-fold increase in integrated emission, respectively (**Table 3.2–3**). Because **6** is better quenched by Cu(II) in 90:10 CH_3CN/H_2O than in pure water, the NO-induced turn-on for **6**–Cu(II) should be greater in 90:10 CH_3CN/H_2O by the same amount. Accordingly, the **6**–Cu(II) complex is 2.3 times less emissive in 90:10 CH_3CN/H_2O than in pure water and the NO-induced turn-on is 2.3 times greater. Unfortunately, treatment of **6**–Cu(II) with NO in buffer yielded a 12% quenching

of fluorescence with an increase in Rayleigh scattering, suggestive of precipitation (**Figure 3.7** and **Table 3.3**). This decrease in emission appears to buffer-specific: no change in integrated emission and no precipitation were observed when the same experiment was performed in pH 7.0, 100 mM NH$_4$OAc.

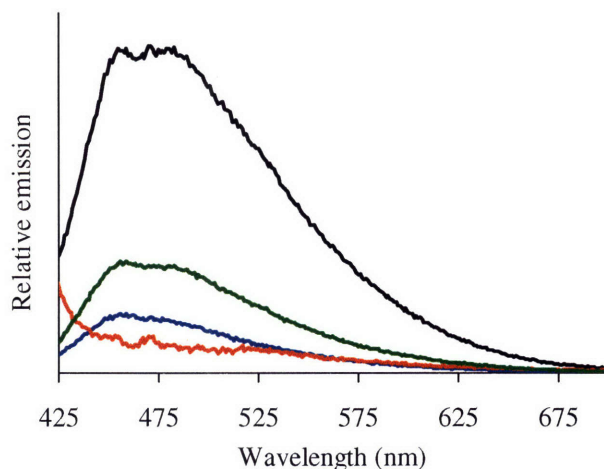### 3.3.19. *Selectivity Studies for 6–Cu(II)*

Rather than being a setback, this lack of reactivity with NO(g) presents a unique opportunity for sensing alternate analytes: in theory, **6**–Cu(II) could be used to detect reactive nitrogen species other than NO(g). Despite considerable interest in developing fluorescent sensors for the detection of nitric oxide,[1,14,15,20–23,27–29,124–127] there has been a surprising lack of progress in sensing other reactive nitrogen species selectively.

No change in fluorescence was observed upon treatment of **6**–Cu(II) with SIN-1-Cl, indicating that this sensor is also unresponsive to peroxynitrite. However, when Na$_2$N$_2$O$_3$ was used, a 6.6-fold increase in integrated emission was observed in pure water. This result is surprising, given that the integrated emission of **6**–Cu(II) in H$_2$O is quenched by 76% relative to that of **6**: a full restoration in fluorescence could yield a *maximum* 4.2-fold enhancement. This greater-than-theoretical turn-on can be understood in terms of pH: introduction of such a large amount of Na$_2$N$_2$O$_3$ to an *unbuffered* aqueous solution will increase the alkalinity of the solution. As observed during the metal quenching studies, we detected an increase in the emission from **6** upon addition of base. Because protons can quench emission and freshly collected Millipore water has pH 6 due to dissolved CO$_2$, there will be some adventitious quenching of the fluorescence from **6** in pure water. As the pH increases, the concentration of protons will decrease, as will the proton-induced quenching. Because the addition of Na$_2$N$_2$O$_3$ in 1.0 M

KOH(aq) causes a reduction to Cu(I) *and* an increase in solution pH, the 'restored' fluorescence is greater than the initial fluorescence of **6** at pH 6.

In contrast, when the addition of $Na_2N_2O_3$ to **6**–Cu(II) was performed in 90:10 CH_3CN/H_2O, the fluorescence only increased 3.3-fold. Presumably, no increase beyond CP-only fluorescence occurs because the pH effects are less pronounced in this solvent system. Because this solution is only 10% H_2O, there are far fewer protons available for quenching the emission of **6**. Furthermore, the large relative CH_3CN composition of the solvent will dramatically affect pK_a values. For example, the pH values for many buffers increase by nearly two log units in going from pure water to 50:50 CH_3CN/H_2O.[128] This deviation becomes more pronounced for simpler, non-buffering molecules as the percent composition of CH_3CN increases. For example, the pK_a of NH_3 increases by more than *seven log units* going when measured in pure CH_3CN compared to pure water due to diminished ion solvation capacity.[129] Presumably, similar behavior would be observed for the pK_a of H_2O.

Figure 3.7. Selectivity studies of **6**–Cu(II) in 50 mM HEPES, 100 mM KCl, pH 7.4 buffer. Addition of Cu(II) to **6** (black trace) forms of **6**–Cu(II) (blue trace). Treatment of **6**–Cu(II) with NO(g) causes 12% quenching of emission (red trace) whereas $Na_2N_2O_3$ causes a 2.1-fold restoration of fluorescence (green trace).

105

To avoid fluctuations in solution pH and to mimic biological milieu more faithfully, we repeated the HNO sensing experiments in buffer. Upon addition of $Na_2N_2O_3$ to 6–Cu(II) in either buffer (HEPES/KCl or NH_4OAc), an immediate 2.1-fold increase in integrated emission was observed (**Figure 3.7**). Because the pH is buffered at 7.4 or 7.0, this change in fluorescence is a genuine response to HNO uncomplicated by pH variations. Thus, 6–Cu(II) is capable of distinguishing HNO from NO(g) under biologically-relevant conditions.

3.3.20. Summary of Results for 6

Replacement of the bipyridyl-based metal binding unit with a weakly-coordinating bithiophene afforded greater quenching efficiency, due to diminished competition between these and the water-solubilizing side-chains. Although 6–Cu(II) displayed a 2.1-fold restoration of emission upon treatment with NO(g) in pure water, there was 12% quenching when performed in 50 mM HEPES, 100 mM KCl, pH 7.4 buffer, most likely due to precipitation of the 6–Cu(I) complex. However, 6–Cu(II) in this same buffer afforded a 2.1-fold increase in fluorescence. There is only one reported example[130] of a sensor selective for HNO over NO(g) and none have been CP-based or fluorescent. Thus, 6–Cu(II) represents the first example of a CMP-based sensor for the turn-on fluorescent detection of HNO in biologically-relevant milieu.

3.4. Conclusions

For the first time, **1a** allowed the fluorescent detection of nitric oxide by a conjugated polymer. Copper(II)-induced quenching of emission of **1a** involved the formation of 2:1 bipyridyl-copper complex-based coordinative cross-links in **1a**–Cu(II). Addition of NO(g) to this CMP afforded a 2.2-fold restoration of emission and a fluorescence spectrum nearly identical to

that for **1a**–Cu(I). Mechanistic studies suggested that reductive nitrosylation caused reduction of the metal to Cu(I), which remains bound to **1a**, and the resulting NO$^+$ is quenched by ethanol.

A systematic variation of metal binding units and spacers revealed insight into the relationship between redox matching and sensor properties. The main-chain bipyridyl **1** and side-chain terpyridyl **3** exhibited the best copper(II) quenching efficiencies, and the PPV-based **_a** and polyfluorene based **_b** displayed comparable K_{SV} values, with **1** > **3** >> **2** and **_a** > **_c** >> **_b**. Copper(II) complexes of **1** and **3** showed good restoration of emission in response to NO(g), but the quantum yields and excitation wavelengths of **3** preclude adaptation to biosensing applications.

Due to synthetic constraints, water-soluble analogs of PPV-based or polyfluorene-based CPs were avoided in favor of those incorporating PPE-type spacers. The water-soluble CPs **4** and **5** were inefficiently quenched by Cu(II) in pure water because of competitive binding by the water-solubilizing side-chains. Unfortunately, treatment of the CP–Cu(II) complexes with NO(g) in water induced fluorescence quenching due to aggregation of the resultant CP–Cu(I) complex. Inclusion of a surfactant prevented this behavior and allowed a turn-on response upon addition of NO(g) to **5**–Cu(II) in 10 mM SDS(aq).

Replacement of the metal binding unit with the weakly-coordinating bithiophene in **6** yielded an improvement in copper(II) quenching efficiency, due to diminished competition. Although **6**–Cu(II) exhibited a 2.1-fold restoration in emission upon reaction with NO(g) in water, the same reaction caused a 12% decrease when performed in 50 mM HEPES, 100 mM KCl, pH 7.4 buffer. No such quenching was observed in 100 mM NH4OAc pH 7.0 buffer. However, treatment of **6**–Cu(II) with an HNO donor in buffer afforded a 2.1-fold increase in integrated emission, demonstrating the ability of this sensor to detect HNO selectively over

NO(g) in biologically-relevant milieu.

These studies have demonstrated the versatility of the conjugated polymer-based scaffold for adaptation to the detection of NO by a turn-on fluorescence response. The inherent modularity of CPs allows simpler modification of sensor properties via alteration of monomers than would be possible in a small-molecule. Thus, exploratory work can be performed under simple conditions (organic solution, etc) and more complicated sensors can be derived from these initial systems by alteration of the nature of the monomers used, such as incorporating water-solubilizing side-chains onto the spacers or altering the balance between metal binding and competition by side-chains. As the need for sensors of greater complexity and specialization grow, so will the demand for CP-based systems.

3.5. References

(1)   Lim, M. H.; Lippard, S. J. "Metal-Based Turn-On Fluorescent Probes for Sensing Nitric Oxide" *Acc. Chem. Res.* **2007,** *40,* 41–51.

(2)   Kálai, T.; Hideg, K. "Synthesis of new, BODIPY-based sensors and labels" *Tetrahedron* **2006,** *62,* 10352–10360.

(3)   Ivanisevic, A.; Reynolds, M. F.; Burstyn, J. N.; Ellis, A. B. "Photoluminescent Properties of Cadmium Selenide in Contact with Solutions and Films of Metalloporphyrins: Nitric Oxide Sensing and Evidence for the Aversion of an Analyte to a Buried Semiconductor– Film Interface" *J. Am. Chem. Soc.* **2000,** *122,* 3731–3738.

(4)   Barker, S. L. R.; Zhao, Y.; Marletta, M. A.; Kopelman, R. "Cellular Applications of a Sensitive and Selective Fiber-Optic Nitric Oxide Biosensor Based on a Dye-Labeled Heme Domain of Soluble Guanylate Cyclase" *Anal. Chem.* **1999,** *71,* 2071–2075.

(5)   Barker, S. L. R.; Clark, H. A.; Swallen, S. F.; Kopelman, R. "Ratiometric and Fluorescence-Lifetime-Based Biosensors Incorporating Cytochrome *c'* and the Detection of Extra- and Intracellular Macrophage Nitric Oxide" *Anal. Chem.* **1999,** *71,* 1767–1772.

(6)   Barker, S. L. R.; Kopelman, R. "Development and Cellular Applications of Fiber Optic Nitric Oxide Sensors Based on a Gold-Adsorbed Fluorophore" *Anal. Chem.* **1998**, *70*, 4902–4906.

(7)   Hirano, T.; Hiromoto, K.; Kagechika, H. "Development of a Library of 6-Arylcoumarins as Candidate Fluorescent Sensors" *Org. Lett.* **2007**, *9*, 1315–1318.

(8)   Kojima, H.; Kiyose, K.; Sasaki, E.; Nishimatsu, H.; Hirata, Y.; Nagano, T. "Development of Near-Infrared Fluorescent Probes for Nitric Oxide and Zinc Ion" *Proc. SPIE* **2007**, *6441*, 1–12.

(9)   Zguris, J.; Pishko, M. V. "Nitric oxide sensitive fluorescent poly(ethylene glycol) hydrogel microstructures" *Sens. Act. B* **2006**, *115*, 503–509.

(10)   Dacres, H.; Narayanaswamy, R. "Evaluation of 1,2-Diaminoanthraquinone (DAA) as a Potential Reagent System for Detection of NO" *Microchim. Acta* **2005**, *152*, 35–45.

(11)   Gabe, Y.; Urano, Y.; Kikuchi, K.; Kojima, H.; Nagano, T. "Highly Sensitive Fluorescence Probes for Nitric Oxide Based on Boron Dipyrromethene Chromophores— Rational Design of Potentially Useful Bioimaging Fluorescence Probe" *J. Am. Chem. Soc.* **2004**, *126*, 3357–3367.

(12)   Chatton, Y.-J.; Broillet, M.-C. "Detection of Nitric Oxide Production by Fluorescent Indicators" *Methods Enzymol.* **2002**, *359*, 134–148.

(13)   Kojima, H.; Nakatsubo, N.; Kikuchi, K.; Kawahara, S.; Kirino, Y.; Nagoshi, H.; Hirata, Y.; Nagano, T. "Detection and Imaging of Nitric Oxide with Novel Fluorescent Indicators: Diaminofluoresceins" *Anal. Chem.* **1998**, *70*, 2446–2453.

(14)   Franz, K. J.; Singh, N.; Lippard, S. J. "Metal-Based NO Sensing by Selective Ligand Dissociation" *Angew. Chem. Int. Ed.* **2000**, *39*, 2120–2122.

(15)   Franz, K. J.; Singh, N.; Spingler, B.; Lippard, S. J. "Aminotroponiminates as Ligands for Potential Metal-Based Nitric Oxide Sensors" *Inorg. Chem.* **2000**, *39*, 4081–4092.

(16)   Bergonzi, R.; Fabbrizzi, L.; Licchelli, M.; Mangano, C. "Molecular switches of fluorescence operating through metal centered redox couples" *Coord. Chem. Rev.* **1998**, *170*, 31–46.

(17)   Hilderbrand, S. A.; Lippard, S. J. "Nitric Oxide Reactivity of Fluorophore Coordinated Carboxylate-Bridged Diiron(II) and Dicobalt(II) Complexes" *Inorg. Chem.* **2004**, *43*, 5294–5301.

(18)   Soh, N.; Imato, T.; Kawamura, K.; Maeda, M.; Katayama, Y. "Ratiometric direct detection of nitric oxide based on a novel signal-switching mechanism" *Chem. Commun.* **2002**, 2650–2651.

(19)   Lim, M. H.; Kuang, C.; Lippard, S. J. "Nitric Oxide-Induced Fluorescence Enhancement by Displacement of Dansylated Ligands from Cobalt" *ChemBioChem* **2006**, *7*, 1571–1576.

(20)   Lim, M. H.; Xu, D.; Lippard, S. J. "Visualization of nitric oxide in living cells by a copper-based fluorescent probe" *Nature Chem. Biol.* **2006**, *2*, 375–380.

(21)   Lim, M. H.; Wong, B. A.; Pitcock Jr., W. H.; Mokshagundam, D.; Baik, M.-H.; Lippard, S. J. "Direct Nitric Oxide Detection in Aqueous Solution by Copper(II) Fluorescein Complexes" *J. Am. Chem. Soc.* **2006**, *128*, 14364–14373.

(22)   Lim, M. H.; Lippard, S. J. "Fluorescent Nitric Oxide Detection by Copper Complexes Bearing Anthracenyl and Dansyl Fluorophore Ligands" *Inorg. Chem.* **2006**, *45*, 8980–8989.

(23)   Lim, M. H.; Lippard, S. J. "Copper Complexes for Fluorescence-Based NO Detection in Aqueous Solution" *J. Am. Chem. Soc.* **2005**, *127*, 12170–12171.

(24)   Khin, C.; Lim, M. D.; Tsuge, K.; Iretskii, A.; Wu, G.; Ford, P. C. "Amine Nitrosation via NO Reduction of the Polyamine Copper(II) Complex Cu(DAC)$^{2+}$" *Inorg. Chem.* **2007**, *46*, 9323–9331.

(25)   Baker, E. S.; Bushnell, J. E.; Wecksler, S. R.; Mark D. Lim; Manard, M. J.; Dupuis, N. F.; Ford, P. C.; Bowers, M. T. "Probing Shapes of Bichromophoric Metal–Organic Complexes Using Ion Mobility Mass Spectrometry" *J. Am. Chem. Soc.* **2005**, *127*, 18222–18228.

(26)   Tsuge, K.; DeRosa, F.; Lim, M. D.; Ford, P. C. "Intramolecular Reductive Nitrosylation: Reaction of Nitric Oxide and a Copper(II) Complex of a Cyclam Derivative with Pendant Luminescent Chromophores" *J. Am. Chem. Soc.* **2004**, *126*, 6564–6565.

(27)   Smith, R. C.; Tennyson, A. G.; Lim, M. H.; Lippard, S. J. "Conjugated Polymer-Based Fluorescence Turn-On Sensor for Nitric Oxide" *Org. Lett.* **2005**, *7*, 3573–3575.

(28)   Smith, R. C.; Tennyson, A. G.; Won, A. C.; Lippard, S. J. "Conjugated Metallopolymers for Fluorescent Turn-On Detection of Nitric Oxide" *Inorg. Chem.* **2006**, *45*, 9367–9373.

(29)   Do, L.; Smith, R. C.; Tennyson, A. G.; Lippard, S. J. "Luminescent Properties of Water-Soluble Conjugated Metallopolymers and Their Application to Fluorescent Nitric Oxide Detection" *Inorg. Chem.* **2006,** *45,* 8998–9005.

(30)   Tennyson, A. G.; Do, L.; Smith, R. C.; Lippard, S. J. "Selective fluorescence detection of nitroxyl over nitric oxide in buffered aqueous solution using a conjugated metallopolymer" *Polyhedron* **2007,** *26,* 4625–4630.

(31)   Tran, D.; Skelton, B. W.; White, A. H.; Laverman, L. E.; Ford, P. C. "Investigation of the Nitric Oxide Reduction of the Bis(2,9-Dimethyl-1,10-phenanthroline) Complex of Copper(II) and the Structure of [Cu(dmp)$_2$(H$_2$O)](CF$_3$SO$_3$)$_2$" *Inorg. Chem.* **1998,** *37,* 2505–2511.

(32)   Chipinda, I.; Simoyi, R. H. "Formation and Stability of a Nitric Oxide Donor: *S*-Nitroso-*N*-acetylpenicillamine" *J. Phys. Chem. B* **2006,** *110,* 5052–5061.

(33)   Nauser, T.; Merkofer, M.; Kissner, R.; Koppenol, W. H. "Gibbs Energy of Formation of Peroxynitrite" *Chem. Res. Toxicol.* **2001,** *14,* 348–350.

(34)   Bonner, F. T.; Ravid, B. "Thermal Decomposition of Oxyhyponitrite (Sodium Trioxodinitrate(II)) in Aqueous Solution" *Inorg. Chem.* **1975,** *14,* 558–563.

(35)   Bielski, B. H. J.; Allen, A. O. "Mechanism of the Disproportionation of Superoxide Radicals" *J. Phys. Chem.* **1977,** *81,* 1048–1050.

(36)   Valentine, J. S.; Curtis, B. "A Convenient Preparation of Solutions of Superoxide Anion and the Reaction of Superoxide Anion with a Copper(II) Complex" *J. Am. Chem. Soc.* **1975,** *97,* 224–226.

(37)   Li, J.; Kendig, C. E.; Nesterov, E. E. "Chemosensory Performance of Molecularly Imprinted Fluorescent Conjugated Polymer Materials" *J. Am. Chem. Soc.* **2007,** *129,* 15911–15918.

(38)   Thomas III, S. W.; Joly, G. D.; Swager, T. M. "Chemical Sensors Based on Amplifying Fluorescent Conjugated Polymers" *Chem. Rev.* **2007,** *107,* 1339–1386.

(39)   Whittell, G. R.; Manners, I. "Metallopolymers: New Multifunctional Materials" *Adv. Mater.* **2007,** *19,* 3439–3468.

(40)   Liu, M. S.; Niu, Y.-H.; Luo, J.; Chen, B.; Kim, T.-D.; Bardecker, J.; Jen, A. K.-Y. "Material and Interface Engineering for Highly Efficient Polymer Light Emitting Diodes" *Polymer Rev.* **2006,** *46,* 7–26.

(41) Voskerician, G.; Weder, C. "Electronic Properties of PAEs" *Adv. Polym. Sci* **2005**, *177*, 209–248.

(42) Toal, S. J.; Trogler, W. C. "Polymer sensors for nitroaromatic explosives detection" *J. Mater. Chem.* **2006**, *16*, 2871–2883.

(43) Aguzzi, A. "Unraveling prion strains with cell biology and organic chemistry" *Proc. Natl. Acad. Sci. USA* **2008**, *105*, 11–12.

(44) Jackson, W. S.; Lindquist, S. "Illuminating aggregate heterogeneity in neurodegenerative disease" *Nature Methods* **2007**, *4*, 1000–1001.

(45) Sigurdson, C. J.; Nilsson, K. P. R.; Hornemann, S.; Manco, G.; Polymenidou, M.; Schwarz, P.; Leclerc, M.; Hammarström, P.; Wüthrich, K.; Aguzzi, A. "Prion strain discrimination using luminescent conjugated polymers" *Nature Methods* **2007**, *4*, 1023–1030.

(46) Liu, Y.; Zhang, S.; Miao, Q.; Zheng, L.; Zong, L.; Cheng, Y. "Fluorescent Chemosensory Conjugated Polymers Based on Optically Active Polybinaphthyls and 2,2'-Bipyridyl Units" *Macromolecules* **2007**, *40*, 4839–4847.

(47) Wang, W.-L.; Xu, J.-W.; Lai, Y.-H. "Bipyridinophane-Containing Conjugated Polymers Modulated with an Intramolecular Aromatic C—H/π Interaction" *J. Polym. Sci. Part A: Polym. Chem.* **2006**, *44*, 4154–4164.

(48) Kokil, A.; Yao, P.; Weder, C. "Organometallic Networks Based on 2,2'-Bipyridine-Containing Poly(*p*-phenylene ethynylene)s" *Macromolecules* **2005**, *38*, 3800–3807.

(49) Zhang, M.; Lu, P.; Ma, Y.; Shen, J. "Metal Ionochromic Effects of Conjugated Polymers: Effects of the Rigidity of Molecular Recognition Sites on Metal Ion Sensing" *J. Phys. Chem. B* **2003**, *107*, 6535–6538.

(50) Liu, B.; Yu, W.-L.; Pei, J.; Liu, S.-Y.; Lai, Y.-H.; Huang, W. "Design and Synthesis of Bipyridyl-Containing Conjugated Polymers: Effects of Polymer Rigidity on Metal Ion Sensing" *Macromolecules* **2001**, *34*, 7932–7940.

(51) Chen, L. X.; Jäger, W. J. H.; Gosztola, D. J.; Niemczyk, M. P.; Wasielewski, M. R. "Ionochromic Effects and Structures of Metalated Poly(p-phenylenevinylene) Polymers Incorporating 2,2'-Bipyridines" *J. Phys. Chem. B* **2000**, *104*, 1950–1960.

(52)   Wang, B.; Wasielewski, M. R. "Design and Synthesis of Metal Ion-Recognition-Induced Conjugated Polymers: An Approach to Metal Ion Sensory Materials" *J. Am. Chem. Soc.* **1997,** *119*, 12–21.

(53)   Nocera, D. G. personal communication.

(54)   He, S.; Iacono, S. T.; Budy, S. M.; Dennis, A. E.; Smith Jr., D. W.; Smith, R. C. "Photoluminescence and ion sensing properties of a bipyridyl chromophore-modified semifluorinated polymer and its metallopolymer derivatives" *J. Mater. Chem.* **2008,** *18*, 1970–1976.

(55)   Chen, L. X.; Jäger, W. J. H.; Niemczyk, M. P.; Wasielewski, M. R. "Effects of π-Conjugation Attenuation on the Photophysics and Exciton Dynamics of Poly(*p*-phenylenevinylene) Polymers Incorporating 2,2'-Bipyridines" *J. Phys. Chem. A* **1999,** *103*, 4341–4351.

(56)   Amrutha, S. R.; Jayakannan, M. "Structure Control of π-Conjugated Polymers for Enhanced Solid-State Luminescence: Synthesis and Liquid Crystalline and Photophysical Properties of New Bulky Poly(*p*-phenylenevinylene)s and Oligo(phenylenevinylene)s Bearing Tricyclodecane Pendants" *Macromolecules* **2007,** *40*, 2380–2391.

(57)   Fakis, M.; Anestopoulos, D.; Giannetas, V.; Persephonis, P. "Influence of Aggregates and Solvent Aromaticity on the Emission of Conjugated Polymers" *J. Phys. Chem. B* **2006,** *110*, 24897–24902.

(58)   Gu, Z.; Bao, Y.-J.; Zhang, Y.; Wang, M.; Shen, Q.-D. "Anionic Water-Soluble Poly(phenylenevinylene) Alternating Copolymer: High-Efficiency Photoluminescence and Dual Electroluminescence" *Macromolecules* **2006,** *39*, 3125–3131.

(59)   Egbe, D. A. M.; Carbonnier, B.; Ding, L.; Mühlbacher, D.; Birckner, E.; Pakula, T.; Karasz, F. E.; Grummt, U.-W. "Supramolecular Ordering, Thermal Behavior, and Photophysical, Electrochemical, and Electroluminescent Properties of Alkoxy-Substituted Yne-Containing Poly(phenylene–vinylene)s" *Macromolecules* **2004,** *37*, 7451–7463.

(60)   Egbe, D. A. M.; Cornelia, B.; Nowotny, J.; Günther, W.; Klemm, E. "Investigation of the Photophysical and Electrochemical Properties of Alkoxy-Substituted Arylene–Ethynylene/Arylene–Vinylene Hybrid Polymers" *Macromolecules* **2003,** *36*, 5459–5469.

(61)   Cho, H.; Kim, E. "Highly Fluorescent and Photochromic Diarylethene Oligomer Bridged by p-Phenylenevinylene" *Macromolecules* **2002,** *35*, 8684–8687.

(62)   Lim, M. D.; Capps, K. B.; Karpishin, T. B.; Ford, P. C. "Further evidence supporting an inner sphere mechanism in the NO reduction of the copper(II) complex Cu(dmp)$_2{}^{2+}$ (dmp = 2,9-dimethyl-1,10-phenanthroline)" *Nitric Oxide* **2005**, *12*, 244–251.

(63)   Albada, G. A. v.; Mohamadou, A.; Mutikainen, I.; Turpeinen, U.; Reedijk, J. "Synthesis, Characterisation, Properties and X-ray Structures of Cu^{II} Coordination Compounds with 5,5'-Dimethylbipyridine and Various Anions: Control of Stoichiometry and Structure by the Counterions" *Eur. J. Inorg. Chem.* **2004**, 3733–3742.

(64)   Fujisawa, K.; Tateda, A.; Miyashita, Y.; Okamoto, K.-i.; Paulat, F.; Praneeth, V. K. K.; Merkle, A.; Lehnert, N. "Structural and Spectroscopic Characterization of Mononuclear Copper(I) Nitrosyl Complexes: End-on versus Side-on Coordination of NO to Copper(I)" *J. Am. Chem. Soc.* **2008**, 1205–1213.

(65)   Schneider, J. L.; Carrier, S. M.; Ruggiero, C. E.; Young Jr., V. G.; Tolman, W. B. "Influences of Ligand Environment on the Spectroscopic Properties and Disproportionation Reactivity of Copper-Nitrosyl Complexes" *J. Am. Chem. Soc.* **1998**, *120*, 11408–11418.

(66)   Ruggiero, C. E.; Carrier, S. M.; Antholine, W. E.; Whittaker, J. W.; Cramer, C. J.; Tolman, W. B. "Synthesis and Structural and Spectroscopic Characterization of Mononuclear Copper Nitrosyl Complexes: Models for Nitric Oxide Adducts of Copper Proteins and Copper-Exchanged Zeolites" *J. Am. Chem. Soc.* **1993**, *115*, 11285–11298.

(67)   Carrier, S. M.; Ruggiero, C. E.; Tolman, W. B.; Jameson, G. B. "Synthesis and Structural Characterization of a Mononuclear Copper Nitrosyl Complex" *J. Am. Chem. Soc.* **1992**, *114*, 4407–4408.

(68)   Marsden, P. A. "Low-molecular-weight *S*-nitrosothiols and blood vessel injury" *J. Clin. Invest.* **2007**, *117*, 2377–2380.

(69)   Hess, D. T.; Matsumoto, A.; Kim, S.-O.; Marshall, H. E.; Stamler, J. S. "Protein S-Nitrosylation: Purview and Parameters" *Nature Rev. Mol. Cell Biol.* **2005**, *6*, 150–166.

(70)   Szaciłowski, K.; Chmura, A.; Stasicka, Z. "Interplay between iron complexes, nitric oxide and sulfur ligands: Structure, (photo)reactivity and biological importance" *Coord. Chem. Rev.* **2005**, *249*, 2408–2436.

(71)   Zhang, Y.; Hogg, N. "*S*-Nitrosothiols: cellular formation and transport" *Free Radic. Biol. Med.* **2005**, *38*, 831–838.

(72)   Carver, J.; Doctor, A.; Zaman, K.; Gaston, B. "S-Nitrosothiol Formation" *Methods Enzymol.* **2005**, *396*, 95–105.

(73)　Marshall, H. E.; Hess, D. T.; Stamler, J. S. "S-nitrosylation: Physiological regulation of NF-κB" *Proc. Natl. Acad. Sci. USA* **2004**, *101*, 8841–8842.

(74)　Smith, J. N.; Dasgupta, T. P. "Kinetics and Mechanism of the Decomposition of *S*-Nitrosoglutathione by L-Ascorbic Acid and Copper Ions in Aqueous Solution to Produce Nitric Oxide" *Nitric Oxide* **2000**, *4*, 57–66.

(75)　Stamler, J. S.; Toone, E. J. "The decomposition of thionitrites" *Curr. Opin. Chem. Biol.* **2002**, *6*, 779–785.

(76)　Kröncke, K.-D.; Kolb-Bachofen, V. "Measurement of Nitric Oxide-Mediated Effects on Zinc Homeostasis and Zinc Finger Transcription Factors " *Methods Enzymol.* **1999**, *301*, 126–135.

(77)　Field, L.; Dilts, R. V.; Ravichandran, R.; Lenhert, P. G.; Carnahan, G. E. "An Unusually Stable Thionitrite from *N*-Acetyl-D,L-penicillamine; X-Ray Crystal and Molecular Structure of 2-(Acetylamino)-2-carboxy-1,1-dimethylethyl Thionitrite" *J. Chem. Soc., Chem. Commun.* **1978**, 249–250.

(78)　Tsikas, D.; Frölich, J. C. "Trouble with the analysis of nitrite, nitrate, *S*-nitrosothiols and 3-nitrotyrosine: freezing-induced artifacts?" *Nitric Oxide* **2004**, *11*, 209–213.

(79)　Vanin, A. F.; Papina, A. A.; Serezhenkov, V. A.; Koppenol, W. H. "The mechanisms of *S*-nitrosothiol decomposition catalyzed by iron" *Nitric Oxide* **2004**, *10*, 60–73.

(80)　Chen, Y.; Irie, Y.; Keung, W. M.; Maret, W. "*S*-Nitrosothiols React Preferentially with Zinc Thiolate Clusters of Metallothionein III through Transnitrosation" *Biochemistry* **2002**, *41*, 8360–8367.

(81)　Kelm, M. "Nitric oxide metabolism and breakdown" *Biochim. Biophys. Acta* **1999**, *1411*, 273–289.

(82)　Dicks, A. P.; Williams, D. L. H. "Generation of nitric oxide from *S*-nitrosothiols using protein-bound Cu^{2+} sources " *Chem. & Biol.* **1996**, *3*, 655–659.

(83)　Singh, S. P.; Wishnok, J. S.; Keshive, M.; Deen, W. M.; Tannenbaum, S. R. "The chemistry of the *S*-nitrosoglutathione/glutathione system" *Proc. Natl. Acad. Sci. USA* **1996**, *93*, 14428–14433.

(84)　Fukuto, J. M.; Dutton, A. S.; Houk, K. N. "The Chemistry and Biology of Nitroxyl (HNO): A Chemically Unique Species with Novel and Important Biological Activity" *ChemBioChem* **2005**, *6*, 612–619.

(85)   Miranda, K. M. "The chemistry of nitroxyl (HNO) and implications in biology" *Coord. Chem. Rev.* **2005**, *249*, 433–455.

(86)   Holliday, B. J.; Swager, T. M. "Conducting metallopolymers: the roles of molecular architecture and redox matching" *Chem. Commun.* **2005**, 23–36.

(87)   Iyer, P. K.; Beck, J. B.; Weder, C.; Rowan, S. J. "Synthesis and optical properties of metallo-supramolecular polymers" *Chem. Commun.* **2005**, 319–321.

(88)   Cameron, C. G.; MacLean, B. J.; Pickup, P. G. "Electron Transport in Conjugated Metallopolymers" *Macromol. Symp.* **2003**, *196*, 165–171.

(89)   Jiang, B.; Zhang, Y.; Sahay, S.; Chatterjee, S.; Jones Jr., W. E. "Conjugated polymers containing pendant terpyridine receptors: Highly efficient sensory materials for transition metal ions" *Proc. SPIE* **1999**, *3856*, 212–223.

(90)   Zhang, Y.; Murphy, C. B.; Jones Jr., W. E. "Poly[p-(phenyleneethynylene)-alt-(thienyleneethynylene)] Polymers with Oligopyridine Pendant Groups: Highly Sensitive Chemosensors for Transition Metal Ions" *Macromolecules* **2002**, *35*, 630–636.

(91)   Weder, C. "Synthesis, processing and properties of conjugated polymer networks" *Chem. Commun.* **2005**, 3578–3589.

(92)   Wosnick, J. H.; Mello, C. M.; Swager, T. M. "Synthesis and Application of Poly(phenylene Ethynylene)s for Bioconjugation: A Conjugated Polymer-Based Fluorogenic Probe for Proteases" *J. Am. Chem. Soc.* **2005**, *127*, 3400–3405.

(93)   Chi, C.; Mikhailovsky, A.; Bazan, G. C. "Design of Cationic Conjugated Polyelectrolytes for DNA Concentration Determination" *J. Am. Chem. Soc.* **2007**, *129*, 11134–11145.

(94)   Åslund, A.; Herland, A.; Hammarström, P.; Nilsson, K. P. R.; Jonsson, B.-H.; Inganäs, O.; Konradsson, P. "Studies of Luminescent Conjugated Polythiophene Derivatives: Enhanced Spectral Discrimination of Protein Conformational States" *Bioconjugate Chem.* **2007**, *18*, 1860–1868.

(95)   Ng, P. K.; Gong, X.; Chan, S. H.; Lam, L. S. M.; Chan, W. K. "The Role of Ruthenium and Rhenium Diimine Complexes in Conjugated Polymers That Exhibit Interesting Opto-Electronic Properties" *Chem. Eur. J.* **2001**, *7*, 4358–4367.

(96)   Peng, Z.; Gharavi, A. R.; Yu, L. "Synthesis and Characterization of Photorefractive Polymers Containing Transition Metal Complexes as Photosensitizer" *J. Am. Chem. Soc.* **1997**, *119*, 4622–4632.

(97)   Lakowicz, J. R., *Principles of Fluorescence Spectroscopy*. 3rd ed.; Springer: New York, 2006.

(98)   Egbe, D. A. M.; Nguyen, L. H.; Schmidtke, K.; Wild, A.; Sieber, C.; Guenes, S.; Sariciftci, N. S. "Combined Effects of Conjugation Pattern and Alkoxy Side Chains on the Photovoltaic Properties of Thiophene-Containing PPE-PPVs" *J. Polym. Sci. Part A: Polym. Chem.* **2007,** *45,* 1619–1631.

(99)   Ishow, E.; Bouffard, J.; Kim, Y.; Swager, T. M. "Anthryl-Based Poly(phenylene ethynylene)s: Tuning Optical Properties with Diels–Alder Reactions" *Macromolecules* **2006,** *39,* 7854–7858.

(100)   Zhao, X.; Pinto, M. R.; Hardison, L. M.; Mwaura, J.; Müller, J.; Jiang, H.; Witker, D.; Kleiman, V. D.; Reynolds, J. R.; Schanze, K. S. "Variable Band Gap Poly(arylene ethynylene) Conjugated Polyelectrolytes" *Macromolecules* **2006,** *39,* 6355–6366.

(101)   Nesterov, E. E.; Zhu, Z.; Swager, T. M. "Conjugation Enhancement of Intramolecular Exciton Migration in Poly(p-phenylene ethynylene)s" *J. Am. Chem. Soc.* **2005,** *127,* 10083–10088.

(102)   Shi, C.; Yang, K.; Cao, Y. "Synthesis and Optical Properties of Soluble Conjugated Poly(*p*-Diethynylbenzenes)s" *Synth. Met.* **2005,** *154,* 121–124.

(103)   Egbe, D. A. M.; Kietzke, T.; Carbonnier, B.; Mühlbacher, D.; Hörhold, H.-H.; Neher, D.; Pakula, T. "Synthesis, Characterization, and Photophysical, Electrochemical, Electroluminescent, and Photovoltaic Properties of Yne-Containing CN–PPVs" *Macromolecules* **2004,** *37,* 8863–8873.

(104)   Lu, S. L.; Yang, M. J.; Luo, J.; Cao, Y.; Bai, F. L. "Synthesis, photophysics and electroluminescent properties of a novel phenylene-ethynylene and bezothiadiazole alternating copolymer" *Synth. Met.* **2004,** *124,* 175–180.

(105)   Huang, Y.-Q.; Fan, Q.-L.; Zhang, G.-W.; Chen, Y.; Lu, X.-M.; Huang, W. "A fluorene-containing water-soluble poly(*p*-phenyleneethynylene) derivative: Highly fluorescent and sensitive conjugated polymer with minor aggregation in aqueous solution" *Polymer* **2006,** *47,* 5233–5238.

(106)   Pal, B.; Yen, W.-C.; Yang, J.-S.; Su, W.-F. "Substituent Effect on the Optoelectronic Properties of Alternating Fluorene-Thiophene Copolymers" *Macromolecules* **2007,** *40,* 8189–8194.

(107)   Zhu, B.; Han, Y.; Sun, M.; Bo, Z. "Water-Soluble Dendronized Polyfluorenes with an Extremely High Quantum Yield in Water" *Macromolecules* **2007,** *40,* 4494–4500.

(108) Liu, X.-M.; Xu, J.; Lu, X.; He, C. "A Comparative Study on Luminescent Copolymers of Fluorene and Carbazole with Conjugated or δ-Si Interrupted Structures: Steric Effects" *Macromolecules* **2006,** *39,* 1397–1402.

(109) Jiang, G.; Wu, J.; Yao, B.; Geng, Y.; Cheng, Y.; Xie, Z.; Wang, L.; Jing, X.; Wang, F. "Synthesis and Characterization of Blue-Light-Emitting Poly(aryl ether)s Containing Oligofluorenes in the Main Chain" *Macromolecules* **2006,** *39,* 7950–7958.

(110) Yang, R.; Garcia, A.; Korystov, D.; Mikhailovsky, A.; Bazan, G. C.; Nguyen, T.-Q. "Control of Interchain Contacts, Solid-State Fluorescence Quantum Yield, and Charge Transport of Cationic Conjugated Polyelectrolytes by Choice of Anion" *J. Am. Chem. Soc.* **2006,** *128,* 16532–16539.

(111) Cagnoli, R.; Mucci, A.; Parenti, F.; Schenetti, L.; Borsari, M.; Lodi, A.; Ponterini, G. "A poly(alkylsulfany)thiophene functionalized with carboxylic groups" *Polymer* **2006,** *47,* 775–784.

(112) Pei, J.; Yu, W.-L.; Ni, J.; Lai, Y.-H.; Huang, W.; Heeger, A. J. "Thiophene-Based Conjugated Polymers for Light-Emitting Diodes: Effect of Aryl Groups on Photoluminescence Efficiency and Redox Behavior" *Macromolecules* **2001,** *34,* 7241–7248.

(113) Chaurin, V.; Constable, E. C.; Housecroft, C. E. "What is the coordination number of copper(II) in metallosupramolecular chemistry?" *New J. Chem.* **2006,** *30,* 1740–1744.

(114) Ziessel, R. "Schiff-based bipyridine ligands. Unusual coordination features and mesomorphic behaviour" *Coord. Chem. Rev.* **2001,** *216–217,* 195–223.

(115) Trouillet, L.; Nicola, A. D.; Guillerez, S. "Synthesis and Characterization of a New Soluble, Structurally Well-Defined Conjugated Polymer Alternating Regioregularly Alkylated Thiophene Oligomer and 2,2'-Bipyridine Units: Metal-Free Form and Ru(II) Complex" *Chem. Mater.* **2000,** *12,* 1611–1621.

(116) Kim, I.-B.; Dunkhorst, A.; Bunz, U. H. F. "Nonspecific Interactions of a Carboxylate-Substituted PPE with Proteins. A Cautionary Tale for Biosensor Applications" *Langmuir* **2005,** *21,* 7985–7989.

(117) Kuroda, K. Thermally Responsive Polymers and Their Applications. Ph.D. Thesis, MIT, Cambridge, 2003.

(118) Duncan, R.; Ringsdorf, H.; Satchi-Fainaro, R. "Polymer Therapeutics: Polymers as Drugs, Drug and Protein Conjugates and Gene Delivery Systems: Past, Present and Future Opportunities" *Adv. Polym. Sci* **2006,** *192,* 1–8.

(119) Kuroda, K.; Swager, T. M. "Fluorescent Semiconducting Polymer Conjugates of Poly(N-isopropylacrylamide) for Thermal Precipitation Assays" *Macromolecules* **2004**, *37*, 716–724.

(120) Kuroda, K.; Swager, T. M. "Synthesis of a nonionic water soluble semiconductive polymer" *Chem. Commun.* **2003**, 26–27.

(121) Stork, M.; Gaylord, B. S.; Bazan, A. J. H. G. C. "Energy Transfer in Mixtures of Water-Soluble Oligomers: Effect of Charge, Aggregation, and Surfactant Complexation" *Adv. Mater.* **2002**, *14*, 361–366.

(122) Sánchez-Delgado, R. A.; Herrera, V.; Bianchini, C.; Masi, D.; Mealli, C. "Simultaneous Coordination of Hydrides and η^1-S Thiophenes Made Possible at Iridium" *Inorg. Chem.* **1993**, *32*, 3766–3770.

(123) Choi, M.-G.; Angelici, R. J. "Sulfur-Coordinated Thiophene and Dibenzothiophene in Cp'(CO)$_2$Re(thiophene) Complexes" *Organometallics* **1991**, *10*, 2436–2442.

(124) Smith, R. C.; Tennyson, A. G.; Lippard, S. J. "Polymer-Bound Dirhodium Tetracarboxylate Films for Fluorescent Detection of Nitric Oxide" *Inorg. Chem.* **2006**, *45*, 6222–6226.

(125) Nagano, T.; Yoshimura, T. "Bioimaging of Nitric Oxide" *Chem. Rev.* **2002**, *102*, 1235–1269.

(126) Lim, M. H.; Lippard, S. J. "Fluorescence-Based Nitric Oxide Detection by Ruthenium Porphyrin Fluorophore Complexes" *Inorg. Chem.* **2004**, *43*, 6366–6370.

(127) Hilderbrand, S. A.; Lim, M. H.; Lippard, S. J. "Dirhodium Tetracarboxylate Scaffolds as Reversible Fluorescence-Based Nitric Oxide Sensors" *J. Am. Chem. Soc.* **2004**, *126*, 4972–4978.

(128) Barbosa, J.; Marqués, I.; Barrón, D.; Sanz-Nebot, V. "The application of factor analysis to solvatochromic parameters and pH$_S$ values for the standardization of potentiometric sensors in mobile phases used in liquid chromatography" *Trends Anal. Chem.* **1999**, *18*, 543–549.

(129) Coetzee, J. F.; Padmanabhan, G. R. "Properties of Bases in Acetonitrile as Solvent. IV. Proton Acceptor Power and Homoconjugation of Mono- and Diamines" *J. Am. Chem. Soc.* **1965**, *87*, 5005–5010.

(130) Martí, M. A.; Bari, S. E.; Estrin, D. A.; Doctorovich, F. "Discrimination of Nitroxyl and Nitric Oxide by Water-Soluble Mn(III) Porphyrins" *J. Am. Chem. Soc.* **2005,** *127*, 4680– 4684.

Chapter 4

Synthesis of $\{Ni(NO)\}^{10}$ and $\{Co(NO)_2\}^{10}$ Complexes Supported by Thiolate Ligands

4.1. Introduction

Nitric oxide plays many roles in biology, including signaling in the central nervous system, activation of immune response, protein regulation, and drug resistance.[1-3] In its active form, mitochondrial aconitase houses a [4Fe–4S] cluster.[4] Structural analysis of the inactive enzyme revealed a [3Fe–4S] cluster with nearly identical geometric parameters. Reaction of the EPR-silent active enzyme with NO affords an EPR spectrum indicative of the [3Fe–4S] cluster and formation of a dinitrosyl iron complex (DNIC).[5] NO also activates the redox-active transcription factor SoxR via DNIC formation from a [2Fe–2S] cluster.[6]

Previous investigations in our laboratory[7,8] and elsewhere[9] into the nitric oxide chemistry of synthetic iron thiolate complexes have provided insight into the formation of iron nitrosyl species supported by thiolate ligands in biology. The conversion of an $[Fe(SR)_4]^{2-}$ iron thiolate complex by NO into a DNIC proceeds through a mononitrosyl iron complex (MNIC). These species have not been unambiguously identified in regulatory roles, but reactions of non-heme monoiron enzymes with NO yield EPR spectra similar to those observed for the synthetic complexes.[10-12] Moreover, the conversion of a [2Fe–2S] cluster into DNICs could involve intermediate formation of two monometallic MNICs or a single dimetallic center containing two mononitrosyl iron units.

In contrast, homoleptic thiolato complexes of nickel and cobalt have never been observed in biology, and very little is known about the nitric oxide chemistry of the few well-characterized nickel and cobalt thiolate species. Methyl-coenzyme M reductase, required in the final step of methane biosynthesis, contains a nickel porphyrinoid active site.[13] Although not a substrate or known inhibitor, NO can bind to various intermediates involved in the catalytic activity of this enzyme,[14] suggesting a possible regulatory role. Similarly, the A cluster of acetyl-coenzyme A

synthase/carbon monoxide dehydrogenase contains a [4Fe–4S] cluster bridged by a cysteine to a three-coordinate homoleptic nickel thiolate center, which is connected to a four-coordinate N_2S_2-bound nickel species. Because iron-sulfur clusters react with NO, and the natural substrate for this enzyme is CO, it is plausible that nitric oxide interacts with the enzyme in vivo at iron, nickel, or sulfur. Although lacking a cobalt(II) thiolate bond, the reduced form of cobalamin binds NO very rapidly and tightly.[15] This cobalt(II) unit is essential for methionine synthesis and C_1 metabolism; treatment of cells with NO donors disrupts these functions,[16] suggesting a role for NO in regulating C_1 metabolism.

Previous reactivity studies of simple iron thiolate complexes with NO suggest that intermediates exist in the formation of multimetallic iron nitrosyl species that have not yet been observed. Low-temperature in situ spectroscopy might reveal their existence, but would not yield as much information as isolation and characterization of discrete complexes. An alternative is to study the nitric oxide chemistry of analogous thiolate complexes of the adjacent transition metals cobalt and nickel. Electronic configurations or geometries that are transient or unstable for iron may be more robust when these other metals are employed. Furthermore, studying the reactivity of simple thiolate complexes of nickel and cobalt with NO would provide insight into how nitric oxide might interact with complexes of these metals in vivo and guide potential future enzymatic investigations. We therefore initiated a program to investigate the reactions of nickel(II) and cobalt(II) thiolate complexes with NO(g), NOBF$_4$, and Ph$_3$CSNO, beginning with the homoleptic [M(SPh)$_4$]$^{2-}$ ions. Despite the simplicity of the system and the availability of the reactants for more than a decade, the previously unexplored chemistry is rich. Our results are reported here.

4.2. Experimental Section

4.2.1. Materials and Methods

Metal salts and porphyrinato complexes purchased Strem Chemicals and organic reagents obtained from Aldrich Chemical Co. or Alfa Aesar were used as received. Solvents were dried and purified by passage through alumina columns under an argon atmosphere. $(Et_4N)_2[Ni(SPh)_4]$ (**1**) and $(Et_4N)_2[Co(SPh)_4]$ (**4**) were prepared by literature methods.[17,18] Ph_3CSNO, supplied by Dr. Zachary Tonzetich in our laboratory, was prepared by a minor modification of an established procedure.[19] Air- and water-sensitive manipulations were carried out under a dry nitrogen or argon atmosphere using standard Schlenk or glovebox techniques. Nitric oxide gas was purified following a reported procedure[20] by passage first through a 2 m stainless steel coil packed with silica and cooled to −78 °C, then through an Ascarite® column. Manipulations and transfers of purified NO(g) were performed with gas-tight syringes under an inert atmosphere.

4.2.2. General Spectroscopic Considerations

NMR spectra were recorded at 22 °C on a 400 MHz Bruker Avance spectrometer and chemical shifts for ^1H and ^{13}C spectra are expressed in ppm relative to residual solvent (CD_2HCN in CD_3CN, 1.94 ppm and 1.24 ppm for ^1H and ^{13}C, respectively). FT-IR spectra were recorded on a ThermoNicolet Avatar 360 spectrophotometer running the OMNIC software. Solid samples were examined in KBr discs. Solution FT-IR spectra were acquired in a gas-tight Graseby-Specac solution cell equipped with CaF_2 windows and 0.1 mm Teflon spacers. UV-visible absorption spectra were recorded on a Cary 50 spectrophotometer at 25 °C. Stirring and temperature control were performed with a Quantum Northwest TC125 Peltier device. All

measurements were performed with a matched pair (blank and sample) of 6Q Spectrosil quartz cuvettes (Starna) with 1 cm path lengths and 3.0 mL sample solution volumes. The sample cuvette was sealed with a gas-tight Teflon-lined screw cap equipped with a septum.

4.2.3. X-Ray Crystallographic Studies

Single crystals were mounted at room temperature within microfiber loops immersed in Paratone-N oil and cooled to 110 K under a stream of cold nitrogen. Intensity data were collected on a Bruker APEX CCD diffractometer running the SMART software package, with Mo Kα radiation (λ = 0.71073 Å). Data reduction protocols and refinement were performed by Dr. Shanta Dhar. The structures were solved by direct methods and refined by using the SHELXTL[21,22] software package. Empirical absorption corrections were applied with SADABS,[23] part of the SHELXTL program package, and the structures were checked for higher symmetry by the program PLATON.[24] All non-hydrogen atoms were refined anisotropically. Hydrogen atoms were placed at calculated positions and assigned thermal parameters equal to either 1.5 (methyl hydrogen atoms) or 1.2 (non-methyl hydrogen atoms) times the thermal parameters of the atoms to which they were attached. Complex **3** crystallizes with one CH$_3$CN molecule in the asymmetric unit and the nitrogen atom was refined in two positions, each with half occupancy. Parameters for **2**, **3**, **5** and **6** are listed in **Tables 4.1–4.4**.

4.2.4. General Procedure for Mass Balance Analyses

Reactions were quenched by addition to 10 volume equiv of Et$_2$O and cooled to −30 °C for 2 h, after which the precipitate and supernatant were separated by filtration. The filtrate was transferred to a Schlenk flask, cycled out of the dry box, and stripped on a vacuum line without

heating (a room-temperature water bath suffices). The residue from the filtrate was washed 3×

with 3 mL of solvent of increasing polarity, Et_2O < THF < CH_3CN, to extract separately the

components present. Each wash was filtered into a separate tared vial, the solvent was removed,

and the mass recorded. A GC-MS of the white solid isolated from the Et_2O fraction was acquired

and compared with that of authentic Ph_2S_2. In the cases where Ph_3CSNO was used as the NO-

donating agent, a statistical mixture of Ph_2S_2, $PhSSCPh_3$, and $Ph_3CSSCPh_3$ was observed. To

calculate the percent yield of disulfide, the average MW was computed from the relative

contributions of each disulfide to the total mixture, *e.g.* for a 1:2:1 mixture: 0.25 × (Ph_2S_2) + 0.5

× ($PhSSCPh_3$) + 0.25 × ($Ph_3CSSCPh_3$) = 0.25 × (218.34) + 0.5 × (384.56) + 0.25 × (550.77) =

384.56 g mol^{-1}. The THF and CH_3CN extracts from the filtrate residue and precipitate were

analyzed separately by IR and ^1H NMR spectroscopy and combined only after confirming their

identities.

4.2.5. Syntheses

4.2.5.1. Synthesis of $(Et_4N)_2[Ni(NO)(SPh)_3]$ (2)

From 1 + NO(g). In 5 mL of CH_3CN was dissolved 75.1 mg of **1** (99.4 μmol) and into

the resulting dark red solution was bubbled 2.5 mL of NO(g) (102 μmol), affording a gradual

color change to blue-green. This reaction was allowed to stir for 30 min at room temperature and

was then added to 100 mL of Et_2O, causing the formation of a white-green suspension. After

cooling this mixture to −30 °C for 2 h, a blue-green microcrystalline product had formed along

with a light green supernatant. The precipitate was collected by filtration and the filtrate was

stripped to afford a mixture of white and blue-green solids. Mass balance analysis was performed

and from this reaction was isolated 9.0 mg of Ph_2S_2 (41 μmol, 82%) and 65 mg of **2** (96 μmol, 97%).

From 1 + Ph₃CSNO. In 5 mL of CH_3CN was dissolved 77.8 mg of **1** (103 μmol) and to the resulting dark red solution was added 32.4 mg of Ph_3CSNO (106 μmol) in 5 mL of CH_3CN, affording a gradual color change to blue-green. This reaction was allowed to stir for 30 min at room temperature and was then added to 100 mL of Et_2O, causing the formation of a white-green suspension. After cooling this mixture to −30 °C for 2 h, a blue-green microcrystalline product had formed along with a light green supernatant. The precipitate was collected by filtration and the filtrate was stripped to afford a mixture of white and blue-green solids. Mass balance analysis was performed and from this reaction was isolated 37 mg of disulfide (96 μmol, 93%) and 66 mg of **2** (98 μmol, 95%).

4.2.5.2. Characterization of 2

^{1}H NMR (CD_3CN): δ 7.54 (br d, 6 H, o-C_6H_5); 6.92 (br t, 6 H, m-C_6H_5); 6.78 (br, 3 H, p-C_6H_5); 3.15 (br q, 16 H, NCH_2CH_3); 1.20 (br t, 24 H, NCH_2CH_3) ppm. ^{13}C NMR (CD_3CN): δ 133.7, 128.1, 120.9, 120.8, 52.9 (t, NCH_2CH_3), 7.59 (NCH_2CH_3) ppm. FT-IR (KBr): 1655 (vs, v_{NO}), 1570 (vs), 1481 (s), 1468 (vs), 1450 (s), 1437 (m), 1390 (s), 1365 (w), 1336 (w), 1304 (w), 1261 (w), 1182 (w), 1173 (m), 1151 (w), 1126 (w), 1082 (s), 1063 (m), 1024 (m), 1003 (m), 993 (m), 964 (w), 904 (vw), 885 (w), 839 (vw), 783 (m), 739 (vs), 694 (vs), 617 (vw), 548 (w), 482 (m), 428 (w) cm^{-1}. FT-IR (CH_3CN, CaF_2): v_{NO} = 1756 (vs) cm^{-1}. UV-vis in CH_3CN, λ (ε) in nm ($M^{-1}cm^{-1}$): 372 (6260), 423 (sh, 2930), 812 (1380). Anal. calcd for $C_{34}H_{55}N_3OS_3Ni$: C, 60.35; H, 8.19; N, 6.21. Found: C, 59.54; H, 8.13; N, 6.09. Blue-green plates (0.14 × 0.09 × 0.04 mm) suitable for X-ray diffraction were grown by cooling a saturated solution of **2** in CH_3CN at room

temperature to −30 °C for 2 weeks.

4.2.5.3. Synthesis of (Et₄N)₂[Ni₂(NO)₂(μ–SPh)₂(SPh)₂] (3)

From 1 + NOBF₄. In 5 mL of CH₃CN was dissolved 156 mg of **1** (206 μmol) and to the resulting dark red solution was added 23.1 mg of NOBF₄ (198 μmol) in 5 mL of CH₃CN, affording a gradual color change to dark brown-green. This reaction was allowed to stir for 30 min at room temperature and was then added to 100 mL of Et₂O, causing the formation of a white-brown suspension. After cooling this mixture to −30 °C for 2 h, a dark brown microcrystalline product had formed along with a dark green supernatant. Mass balance analysis was performed and from this reaction was isolated 41 mg of Ph₂S₂ (188 μmol, 95%), 40 mg of Et₄NBF₄ (184 μmol, 93%), and 86 mg of **3** (98 μmol, 99%).

From 2 + Me₃OBF₄. In 5 mL of CH₃CN was dissolved 67.7 mg of **2** (100 μmol) and to the resulting dark blue-green solution was added 14.7 mg of Me₃OBF₄ (99.4 μmol) in 3 mL of CH₃CN, affording a gradual color change to dark green. This reaction was allowed to stir for 30 min at room temperature and was then added to 100 mL of Et₂O, causing the formation of a white-green suspension. After cooling this mixture to −30 °C for 2 h, a white solid had formed along with a dark green supernatant. Mass balance analysis was performed and from this reaction was isolated 21 mg of Et₄NBF₄ (97 μmol, 98%) and 43 mg of **3** (49 μmol, 98%).

4.2.5.4. Characterization of 3

^{1}H NMR (CD₃CN): δ 7.82 (br, *o*-C₆H_5, 8H); 7.13 (br, *m*-C₆H_5, 8H); 6.92 (br, *p*-C₆H_5, 2H); 3.12 (q, NCH_2CH₃, 16H); 1.17 (tt, NCH₂CH_3, 24H) ppm. ^{13}C NMR (CD₃CN): δ 134.1, 137.8, 128.5, 123.1, 53.0 (t, NCH₂CH₃), 7.62 (NCH₂CH₃) ppm. FT-IR (KBr): 1709 (vs, ν$_{NO}$),

1574 (s), 1471 (s), 1433 (m), 1392 (m), 1367 (w), 1338 (vw), 1302 (w), 1265 (w), 1182 (w), 1171 (m), 1082 (s), 1065 (m), 1055 (m), 1024 (m), 1001 (m), 976 (w), 895 (w), 854 (w), 789 (m), 742 (vs), 694 (vs), 671 (vw), 615 (vw), 569 (w), 482 (m), 426 (w). FT-IR (THF, CaF$_2$): ν_{NO} = 1751 (vs), 1721 (vs) cm^{-1}. UV-vis in CH$_3$CN, λ in nm (ε in M^{-1}cm^{-1}): 365 (7990), 431 (sh, 3360), 639 (sh, 989), 808 (1650). Anal. calcd for C$_{41}$H$_{61.5}$N$_{4.5}$O$_2$S$_4$Ni$_2$: C, 55.01; H, 6.93; N, 7.04. Found: C, 54.64; H, 6.60; N, 7.34. Dark green blocks (0.20 × 0.20 × 0.05 mm) suitable for X-ray diffraction were grown by vapor diffusion of Et$_2$O into a solution of **3** in CH$_3$CN at −30 °C over 3 days.

4.2.5.5. Synthesis of (Et$_4$N)[Co(NO)$_2$(SPh)$_2$] (5)

From NO(g). In 5 mL of CH$_3$CN was dissolved 75.6 mg of **4** (100 μmol) and into the resulting dark green solution was bubbled 10.0 mL of NO(g) (406 μmol), affording a gradual color change to dark brown. This reaction was allowed to stir for 30 min at room temperature and was then added to 100 mL of Et$_2$O, causing the formation of a white-brown suspension. After cooling this mixture to −30 °C for 2 h, a dark brown microcrystalline product had formed along with a white precipitate and a dark brown supernatant. The solids were collected by filtration and the filtrate was stripped to afford a mixture of white and dark brown solids. Mass balance analysis was performed and from this reaction was isolated 10 mg of disulfide (46 μmol, 92%), 24 mg of Et$_4$NSPh (100 μmol, 100%), and 41 mg of **5** (88 μmol, 88%).

From Ph$_3$CSNO. In 5 mL of CH$_3$CN was dissolved 76.1 mg of **4** (101 μmol) and to the resulting dark green solution was added 62.0 mg of Ph$_3$CSNO (204 μmol) in 5 mL of CH$_3$CN, affording a gradual color change to dark brown. The reaction was allowed to stir for 30 min at room temperature and was then added to 100 mL of Et$_2$O, causing the formation of a white-

brown suspension. After cooling this mixture to −30 °C for 2 h, a dark brown microcrystalline product had formed along with a dark brown supernatant. The precipitate was collected by filtration and the filtrate was stripped to afford a commixture of white and dark brown solids. Mass balance analysis was performed and from this reaction was isolated 56 mg of disulfide (85 μmol, 84%), 19 mg of Et$_4$NSPh (79 μmol, 77%), and 44 mg of **5** (93 μmol, 92%).

From NOBF$_4$. In 5 mL of CH$_3$CN was dissolved 76.8 mg of **4** (102 μmol) and to the resulting dark green solution was added 11.8 mg of NOBF$_4$ (101 μmol) in 5 mL of CH$_3$CN, affording a color change to dark brown with a purple colloid. This reaction was allowed to stir for 30 min at room temperature and was then added to 100 mL of Et$_2$O, causing the formation of a white-brown suspension. After cooling this mixture to −30 °C for 2 h, a dark brown microcrystalline product had formed along with a dark brown supernatant. Mass balance analysis was performed and from this reaction was isolated 11 mg of Ph$_2$S$_2$ (50 μmol, 100%), 22 mg of Et$_4$NBF$_4$ (101 μmol, 100%), 21 mg of **5** (45 μmol, 90%), and an intractable dark purple solid.

4.2.5.6. Characterization of 5

^{1}H NMR (CD$_3$CN): δ = 7.30 (dd, *o*-C$_6$H$_5$, 4H), 7.00 (tt, *m*-C$_6$H$_5$, 4H), 6.84 (tt, *p*-C$_6$H$_5$, 2H), 3.14 (br q, NC*H*$_2$CH$_3$, 8H), 1.18 (br t, NCH$_2$C*H*$_3$, 12H) ppm. ^{13}C NMR (CD$_3$CN): δ = 148.9, 133.2, 128.3, 122.5, 53.0 (t, N*C*H$_2$CH$_3$), 7.68 (NCH$_2$*C*H$_3$) ppm. FT-IR (KBr): ν = 1756 (vs, ν$_{NO}$), 1678 (vs, ν$_{NO}$), 1573 (s), 1558 (m), 1479 (s), 1473 (s), 1460 (s), 1433 (s), 1390 (s), 1374 (w), 1366 (m), 1335 (w), 1311 (w), 1295 (w), 1265 (w), 1170 (s), 1083 (s), 1067 (m), 1056 (m), 1020 (m), 998 (m), 895 (w), 844 (w), 781 (m), 753 (s), 749 (s), 696 (s), 480 (w), 421 (w) cm^{-1}. FT-IR (THF, CaF$_2$): ν$_{NO}$ = 1769 (vs), 1699 (vs) cm^{-1}. UV-vis in CH$_3$CN, λ (ε) in nm (M^{-1}cm^{-1}): 346 (sh, 6060). Anal. calcd for C$_{20}$H$_{30}$N$_3$O$_2$S$_2$Co: C, 51.38; H, 6.47; N, 8.99. Found:

C, 51.65; H, 6.58; N, 8.79. Dark brown-black needles (0.25 × 0.08 × 0.03 mm) suitable for X-ray diffraction were grown by vapor diffusion of Et_2O into a solution of **5** in THF at -30 °C overnight.

4.2.5.7. Synthesis of $[Co_3(NO)_6(\mu\text{–}SPh)_3]$ (**6**)

In 5 mL of CH_3CN was dissolved 70.0 mg of **5** (150 μmol) and to the resulting dark brown solution was added 22.7 mg of Me_3OBF_4 (153 μmol) in 3 mL of CH_3CN, affording a gradual color change to dark red-orange. This reaction was allowed to stir for 30 min at room temperature and was then added to 100 mL of Et_2O, causing the formation of cloudy red-orange solution. After cooling this mixture to -30 °C for 2 h, a light grey precipitate had formed along with a red-orange supernatant. Mass balance analysis was performed and from this reaction was isolated 32 mg of Et_4NBF_4 (147 μmol, 98%) and 33 mg of **6** (48 μmol, 96%).

4.2.5.8. Characterization of **6**

^1H NMR (CD_3CN): δ = 7.53 (d, o-C_6H_5, 6H), 7.28 (t, m-C_6H_5, 6H), 7.19 (t, p-C_6H_5, 3H) ppm. ^{13}C NMR (CD_3CN): δ = 134.4, 130.5, 128.3 ppm. FT-IR (KBr): ν = 1840 (s, NO), 1817 (s, NO), 1779 (s, NO), 1744 (s, NO), 1575 (vw), 1473 (w), 1435 (w), 1385 (vw), 1295 (vw), 1261 (w), 1152 (vw), 1011 (vw), 1080 (vw), 1066 (w), 1021 (w), 999 (vw), 800 (w), 740 (vs), 687 (s), 479 (m) cm^{-1}. FT-IR (THF, CaF_2): ν_{NO} = 1844 (m sh), 1819 (vs), 1780 (vs), 1764 (s sh) cm^{-1}. UV-vis in CH_3CN, λ (ε) in nm ($M^{-1}cm^{-1}$): 325 (sh, 12500), 421 (br sh, 6670), 656 (sh, 757). Anal. calcd for $C_{18}H_{15}N_6O_6S_3Co_3$: C, 31.59; H, 2.21; N, 12.28. Found: C, 31.28; H, 2.25; N, 12.20. Dark brown-red plates (0.20 × 0.20 × 0.02 mm) suitable for X-ray diffraction were grown by cooling a saturated solution of **6** in Et_2O at room temperature to -30 °C for 1 week.

Table 4.1. Summary of crystal data, intensity collection, and refinement parameters for **2**.

	2
formula	$C_{34} H_{55} N_3 Ni O S_3$
MW (g mol^{-1})	676.60
morphology	blue-green plates
dimensions (mm)	$0.20 \times 0.20 \times 0.08$
crystal system	orthorhombic
space group	$Pca2_1$
a (Å)	17.879(5)
b (Å)	12.945(5)
c (Å)	31.057(5)
V (Å^3)	7188(4)
Z	8
ρ_{calc} (g cm^{-3})	1.251
μ (mm^{-1})	0.744
F(000)	2912
θ range (deg)	2.34 – 25.00
total / unique reflections	56522 / 12656
completeness to 2θ (%)	99.8
data / restraints / parameters	12656 / 1 / 745
GoOF	1.230
R_1 [a]	0.0841
wR_2 [b]	0.1717
Largest diff. peak & hole (e Å^{-3})	1.278 and −0.888

[a] $R_1 = \Sigma \mid |F_o| - |F_c| \mid / \Sigma |F_o|$; [b] $wR_2 = \{\Sigma [w(F_o^2 - F_c^2)^2] / \Sigma [w(F_o^2)^2]\}^{1/2}$

Table 4.2. Summary of crystal data, intensity collection, and refinement parameters for **3**.

	3•CH₃CN
formula	$C_{42} H_{60} N_5 O_2 S_4 Ni_2$
MW (g mol⁻¹)	912.61
morphology	dark green blocks
crystal system	monoclinic
dimensions (mm)	$0.25 \times 0.25 \times 0.20$
space group	$P2_1/n$
a (Å)	11.428(5)
b (Å)	12.295(5)
c (Å)	16.705(7)
β (deg)	106.599(6)
V (Å³)	2249.4(15)
Z	2
ρ_{calc} (g cm⁻³)	1.347
μ (mm⁻¹)	1.063
F(000)	966
θ range (deg)	2.09 – 28.40
total / unique reflections	30222 / 5585
completeness to 2θ (%)	98.6
data / restraints / parameters	5585 / 0 / 373
GoOF	1.169
R₁ [a]	0.0685
wR₂ [b]	0.1022
Largest diff. peak & hole (e Å⁻³)	0.495 and −0.423

[a] $R_1 = \Sigma \, | \, |F_o| - |F_c| \, | \, / \, \Sigma \, |F_o|$; [b] $wR_2 = \{ \Sigma \, [w(F_o^2 - F_c^2)^2] \, / \, \Sigma \, [w(F_o^2)^2] \}^{1/2}$

Table 4.3. Summary of crystal data, intensity collection, and refinement parameters for **5**.

	5
formula	$C_{20} H_{30} N_3 O_2 S_2 Co$
MW (g mol^{-1})	467.53
morphology	brown-black needles
dimensions (mm)	$0.25 \times 0.08 \times 0.03$
crystal system	monoclinic
space group	$P2_1/c$
a (Å)	13.4199(17)
b (Å)	16.051(2)
c (Å)	11.0093(14)
β (deg)	108.937(6)
V (Å^3)	2243.0(5)
Z	4
ρ_{calc} (g cm^{-3})	1.384
μ (mm^{-1})	0.971
F(000)	984
θ range (deg)	2.33 – 28.30
total / unique reflections	9719 / 5495
completeness to 2θ (%)	98.6
data / restraints / parameters	5495 / 0 / 257
GoOF	1.080
R_1 [a]	0.0787
wR_2 [b]	0.1104
Largest diff. peak & hole (e Å^{-3})	0.886 and –0.402

[a] $R_1 = \Sigma \mid \mid F_o \mid - \mid F_c \mid \mid / \Sigma \mid F_o \mid$; [b] $wR_2 = \{ \Sigma [w(F_o^2 - F_c^2)^2] / \Sigma [w(F_o^2)^2] \}^{1/2}$

Table 4.4. Summary of crystal data, intensity collection, and refinement parameters for **6**.

	6
formula	$C_{18} H_{15} N_6 O_6 S_3 Co_3$
MW (g mol^{-1})	684.33
morphology	brown-red plates
dimensions (mm)	$0.20 \times 0.20 \times 0.02$
crystal system	orthorhombic
space group	Pbca
a (Å)	17.050(3)
b (Å)	9.0194(15)
c (Å)	32.227(6)
V (Å^3)	4955.8(15)
Z	8
ρ_{calc} (g cm^{-3})	1.834
μ (mm^{-1})	2.285
F(000)	2736
θ range (deg)	2.39 − 28.44
total / unique reflections	47123 / 6185
completeness to 2θ (%)	99.1
data / restraints / parameters	6185 / 0 / 385
GoOF	1.052
R_1 [a]	0.0685
wR_2 [b]	0.0995
Largest diff. peak & hole (e Å^{-3})	0.993 and −0.465

[a] $R_1 = \Sigma \mid |F_o| - |F_c| \mid / \Sigma |F_o|$; [b] $wR_2 = \{\Sigma [w(F_o^2 - F_c^2)^2] / \Sigma [w(F_o^2)^2]\}^{1/2}$

4.2.6. NO Transfer Reactions

4.2.6.1. UV-vis Spectroscopic Parameters

Using the Cary scanning kinetics software, the scan window range was set to 800–200 nm, with 50 ms averaging time, 1.00 nm resolution, 1200 nm/min scan rate, and scans were acquired every 60 s for 2 h. The first scan of each experiment consisted of metalloporphyrin alone. An aliquot of metal nitrosyl was added and the solution was vigorously shaken for 3 s then allowed to stand for an additional 7 s before beginning the second scan. Thus, a total of 10 s elapsed between injection of the metal nitrosyl and the beginning of the second scan.

4.2.6.2. Metal Nitrosyl Reactions with [Fe(TPP)Cl]

A 762 μM stock solution of [Fe(TPP)Cl] in THF was prepared, from which a 7.62 μM working solution in THF was obtained. A 2.3 mM stock solution of metal nitrosyl (**2** in CH$_3$CN, **3** or **5** in THF) was prepared. After acquiring a blank in THF, the spectrum of a 3 mL aliquot of the working solution of [Fe(TPP)Cl] was obtained to verify the concentration by measuring the absorption of the Soret band (λ = 417 nm, ε = 1.11 × 10^5 M^{-1}cm^{-1}). Simple NO coordination would afford [Fe(TPP)(NO)Cl], a process that does not significantly alter the UV-vis spectrum in the 400–1000 nm region.[25] A reductive nitrosylation reaction would afford [Fe(TPP)(NO)] with a concomitant hypsochromic shift in the Soret band (λ = 405 nm, ε = 1.00 × 10^5 M^{-1}cm^{-1}).[26]

4.2.6.3. Reaction of 2 with [Fe(TPP)Cl]

In 5 mL of THF was dissolved 70.9 mg of [Fe(TPP)Cl] (101 μmol) and to the resulting dark red solution was added 67.1 mg of **2** (99.2 μmol) in 3 mL of CH$_3$CN, affording no

perceptible color change. This reaction was allowed to stir for 30 min at room temperature and was then added to 100 mL of Et_2O causing the formation of a red-brown solution. After cooling this mixture to -30 °C for 2 h, a sticky dark green precipitate had formed along with a red-brown supernatant. No Ph_2S_2 was isolated from the supernatant and the IR spectrum of the dark green precipitate was identical to that of authentic **3**, with an NO stretch at 1709 cm^{-1}. Mass balance analysis could not be performed due to the similar solubilities of **3** and the porphyrin-containing product.

4.2.6.4. NO transfer to [Co(TPP)]

A 2.01 mM stock solution of [Co(TPP)] in THF was prepared, from which a 5.03 μM working solution in THF was obtained. A 2.0 mM stock solution of **2** in CH_3CN was prepared. After acquiring a blank in THF, the spectrum of a 3 mL aliquot of the working solution of [Co(TPP)] was obtained to verify the concentration by measuring the absorption of the Soret band (λ = 409 nm, ε = 2.05 × 10^5 $M^{-1}cm^{-1}$).[27] A simple NO coordination would afford [Co(TPP)(NO)] with a concomitant bathochromic shift in the Soret band and increase in absorptivity (λ = 411 nm, ε = 1.77 × 10^6).[28] In comparison, the Soret band for cobalt-reconstituted guanylyl cyclase [Co(sGC)] (λ = 401 nm, ε = 1.14 × 10^5 $M^{-1}cm^{-1}$) shifts hypsochromically with a decrease in absorptivity upon binding NO (λ = 390 nm, ε = 1.07 × 10^5 $M^{-1}cm^{-1}$).[29]

4.3. Results and Discussion

4.3.1. Synthesis and Properties of the First Anionic {Ni(NO)}^{10} Complex (2)

Addition of a stoichiometric amount of Ph_3CSNO to a solution of **1** in CH_3CN caused an immediate color change from dark red to dark blue-green. Mass balance analysis indicated that one equiv of disulfide and one equiv of $(Et_4N)_2[Ni(NO)(SPh)_3]$ (**2**) were produced per equiv of **1** consumed (**Scheme 4.1**). Compound **2** is diamagnetic and ^1H NMR spectroscopy reveals a 2:3 ratio of Et_4N^+ to PhS^- protons (**Table 4.5**). The NO stretch for **2** occurs at 1655 cm^{-1} in the solid state (KBr) but shifts to 1756 cm^{-1} in solution (CH_3CN). Monometallic {Ni(NO)}^{10} complexes can exhibit solvent-dependent variations in v_{NO} by up to 50 cm^{-1} from the value measured in the solid state.[30] The source of this behavior is believed to be a result of a Lewis acid-base interaction between the nitrosyl and solvent,[31] but the limited solubility of **2** precludes a study of

Scheme 4.1. Syntheses of **2** and **3**.
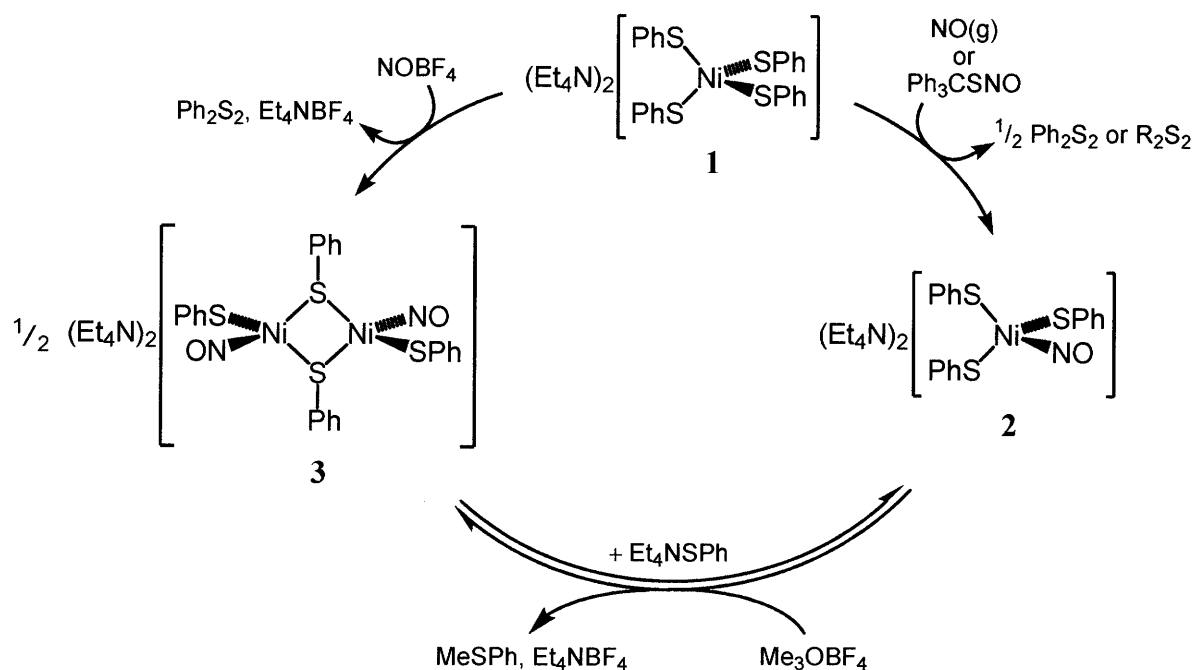
ν_{NO} dependence on solvent acceptor number. Dissolving **2** in CH_3CN, removing the solvent in vacuo, and acquiring the IR spectrum in KBr reveals the same ν_{NO} band at 1655 cm^{-1}. According to the Enemark-Feltham convention,[32] **2** has a $\{Ni(NO)\}^{10}$ core and complexes of this type are well-known. Other four-coordinate, monometallic $\{Ni(NO)\}^{10}$ complexes are diamagnetic and display a range of NO stretching frequencies from 1558 to 1867 cm^{-1} (avg = 1742 ± 68 cm^{-1}).[30,33–44] Presumably, the ν_{NO} value in KBr is significantly below average because the $\{Ni(NO)\}^{10}$ core is supported by three thiolates in a dianionic molecule, whereas the other complexes are cationic or charge neutral. Complex **2** contains the first reported example of a $\{Ni(NO)\}^{10}$ species contained within an anionic molecule.

Table 4.5. ^1H NMR chemical shifts for PhS ligands and ratio of Et_4N:PhS integrals for **1–6**.

	ortho	meta	para	Et_4N:PhS
1	1.91	21.7	−12.5	1:2
2	7.54	6.92	6.78	2:3
3	7.82	7.13	6.92	1:2
4	17.3	−24.5	−33.0	1:2
5	7.30	7.00	6.84	1:2
6	7.54	7.28	7.19	—

A preliminary reactivity study of **1** with *S*-nitroso-*N*-acetylpenicillamine (SNAP) also afforded **2**, judging by FT-IR spectroscopy, but the insolubility of SNAP in CH_3CN prevented reaction homogeneity and accurate mass balance analysis. *S*-Nitrosothiols (RSNOs) like SNAP are prevalent in biology and believed by some to be the predominant carrier of NO. Nevertheless, the mechanism by which an RSNO delivers NO is controversial.[45–50] The two limiting cases are RSNO delivery of NO, termed nitrosylation, and delivery of NO^+, termed nitrosation.[51] To determine whether the RSNO species were behaving as NO or NO^+ donors, we compared the reactivity of Ph_3CSNO and SNAP with that of NO(g). Addition of stoichiometric

NO(g) to **1** afforded slow conversion to 0.5 equiv of Ph_2S_2 and one equiv of **2** (**Scheme 4.1**). Because the reaction of **1** with either Ph_3CSNO or SNAP yielded **2**, we conclude that these *S*-nitrosothiols are functioning as NO donors and such behavior has been observed previously by us[8] and others.[9]

Slow vapor diffusion of Et_2O into a solution of **2** in CH_3CN at –30 °C over 2 weeks afforded crystals suitable for X-ray diffraction, which confirmed the structural assignment of **2** (**Figure 4.1**). The average nickel nitrosyl structural parameters for **2** (Ni–N–O = 156.6°, N–O = 1.171 Å, Ni–N = 1.663 Å, **Table 4.6**) fall within the range of reported values for other four-coordinate, monometallic $\{Ni(NO)\}^{10}$ complexes (Ni–N–O = 149.1–180.0°, avg = 165.8 ± 11.1°; N–O = 1.120–1.185 Å, avg = 1.160 ± 0.017 Å; Ni–N = 1.581–1.692 Å, avg = 1.645 ± 0.032 Å).[30,33–44] Because the mean Ni–N–O angle for **2** is more acute than average, and the N–O and Ni–N distances are longer, we conclude that the nickel atom in **2** provides greater π-backbonding to the nitrosyl. This result is consistent with the anionic environment and ligand donation ability in the nickel nitrosyl fragment of **2**, whereas other reported $\{Ni(NO)\}^{10}$ complexes are neutral or cationic and are not bound by thiolates.

Of the structurally characterized, four-coordinate, monometallic $\{Ni(NO)\}^{10}$ complexes, only two are supported by sulfur donor ligands.[33,37] For comparison, the structural parameters for these complexes and their v_{NO} values are reported in **Table 4.6**. Complexes **IIa–b** both contain $\{Ni(NO)\}^{10}$ cores supported by monoanionic, $\kappa^3\text{-}S_3$ ligands and are arranged according to increasing v_{NO}. Unfortunately, no clear trends are apparent in this comparison. Complex **2** most closely resembles **IIa** based on the M–N bond length and the S–M–N and S–M–S angles. However, the N–O and M–S distances in **2** are most similar to those in **IIb**, whereas the Ni–N–O angle and solid state NO stretching energy are substantially different from the other complexes
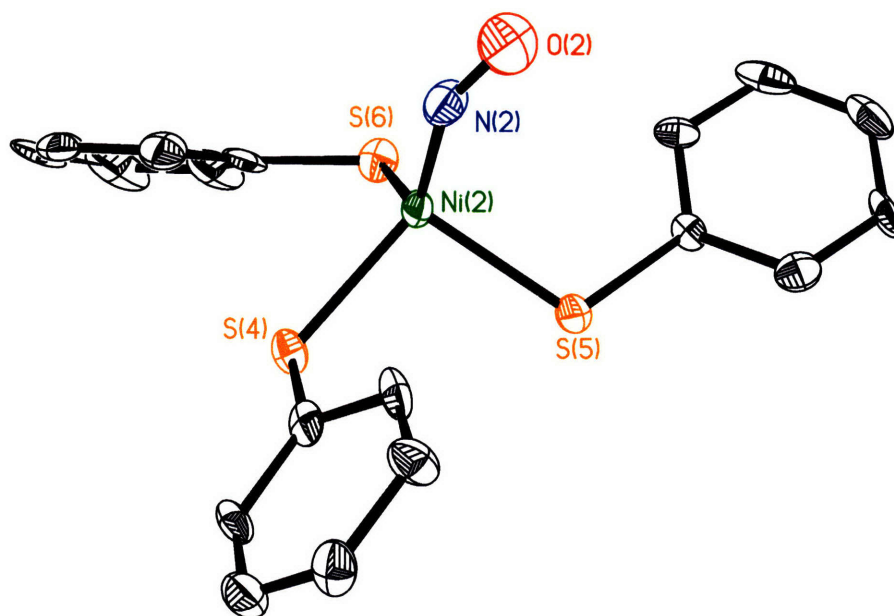
Figure 4.1. ORTEP diagram showing 50% probability thermal ellipsoids and selected atom labels for one of the two crystallographically distinct molecules of **2** in the crystal lattice. The Et_4N^+ cations and H atoms are omitted for clarity. Selected bond distances (Å) and angles (deg): N1–O1, 1.178(9); Ni1–N1, 1.651(7); Ni1–S1, 2.339(2); Ni1–S2, 2.307(2); Ni1–S3, 2.279(2); Ni1–N1–O1, 159.0(6); S1–Ni1–N1, 121.6(2); S2–Ni1–N1, 119.9(2); S3–Ni1–N1, 105.5(2); S1–Ni1–S2, 99.67(7); S1–Ni1–S3, 106.82(7); S2–Ni1–S3, 101.14(7); N2–O2, 1.164(8); Ni2–N2, 1.674(7); Ni2–S4, 2.295(2); Ni2–S5, 2.270(2); Ni2–S6, 2.317(2); Ni2–N2–O2, 154.2(6); S4–Ni2–N2, 126.0(2); S5–Ni2–N2, 103.0(2); S6–Ni2–N2, 118.2(2); S4–Ni2–S5, 98.71(8); S4–Ni2–S6, 99.19(8); S5–Ni2–S6, 109.80(8).

comprising $\{Ni(NO)\}^{10}$ cores bound to three sulfur atoms. A similar lack of any straightforward trend in structural parameters is also observed for manganese nitrosyls,[52] for which the ν_{NO} is recommended as the most reliable measure of the {M(NO)} electron count. Complexes containing $\{Cu(NO)\}^{11}$ cores are very rare, and the structurally characterized examples with C_{3v} geometries exhibit ν_{NO} values ranging from 1698 to 1742 cm^{-1} (avg = 1712 ± 18 cm^{-1}).[53,54] Because $\{Cu(NO)\}^{11}$ formally contains one more electron in the metal nitrosyl unit than

{Ni(NO)}^{10}, complexes with this unit should display lower v_{NO} values. This behavior is observed for the average NO stretching energies for {Cu(NO)}^{11} and {Ni(NO)}^{10} complexes with similar geometries (1712 cm^{-1} vs. 1742 cm^{-1}). However, complex **2** exhibits a v_{NO} value in KBr nearly 50 cm^{-1} lower than the lowest measured value for a {Cu(NO)}^{11} complex, despite the latter having greater electron density within the metal nitrosyl unit. These results suggest that the electronic properties of a {M(NO)} core depend heavily on the electron donating ability of the ligands and the overall charge of the molecule.

Table 4.6. List of Bond Lengths (Å), Angles (deg) and v_{NO} (cm^{-1}) Values for **2** and **IIa–c**.[a]

	2[b,c]	**IIa**	**IIb**	**IIc**
N–O	1.171(10)	1.131(4)	1.173(2)	1.169(6)
M–N	1.663(16)	1.665(3)	1.683(2)	1.682(5)
M–S	2.328(16)	2.3503(11)	2.2915(5)	2.2780(13)
	2.301(8)	2.3432(11)	2.2838(5)	2.2696(12)
	2.275(6)	2.3190(10)	2.2775(5)	2.2670(14)
M–N–O	156.6(34)	173.9(4)	167.0(2)	164.6(5)
S–M–N	123.8(31)	121.34(11)	130.48(7)	116.52(16)
	119.1(12)	114.47(10)	117.99(6)	109.19(18)
	104.3(18)	114.01(11)	117.48(8)	108.69(18)
S–M–S	108.3(21)	103.87(4)	95.67(2)	109.47(5)
	100.2(14)	101.34(4)	94.54(2)	108.35(5)
	99.19(7)	99.30(4)	92.99(2)	103.87(5)
v_{NO} (solid)	1655	—	1785	—
v_{NO} (soln)	1756	1752	—	1732

[a]**IIa** = [Ni(NO)(C$_{30}$H$_{28}$BN$_6$S$_3$)],[37] **IIb** = [Ni(NO)(C$_{21}$H$_{38}$BS$_3$)],[33] **IIc** = (Et$_4$N)[Fe(NO)(SPh)$_3$].[9] [b]Structural parameters are averaged from the two crystallographically distinct molecules. [c]Numbers in parentheses represent standard deviation from mean, not ESD values.

Interestingly, **2** has structural characteristics similar to those of the MNIC (Et$_4$N)[Fe(NO)(SPh)$_3$] (**IIc**, **Table 4.6**).[9] The most notable differences between the two structures are a more acute M–N–O angle in **2**, a greater average M–S distance (2.301 Å vs. 2.271 Å), and a more acute average S–M–S angle (102.7° vs. 107.2°). These differences are consistent with the

fact that **2** contains a $\{Ni(NO)\}^{10}$ core and **IIc** a $\{Fe(NO)\}^7$ core; greater electron density in the $\{M(NO)\}$ unit will result in more π-backbonding. As the backbonding increases, the nitrosyl will become more reduced and adopt a more bent geometry. Furthermore, as the M–N bond develops multiple bonding character, its length will decrease and the thiolates will be pulled closer together and lie farther away from the metal atom.

4.3.2. Synthesis and Properties of 3

Treatment of a solution of **1** in CH_3CN with 1 equiv of $NOBF_4$ produced an immediate color change from dark red to brown-green. Product and mass balance analysis revealed that 1 equiv of Ph_2S_2, 1 equiv of Et_4NBF_4, and 0.5 equiv of $(Et_4N)_2[Ni_2(NO)_2(\mu-SPh)_2(SPh)_2]$ (**3**) were produced per equiv of **1** consumed (**Scheme 4.1**). Complex **3** is also diamagnetic, and ^1H NMR spectroscopy revealed a 1:2 ratio of Et_4N^+ to PhS^- protons; the aryl resonances of **3** are distinct from those in **2** (**Table 4.5**). In the solid state (KBr), only one NO stretch is observed for **3** at 1709 cm^{-1}, but in THF solution, **3** displays two NO stretching modes at 1751 and 1721 cm^{-1}. Like **2**, complex **3** contains a $\{Ni(NO)\}^{10}$ core, and dimetallic complexes of this unit have been previously reported. There are examples of structurally characterized diamagnetic complexes comprising two $\{Ni(NO)\}^{10}$ moieties bridged by anionic[55–57] or neutral[58] ligands with NO stretching frequencies ranging from 1718 to 1817 cm^{-1} (avg = 1771 ± 29 cm^{-1}). Furthermore, some of these complexes display one v_{NO} value in the solid state and two in solution.[57] For example, the $[Ni_2(NO)_2(\mu-N_2C_5H_7)_2(PPh_3)_2]$ dimer, consisting of two $\{Ni(NO)\}^{10}$ units bridged by 3,5-dimethylpyrazolates, exhibits one NO stretching mode at 1728 cm^{-1} in a Nujol mull and two at 1804 and 1758 cm^{-1} in cyclohexane solution. The solid state IR spectrum of **3** suggests a C_i geometric configuration with *anti* nitrosyls and *trans* bridging thiolates. Only this arrangement

of nitrosyl and thiolate ligands would afford an IR spectrum with one NO stretching band, of A_u symmetry. The other possible arrangements, *anti* nitrosyls and *cis* thiolates (C_s), *syn* nitrosyls and *cis* thiolates (C_{2v}), or *syn* nitrosyls and *trans* thiolates (C_s), are expected to display two IR active NO stretching modes. Dipole-dipole interaction between solvent and **3** may allow the symmetric (A_g) stretching mode to become IR active, or a different nitrosyl/thiolate geometric arrangement may be preferred in solution.

Reaction of **2** with 1 equiv of Me_3OBF_4 in CH_3CN yielded 0.5 equiv of **3** and 1 equiv of Et_4NBF_4 (**Scheme 4.1**). Because no Ph_2S_2 is formed, we presume that Me_3OBF_4 converts one PhS^- ligand to MeSPh, which cannot not be isolated or quantified due to its volatility. Additionally, cooling a saturated solution of **3** in THF to −30 °C afforded **2**. This result is not surprising given that **2** is THF-insoluble and could be formed by simple association of Et_4NSPh with **3**. Even if the equilibrium favors **3**, **2** will selectively crystallize from THF solution and its generation will be irreversible. Qualitative IR analysis of the reaction of **3** with Et_4NSPh similarly indicated formation of **2**.

Crystals suitable for X-ray diffraction were grown from vapor diffusion of Et_2O into a solution of **3** in CH_3CN at −30 °C over 3 days. The structure confirms the assignment of **3** as containing a thiolate-bridged dimer of two $\{Ni(NO)\}^{10}$ units (**Figure 4.2**). The nickel nitrosyl structural parameters for **3**, Ni–N–O = 161.5(2)°, N–O = 1.168(3) Å, Ni–N = 1.657(2) Å (**Table 4.7**), fall close to or within the range of values reported for analogous complexes containing two $\{Ni(NO)\}^{10}$ cores bridged by anionic or neutral ligands (Ni–N–O = 166.4–178.9°, avg = 172.6 ± 5.4°; N–O = 1.13–1.183 Å, avg = 1.154 ± 0.024 Å; Ni–N = 1.591–1.670 Å, avg = 1.638 ± 0.033 Å).[55–58] There are no examples of dimers of $\{Ni(NO)\}^{10}$ units supported by terminal or bridging thiolates. The closest analog of **3** that has been structurally characterized,
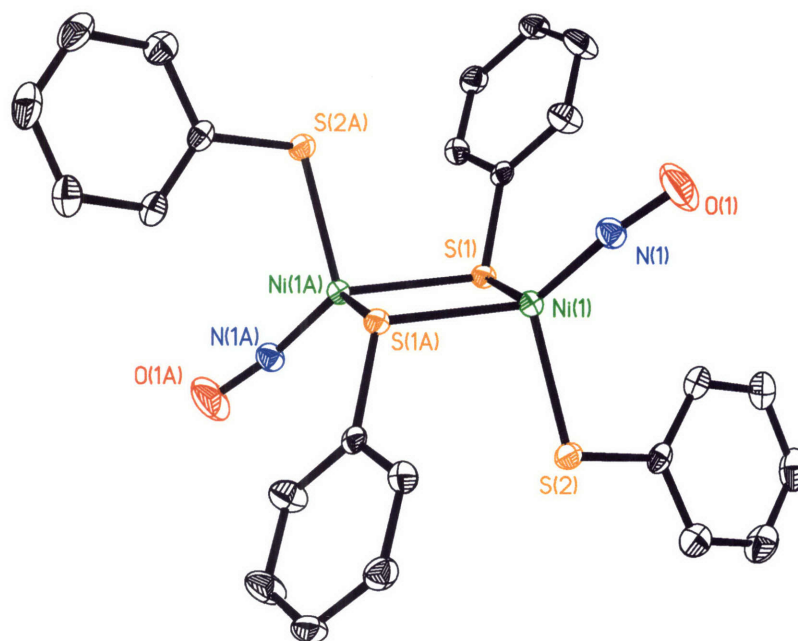
Figure 4.2. ORTEP diagram showing 50% probability thermal ellipsoids and selected atom labels for **3**. The Et_4N^+ cations, H atoms, and disordered CH_3CN have been omitted for clarity. Selected bond distances (Å) and angles (deg): N1–O1, 1.168(3); Ni1–N1, 1.657(2); Ni1–S1, 2.2923(9); Ni1–S1A, 2.3320(10); Ni1–S2, 2.2733(11); Ni1–N1–O1, 161.5(2); S1–Ni1–N1, 118.56(8); S1A–Ni1–N1, 127.12(9); S2–Ni1–N1, 116.58(8); S1–Ni1–S1A, 89.24(4); S1–Ni1–S2, 100.80(3); S1A–Ni1–S2, 98.65(3).

$[Ni(NO)_2(\mu–C_{10}H_{10}P_3)_2(PPh_3)_2]$ (**IIIa**), contains two $\{Ni(NO)\}^{10}$ cores bridged by two triphospholyl ligands (**Table 4.7**).[55] Despite the fact that the bridging and terminal ligands are different, and that **3** is dianionic whereas **IIIa** is neutral, the average bond lengths are nearly identical. However, the average S–Ni–N angle in **3** (120.8°) is more obtuse than the average P–Ni–N angle in **IIIa** (114.6°), and the average S–Ni–S angle in **3** is more acute than the average P–Ni–P angle in **IIIa** (96.23° vs. 103.6°). Although both **3** and **IIIa** contain dimers of $\{Ni(NO)\}^{10}$ cores, complex **3** has an overall 2– charge and is supported by thiolate ligands. As a

result, the nickel atom in **3** will be more electron rich than in **IIIa**, resulting in greater π-backbonding.

Table 4.7. List of Bond Lengths (Å), Angles (deg) and v_{NO} (cm^{-1}) Values for **3** and **IIIa–b**.[a]

	3	**IIIa**	**IIIb**
N–O	1.168(3)	1.169(5)	1.161(2)
M–N	1.657(2)	1.662(3)	1.6725(16)
M–A$_t$	2.2733(11)	2.3304(11)	—
M–A$_b$	2.3320(10)	2.2874(11)	2.2569(5)
	2.2923(9)	2.2626(11)	2.2527(5)
M–N–O	161.5(2)	166.4(3)	167.0(2)
A$_t$–M–N	116.58(8)	124.56(12)	—
A$_b$–M–N	127.12(9)	111.67(12)	108.91(6)
	118.56(8)	107.44(12)	107.73(8)
A$_b$–M–A$_t$	100.80(3)	105.50(4)	—
	98.65(3)	103.54(4)	—
A$_b$–M–A$_b$	89.24(4)	101.74(4)	106.060(17)
v_{NO} (solid)	1709	1751	1775, 1749
v_{NO} (soln)	1751, 1721	—	1783, 1765, 1722

[a] **IIIa** = [Ni(NO)$_2$(μ-C$_{10}$H$_{10}$P$_3$)$_2$(PPh$_3$)$_2$],[55] **IIIb** = [Fe$_2$(NO)$_4$(μ-SBz)$_2$].[8] A$_t$ = atom coordinated to metal from terminal, non-nitrosyl ligand. A$_b$ = atom coordinated to metal from bridging, non-nitrosyl ligand.

Although no iron analog of **3** is known, the structure of **3** suggests a possible intermediate in the conversion of one equiv of [Fe$_2$S$_2$(SR)$_2$]$^{2-}$ to two equiv of the DNIC [Fe(NO)$_2$(SR)$_2$]$^-$. This process requires a net gain of four equiv of NO and a net loss of two equiv of sulfur, of unknown allotropic form. Coordination of two equiv of NO followed by extrusion of sulfur might afford [Fe$_2$(NO)$_2$(μ-SR)$_2$(SR)$_2$]$^{2-}$, the iron analog of **3** containing two {Fe(NO)}^{8} units (**Scheme 4.2**). Subsequent binding of 1 equiv of NO to each metal could break apart the dimer to yield two equiv of DNIC. Preliminary experiments performed in our laboratory have suggested that such an intermediate exists.[59] This observation suggests a possible intermediate in the breakdown of [2Fe–2S] clusters into DNICs in vivo.

Scheme 4.2. Proposed Conversion of a [2Fe–2S] Cluster into DNICs.
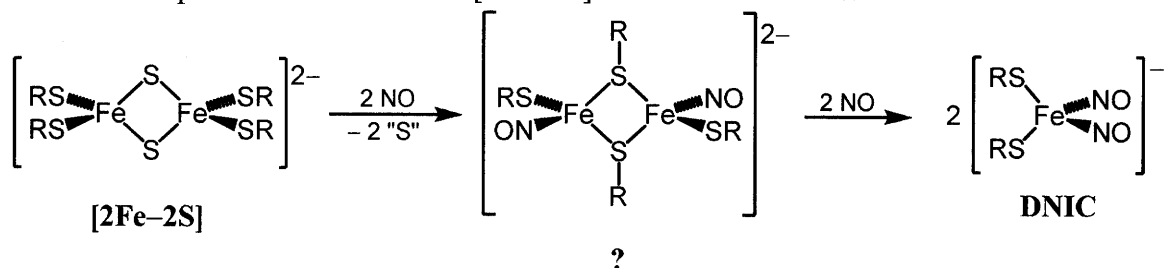
Crystal structures of Roussin red ester (RRE) complexes of the general formula [Fe$_2$(NO)$_4$(μ–SR)$_2$] have been known for decades.[60] For comparison, we have juxtaposed the structural parameters of **3** with those previously obtained for the RRE [Fe$_2$(NO)$_4$(μ–SBz)$_2$] (**IIIb**) in **Table 4.7**.[8] The M–N and N–O bond lengths are nearly identical, whereas the bridging thiolate-metal bonds are slightly longer in **3** than in **IIIb** (2.3122 Å vs. 2.2548 Å). Unsurprisingly, the M–N–O angle is more acute in **3** than in **IIIb**. Because **3** contains a {Ni(NO)}^{10} core, there are more electrons spread over fewer NO moieties than in the {Fe(NO)$_2$}^{9} complex, and therefore π-backbonding is better. The greater multiple-bond character between the metal and nitrosyl in **3** shortens the M–N bond with concomitant lengthening of the M–S bonds. One nitrosyl will cause the three other ligands in a pseudotetrahedral configuration to draw closer together; two nitrosyls will prefer a wider separating angle and cause the bridging thiolates to spread farther apart. An additional difference between **3** and **IIIb** is the ability of the two {Fe(NO)$_2$}^{9} units in the latter to interact via an Fe–Fe bond, which is not possible for two {Ni(NO)}^{10} units.

Attempts to prepare a nickel dinitrosyl complex by reacting **2** with NO(g) or Ph$_3$CSNO failed, yielding only slow conversion to **3**. This result is consistent with the fact that there are no structurally characterized complexes containing a {Ni(NO)$_2$} fragment of any electron count.

Scheme 4.3. Syntheses of **5** and **6**.
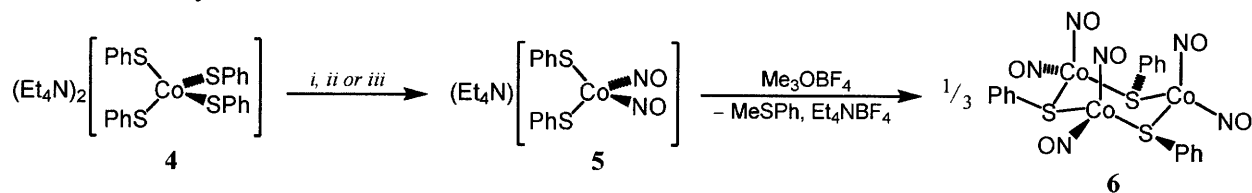
(*i*) +2 equiv of Ph$_3$CSNO, −1.5 equiv of R$_2$S$_2$ and 1 equiv of Et$_4$NSPh, (*ii*) +excess NO(g), −0.5 equiv of Ph$_2$S$_2$ and 1 equiv of Et$_4$NSPh, (*iii*) +1 equiv of NOBF$_4$, −0.5 equiv of Ph$_2$S$_2$ and 1 equiv of Et$_4$NBF$_4$ (to afford 0.5 equiv of **5**).

4.3.3. Synthesis and Properties of the First Anionic {Co(NO)$_2$}^{10} Complex (5)

Upon addition of two equiv of Ph$_3$CSNO to a solution of **4** in CH$_3$CN, the solution color immediately changed from dark green to dark brown. Mass balance analysis revealed that 1.5 equiv of disulfide, one equiv of Et$_4$NSPh and one equiv of (Et$_4$N)[Co(NO)$_2$(SPh)$_2$] (**5**) were produced per equiv of **4** consumed (**Scheme 4.3**, *Route i*). Complex **5** is diamagnetic and its ^{1}H NMR spectrum displays a 1:2 ratio of Et$_4$N$^+$ to PhS$^-$ protons (**Table 4.5**). The asymmetric and symmetric NO stretching modes for **5** occur at 1678 and 1756 cm^{-1} in the solid state (KBr) and shift to 1699 and 1769 cm^{-1} in solution (THF), respectively. Complex **5** contains a {Co(NO)$_2$}^{10} core and other four-coordinate, monometallic complexes with this configuration have asymmetric v_{NO} values ranging from 1730 to 1798 cm^{-1} (avg = 1766 ± 20 cm^{-1}) and symmetric v_{NO} values ranging from 1809 to 1870 (avg = 1837 ± 18 cm^{-1}).[61–67] Presumably, the asymmetric and symmetric v_{NO} modes for **5** are nearly 100 cm^{-1} lower than the average values observed with other {Co(NO)$_2$}^{10} complexes because the previously reported complexes of this configuration have been overall charge neutral or cationic. Complex **5** represents the first example of a {Co(NO)$_2$}^{10} species contained within an anion. The formation of **5** from **4** may proceed through a cobalt mononitrosyl intermediate, but attempts to observe such a species by IR or UV-vis spectroscopy were unsuccessful. Addition of fewer than two equiv of NO(g) or Ph$_3$CSNO yields

148

incomplete conversion to **5**.

As with the Ph₃CSNO reactivity, addition of excess NO(g) to **4** yielded 0.5 equiv of Ph₂S₂, one equiv of Et₄NSPh, and one of equiv **5** (**Scheme 4.3**, *Route ii*). Surprisingly, addition of one equiv of NOBF₄ to a solution of **4** in CH₃CN yielded 0.5 equiv of Ph₂S₂, one equiv of Et₄NBF₄, and 0.5 equiv of **5**, as well as an intractable plum-colored solid, the IR spectrum of which showed bands only for the Et₄N⁺ and PhS⁻ moieties (**Scheme 4.3**, *Route iii*). The combination of mass balance analysis and the IR spectrum of this material suggests it could have the formula (Et₄N)[Co(SPh)₄]. Such a product would be consistent with a possible mechanism by which **5** might form. Oxidation of **4** by NOBF₄ would yield 0.5 equiv of Ph₂S₂, one equiv of Et₄NBF₄, one equiv of NO and one equiv of "(Et₄N)[Co(SPh)₃]." Presumably, this cobalt(II) thiolate complex would rapidly bind NO to produce a cobalt(II) nitrosyl. Previous studies have demonstrated that [Co^{II}(NO)(L)] complexes disproportionate to form 0.5 equiv of [Co^{I}(NO)₂] and 0.5 equiv of [Co^{III}(L)₂].[68,69]

Crystals suitable for X-ray diffraction were grown by cooling a saturated solution of **5** in THF to −30 °C overnight. The structure confirms the assignment of **5** as containing a {Co(NO)₂}^{10} fragment supported by two thiolates (**Figure 4.3**). The cobalt nitrosyl structural parameters for **5** (Co–N–O = 161.4(3)° and 174.9(2)°, N–Co–N = 110.35(14)°, N–O = 1.106(3) and 1.126(3) Å, Co–N = 1.651(3) and 1.684(3) Å, **Table 4.8**) fall close to or within the range of reported values for four-coordinate, monometallic {Co(NO)₂}^{10} complexes (Co–N–O = 162.2–176.6°, avg = 169.2 ± 4.9°; N–Co–N = 115.6–131.7°, avg = 121.7 ± 6.6°; N–O = 1.12–1.156 Å, avg = 1.142 ± 0.011 Å; Co–N = 1.641–1.671 Å, avg = 1.654 Å ± 0.010 Å). The [Co(NO)₂(S₂C₅H₇)] dinitrosyl complex (**Va**) is the only structurally characterized, monometallic {Co(NO)₂}^{10} unit coordinated by sulfur atoms. A summary of its bond lengths and angles is

149
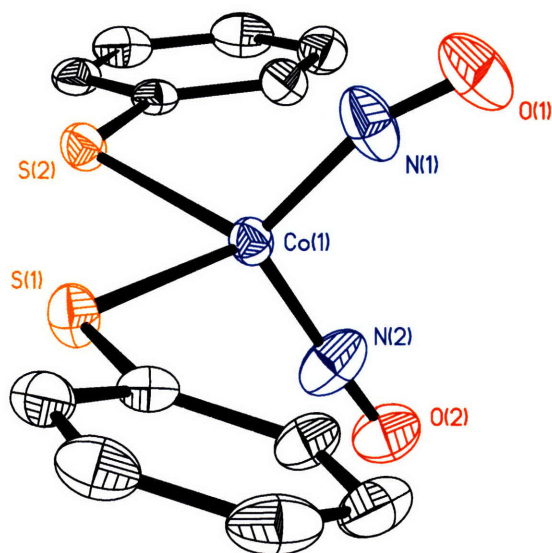
Figure 4.3. ORTEP diagram showing 50% probability thermal ellipsoids and selected atom labels for **5**. The Et_4N^+ cation and H atoms have been omitted for clarity. Selected bond distances (Å) and angles (deg): N1−O1, 1.106(3); N2−O2, 1.126(3); Co1−N1, 1.684(3); Co1−N2, 1.651(3); Co1−S1, 2.2478(8); Co1−S2, 2.2565(8); Co1−N1−O1, 161.4(3); Co1−N2−O2, 174.9(2); N1−Co−N2, 110.35(14); S1−Co1−N1, 111.56(9); S1−Co1−N2, 118.38(9); S2−Co1−N1, 116.26(9); S2−Co1−N2, 111.67(10); S1−Co1−S2, 87.14(3).

presented in **Table 4.8**.[70] The average cobalt nitrosyl structural parameters for **5** are similar to those for **Va**, but the Co−S bonds are longer and the S−M−S angle is more acute. Presumably, the greater Co−S distances in **5** are due to increased electron density at the metal compared to **Va**. Although the smaller S−M−S angle in **5** may reflect greater π-backbonding from the metal to the nitrosyls compared to **Va**, the ligand supporting the latter complex is bidentate and its geometry is dictated by the delocalized π-system. An idealized five-membered chelate ring would exhibit an S−M−S angle of 108° and an idealized six-membered chelate ring would display an angle of 120°. Because five of the six atoms in the chelate ring for **Va** are sp^2

hybridized, whereas the cobalt atom in **5** contains only monodentate ligands, the S–M–S angle in

Va will be necessarily greater, independent of any electronic effects.

Table 4.8. List of Bond Lengths (Å), Angles (deg) and v_{NO} (cm^{-1}) Values for **5** and **Va–c**.[a]

	5	**Va**[b]	**Vb**	**Vc**
N–O	1.126(3)	1.120(5)	1.181(2)	1.189(3)
	1.106(3)	—	1.179(2)	1.188(4)
M–N	1.684(3)	1.650(6)	1.680(2)	1.650(3)
	1.651(3)	—	1.678(2)	1.648(3)
M–S	2.2565(8)	2.224(2)	2.288(1)	—
	2.2478(8)	2.217(2)	2.272(1)	—
M–N–O	174.9(2)	168.9(5)	169.4(2)	170.1(3)
	161.4(3)	—	168.5(2)	167.5(3)
N–M–N	110.35(14)	115.5(3)	117.36(9)	117.33[c]
S–M–N	118.38(9)	111.1(2)	111.47(6)	—
	116.26(9)	109.1(2)	110.81(6)	—
	111.67(10)	—	103.88(6)	—
	111.56(9)	—	103.61(6)	—
S–M–S	87.14(3)	100.0(1)	109.73(2)	—
v_{NO} (solid)	1756, 1678	—	1743, 1683	—
v_{NO} (soln)	1769, 1699	1820, 1750	1737, 1693	1673, 1617

[a]**Va** = $[Co(NO)_2(S_2C_5H_7)]$,[70] **Vb** = $(Et_4N)[Fe(NO)_2(SPh)_2]$,[72] **Vc** = $[Fe(NO)_2(C_4H_6N_2)_2]$.[71] [b]Structural parameters averaged for metal nitrosyl moieties in original report but errors were propagated. [c]For the nitrosyl nitrogens.

Although the NO stretching bands in **5** are well below the range of those reported for

other complexes, the IR spectrum for the DNIC $(Et_4N)[Fe(NO)_2(SPh)_2]$ (**Vb**) strongly resembles

that of **5**. This result is unexpected, given that **5** is $\{M(NO)_2\}^{10}$ and **Vb** is $\{M(NO)_2\}^9$ – these

complexes should exhibit a more dramatic difference in electron density in the metal nitrosyl

core than is actually observed. The average M–N distance in **5** is shorter than that in **Vb**,

consistent with greater π-backbonding, but the N–O lengths are significantly shorter. A DNIC

containing a $\{Fe(NO)_2\}^{10}$ core supported by 1-methylimidazole ligands (**Vc**)[71] should be a better

molecule for comparison to **5** because it has the same number of electrons in its $\{M(NO)_2\}$

framework. However, the M–N bonds in **Vc** are shorter and the N–O distances are greater, suggesting more π-backbonding in **Vc** than **5**. Consistent with this speculation, the symmetric and asymmetric v_{NO} values in **Vc** are nearly 100 cm^{-1} lower in energy than those observed in **5**. Discussion of electronic configuration of metal nitrosyl complexes based solely on structural parameters can be counterproductive, but the v_{NO} values should be consistent with the Enemark-Feltham configuration of the complex. Perhaps the use of σ,π-donor thiolates negates the validity of considering the metal nitrosyl core as an independent moiety.

4.3.4. Synthesis and Properties of 6

Addition of stoichiometric Me_3OBF_4 to a solution of **5** in CH_3CN caused an immediate color change from dark brown to dark red-orange. Product and mass balance analyses indicated that one equiv of Et_4NBF_4 and $\frac{1}{3}$ equiv of $[Co_3(NO)_6(\mu-SPh)_3]$ (**6**) were formed per equiv of **5** consumed (**Scheme 4.3**). Compound **6** is diamagnetic and ^1H NMR spectroscopy reveals only PhS$^-$ protons (**Table 4.5**). The NO stretches of **6** occur at 1840, 1817, 1779, and 1744 cm^{-1} in the solid state (KBr). The v_{NO} values in THF solution do not shift significantly and appear at 1844, 1819, 1780 and 1764 cm^{-1}. Both solid state and solution v_{NO} values for **6** lie within the range of previously observed values for complexes comprising one $\{Co(NO)_2\}^{10}$ unit (*vide supra*) or multiple ligand-bridged $\{Co(NO)_2\}^{10}$ units (1750–1878 cm^{-1}, avg = 1815 ± 41 cm^{-1}).[73–76] Synthesis of a *dimetallic* $[Co_2(NO)_4(\mu-SPh)_2]$ compound from $[Co_2(NO)_4(\mu-Cl)_2]$ and LiSPh has been reported.[77] Although the NO stretches at 1842, 1820, 1783 and 1767 cm^{-1} in this complex are nearly identical to those observed for **6**, the only other characterization provided was its mass spectrum. In the solid state, **6** displays C_{3v} symmetry (**Figure 4.4**), the six nitrosyls of which should give rise to four IR active modes $(2A_1 + 2E)$, as we observe. If **6** were a

dimetallic species with the same solid state structure as RRE (C_{2h}), only two NO stretching modes would be IR active ($A_u + B_u$). Because four overlapping NO stretching bands are observed in the solid state and solution IR, we conclude that the trimetallic formulation is retained in solution. The ν_{NO} values for **6** are in excellent agreement with other reported $[Co(NO)_2(\mu-SR)]_n$ complexes.[77]
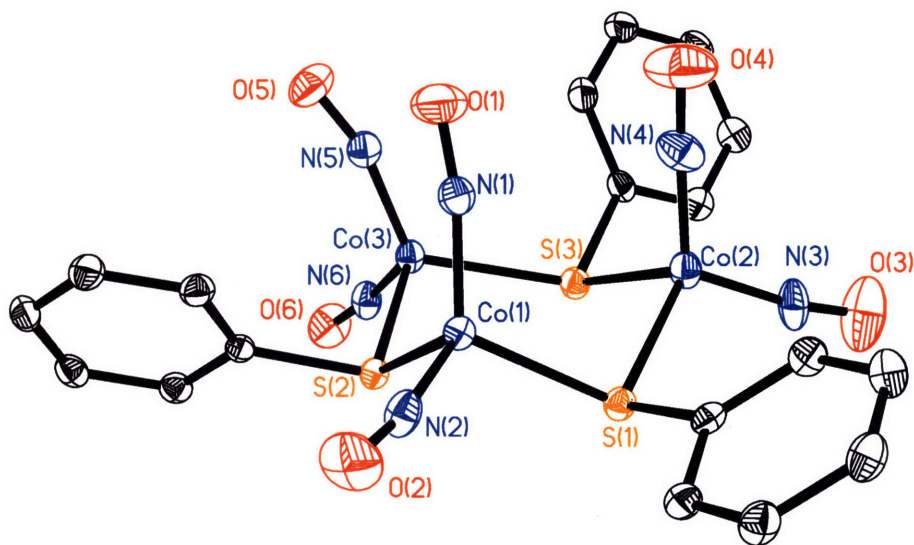
Figure 4.4. ORTEP diagram showing 50% probability thermal ellipsoids and selected atom labels for **6**. The H atoms have been omitted for clarity. Selected bond distances (Å) and angles (deg): N1–O1, 1.139(4); N2–O2, 1.131(4); N3–O3, 1.135(4); N4–O4, 1.127(4); N5–O5, 1.154(4); N6–O6, 1.147(4); Co1–N1, 1.663(3); Co1–N2, 1.675(3); Co2–N3, 1.672(3); Co2–N4, 1.668(3); Co3–N5, 1.674(3); Co3–N6, 1.669(3); Co1–S1, 2.3093(9); Co1–S2, 2.2814(9); Co2–S1, 2.2832(9); Co2–S3, 2.2811(10); Co3–S2, 2.2984(9); Co3–S3, 2.3027(9); Co1–N1–O1, 170.2(3); Co1–N2–O2, 171.1(3); Co2–N3–O3, 170.1(3); Co2–N4–O4, 175.8(3); Co3–N5–O5, 164.3(3); Co3–N6–O6, 173.0(3); N1–Co1–N2, 119.30(5); N3–Co2–N4, 118.05(16); N5–Co3–N6, 119.60(14); S1–Co1–N1, 114.97(10); S1–Co1–N2, 110.72(10); S1–Co2–N3, 111.86(11); S1–Co2–N4, 112.51(11); S2–Co1–N1, 106.97(10); S2–Co1–N2, 106.88(10); S2–Co3–N5, 102.13(10); S2–Co3–N6, 107.40(10); S3–Co2–N3, 102.36(11); S3–Co2–N4, 111.66(11); S3–Co3–N5, 121.29(10); S3–Co3–N6, 105.12(10); S1–Co1–S2, 94.59(3); S1–Co2–S3, 98.07(4); S2–Co3–S3, 98.22(3).

Crystals suitable for X-ray diffraction were grown by cooling a saturated solution of **6** in

Et_2O to -30 °C overnight. The structure reveals that **6** contains a trimer of thiolate-bridged

$\{Co(NO)_2\}^{10}$ fragments (**Figure 4.4**). The average bond lengths and angles for the $\{Co(NO)_2\}^{10}$

units in **6** (N–Co–N = 119.0°, Co–N–O = 170.8°, N–O = 1.139 Å, Co–N = 1.670 Å, **Table 4.9**)

fall within the range of reported values for four-coordinate, monometallic (*vide supra*) or

multimetallic $\{Co(NO)_2\}^{10}$ complexes (Co–N–O = 161.6–173.5°, avg = 168.2 ± 5.1°; N–Co–N

= 109.8–118.3°, avg = 112.5 ± 3.2°; N–O = 1.11–1.19 Å, avg = 1.146 ± 0.022 Å; Co–N =

1.60–1.68 Å, avg = 1.648 Å ± 0.030 Å).[73–76]

Table 4.9. List of Bond Lengths (Å), Angles (deg) and v_{NO} (cm^{-1}) Values for **6** and **VIa–e**.[a]

	6[b]	**VIa**[b]	**VIb**[b]	**VIc**[b]	**VId**[b,c]	**VIe**[b]
N–O	1.139	—	—	—	1.162	1.19
M–N	1.670	—	—	—	1.669	1.650
M–S	2.293	2.292	2.369	2.356	2.256	—
M–N–O	170.8	—	—	—	166.4	171.7
N–M–N	119.0	—	—	—	115.3	116.9
S–M–N	109.49	—	—	—	110.4	—
S–M–S	96.96	132.61	94.8	100.5	104.07	—
v_{NO} (solid)	1840, 1817, 1779, 1744	—	—	—	—	—
v_{NO} (soln)	1844, 1819, 1780, 1764	—	—	—	1795, 1743 1708	1733, 1721 1687, 1668

[a]**VIa** = $[Co_3(C_{10}H_{21}N_2S)_3]^{3+}$,[78] **VIb** = $[Ir_3(CO)_6(C_5H_9S_3)]$,[79] **VIc** = $(Et_4N)_3[Fe_3Cl_6(\mu–SPh)_3]$,[81] **VId** = $(Et_4N)[Fe_4S_3(NO)_7]$,[82] **VIe** = $[Fe_2(NO)_4(C_{25}H_{22}P_2)_2]$.[83] [b]Bond lengths and angles are averaged for all similar occurrences. [c]Excluding apical $\{Fe(NO)\}^7$ unit.

Although there are no structurally characterized complexes with three ligand-bridged

$\{Co(NO)_2\}^{10}$ units, dimers[73,74] and infinite chains[75,76] are known. Only one thiolate-bridged

trimetallic complex containing four-coordinate cobalt centers (**VIa**) has been structurally

characterized. Although the average Co–S lengths are similar, the average S–Co–S angle is

wider in **6**, most likely due to the geometric constraints imposed by the ligand (**Table 4.9**).[78] A

154

trimer of {Ir(CO)$_2$} units bridged by alkyl thiolates (**VIb**)[79] is a better structural analog of the metal thiolate core in **6** and displays a comparable average S–M–S angle; the greater average M–S length in **VIb** is most likely a consequence of the greater ionic radius of iridium (0.69 vs. 0.82 Å for Co(III) vs. Ir(III) in octahedral, high-spin configurations).[80] The M$_3$S$_3$ core of **VIb** also more closely resembles the cyclohexane-like configuration of **6** than does **VIa**.

Although no iron analog of **6** has been reported, (Et$_4$N)$_3$[Fe$_3$Cl$_6$(μ–SPh)$_3$] (**VIc**) shares its M$_3$S$_3$ core configuration.[81] Despite having an average S–M–S angle similar to that in **6**, **VIc** exhibits a much longer M–S distance and a planar M$_3$S$_3$ core. An iron nitrosyl complex with similar structural parameters and v_{NO} values to those in **6** is the Roussin black salt (RBS) (Et$_4$N)[Fe$_4$S$_3$(NO)$_7$] (**VId**).[82] The greater average N–O distance in **VId** compared to **6**, the more acute average M–N–O and more obtuse S–M–S angle in **VId**, and the lower v_{NO} values suggest that there is greater M–NO π-backbonding in **VId** than in **6**. Although **6** contains three {Co(NO)$_2$}[10] units and **VId** three equatorial {Fe(NO)$_2$}[9] units, the latter are bridged by sulfides and the complex is overall anionic, thus providing a more electron rich environment for the metal centers in **VId**. An analog of RRE containing {Fe(NO)$_2$}[10] units bridged by two bis(diphenylphosphino)methane ligands (**VIe**)[83] displays nearly identical metal nitrosyl angles, but the average M–N distance is shorter and average N–O length is greater than in **6**, indicating better π-backbonding in **VIe**. In support of this observation, the NO stretching energies in **VIe** are nearly 100 cm^{-1} lower in energy than those in **6**. Although **6** and **VIe** both contain {M(NO)$_2$}[10] cores, and the cobalt complex is supported by σ,π-donor ligands, the iron complex exhibits structural and spectroscopic parameters consistent with greater electron density residing within the M–NO units. Because **6** and **VIe** have the same Enemark-Feltham configuration, the iron must be in a more reduced state and will thus be more electron releasing than the cobalt.

155

The results for the nickel and cobalt nitrosyls supported by thiolates, especially in comparison with similar metal nitrosyl thiolate complexes, suggest that the nature of the metal and supporting ligands can have non-trivial influence on the structural and vibrational properties of the "independent" $\{M(NO)_x\}^n$ core. Comparison to other complexes containing similar metal nitrosyl units has revealed the importance of the electron donating ability of the ligand and the overall charge of the molecule in influencing the electronic properties of the metal nitrosyl core. These relationships are currently being explored via computational methods and will be reported at a later date.

4.3.5. NO Transfer to [Fe(TPP)Cl]

Our lab has previously employed [Fe(TPP)Cl] to measure the ability of a metal nitrosyl complex to donate or transfer NO by monitoring the response of the Soret band at 417 nm.[8] The reaction between [Fe(TPP)Cl] and the MNIC $(Et_4N)[Fe(NO)(S^tBu)_3]$ under ambient fluorescent lighting afforded [Fe(TPP)(NO)] with the expected hypsochromic shift to 405 nm and small decrease in absorptivity. However, [Fe(TPP)(NO)] is only obtained by reductive nitrosylation of [Fe(TPP)Cl] – an exogenous electron must be supplied with the displaced chloride being trapped by the NO donor.[25] In the absence of a reducing agent, reaction of a stoichiometric amount of NO(g) with [Fe(TPP)Cl] in aprotic solvent affords [Fe(TPP)(NO)Cl], a complex that is optically indistinguishable from [Fe(TPP)Cl].[25] When solutions of this six-coordinate nitrosyl are allowed to stand, they gradually lose NO and the spectrum of the original [Fe(TPP)Cl] is restored, and this process is greatly accelerated upon exposure to vacuum.
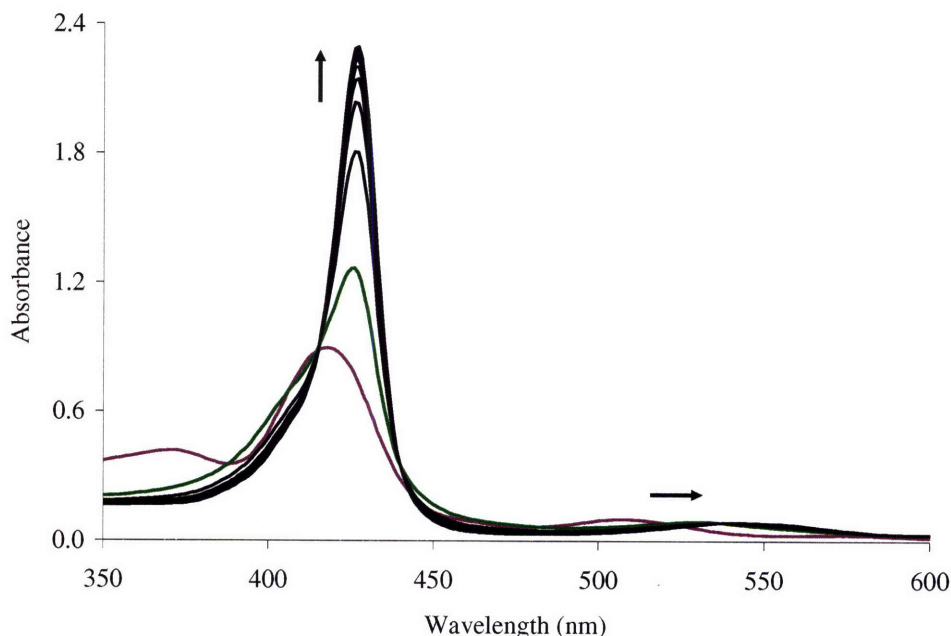
Figure 4.5. Reaction of [Fe(TPP)Cl] with **2** in THF without illumination. The Soret band for [Fe(TPP)Cl] (purple trace) shifts hypsochromically and increases in intensity upon addition of **2** (green trace). Scans every 60 s thereafter (black traces) show increasing absorptivity that is complete within 10 min.

Contrary to our expectations, addition of one equiv of **2**, 0.5 equiv of **3** or one equiv of **5** to [Fe(TPP)Cl] in THF produced a *bathochromic* shift in the Soret band from 417 nm to 426 nm with dramatic increases in absorption *in the dark* (**Figure 4.5**). Because the Soret band moves to lower energy and the absorptivity increases, we can exclude the formation of either [Fe(TPP)(NO)Cl] or [Fe(TPP)(NO)]. Iron porphyrin nitrosyl complexes have been extensively studied and coordination of a sixth ligand to [Fe(TPP)(NO)] can cause a significant change in the optical spectrum. The six-coordinate [Fe(TPP)(NO)(MeIm)] complex, where MeIm is 1-methylimidazole, has a Soret band at 425 nm with $\lambda = 1.54 \times 10^6$ $M^{-1}cm^{-1}$.[84] However, product analysis from a preparative scale reaction of **2** with [Fe(TPP)Cl] revealed an IR spectrum identical to that of **3** and no evidence for formation of Ph_2S_2. We therefore conclude that **2** transfers PhS^- to [Fe(TPP)Cl] with concomitant formation of **3** and Et_4NCl. Because **3** and **5**

157

have the same optical response, we propose that these complexes also undergo thiolate-chloride ligand exchange.
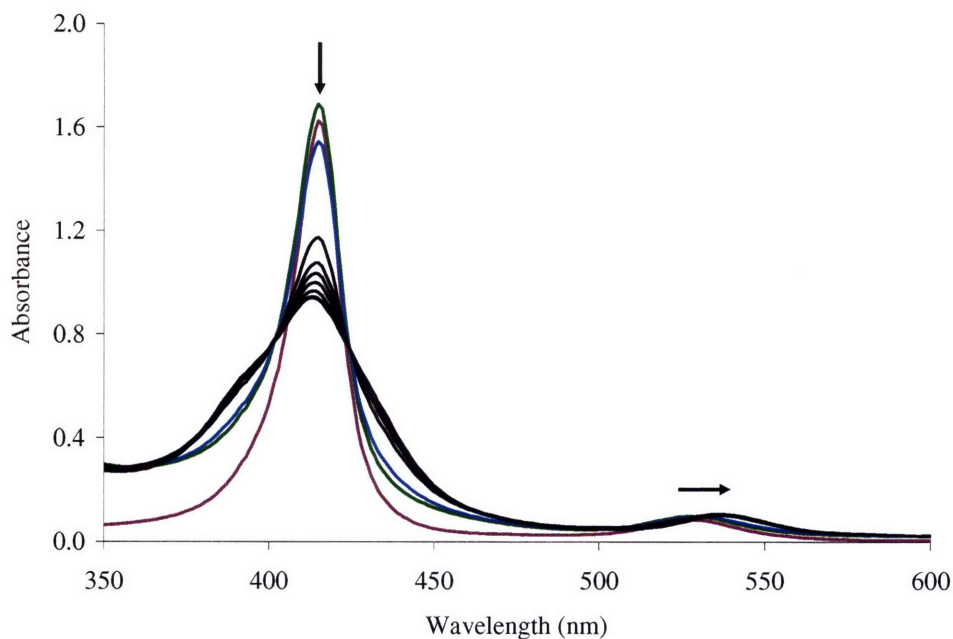
Figure 4.6. Reaction of [Co(TPP)] and **2** in THF with illumination. The Soret band for [Co(TPP)] (purple trace) is unaffected by the addition of **2** (green trace). After 60 s of exposure to ambient lighting, the intensity had decreased (blue trace). Scans every 5 min thereafter (black traces) show decreasing absorptivity that is complete within 30 min.

4.3.6. NO Transfer to [Co(TPP)]

To avoid the mechanistic complications of [Fe(TPP)Cl], we studied the NO transfer ability of one of our nitrosyl complexes to [Co(TPP)]. Addition of **2** to [Co(TPP)] in THF did not significantly alter the optical spectrum when shielded from light. A small increase in intensity of the Soret band was noted due to the absorption of **2** at this wavelength. Exposure of the [Co(TPP)] + **2** solution to ambient fluorescent lighting after 60 s and at 5 min intervals thereafter produced a rapid decrease in absorption along with a slight hypsochromic shift (**Figure 4.6**). The final spectrum obtained from this reaction matched that for [Co(TPP)] + NO(g) or Ph₃CSNO but

not the previously reported values for the Soret band wavelength and absorptivity of [Co(TPP)(NO)].[28] As a control, the reaction of [Co(TPP)] with Ph_3CSNO was performed on a preparative scale, and the v_{NO} value observed was 1697 cm^{-1}. This value is in good agreement with that previously observed for [Co(TPP)(NO)]. The cause of the disparity between the results from IR and UV-vis spectroscopy is unclear, but the optical spectrum of [Co(TPP)(NO)] may depend on solvent, since our measurements were performed in THF and the literature values[28] were acquired in CH_2Cl_2. By comparison, cobalt(II)-reconstituted soluble guanylyl cyclase displays a slight hypsochromic shift in the Soret band upon coordination of NO with a decrease in absorptivity to 1.07×10^5 $M^{-1}cm^{-1}$.[29]

4.4. Conclusions

Reaction of **1** with Ph_3CSNO or NO(g) yielded the monometallic $\{Ni(NO)\}^{10}$ species **2**, which displays one of the lowest recorded v_{NO} values and shares similar structural parameters with MNIC **IIc**. Compound **2** is the first example of an anionic complex containing a $\{Ni(NO)\}^{10}$ moiety. Although **IIc** is light- and temperature-sensitive and readily converts to a DNIC, **2** is stable and our efforts to prepare the corresponding nickel dinitrosyl complex have been unsuccessful. The similarity in reactivity of Ph_3CSNO and NO(g) indicates that Ph_3CSNO functions as an NO donor under these reaction conditions. In contrast, addition of $NOBF_4$ to **1** produced a dimetallic $\{Ni(NO)\}^{10}$ species that exhibited ^1H NMR and IR spectra different from those of **2**. The resulting thiolate-bridged dimer **3** suggests a possible intermediate in the conversion of a [2Fe–2S] cluster into two DNICs that has not yet been observed. Complex **3** was also prepared by addition of Me_3OBF_4 to **2**, demonstrating the ability of these two $\{Ni(NO)\}^{10}$ species to interconvert by simple ligand dissociation or association reactions.

The $\{Co(NO)_2\}^{10}$ complex **5** can be obtained by reaction of **4** with Ph_3CSNO, NO(g) or $NOBF_4$ and displays the lowest recorded v_{NO} values for any dinitrosylcobalt complex with this electron count. Furthermore, **5** is the first example of an anionic complex containing a $\{Co(NO)_2\}^{10}$ moiety. Attempts to isolate or observe a cobalt mononitrosyl were unsuccessful, presumably due to rapid disproportionation into a cobalt(I) dinitrosyl and a cobalt(III) species. Reaction of **5** with Me_3OBF_4 afforded a trinuclear analog of RRE **6** composed of three $\{Co(NO)_2\}^{10}$ units. The existence of this complex suggests a pathway by which RRE might be converted into RBS. RRE might be in equilibrium among various $[Fe(NO)_2(\mu–SPh)]_n$ species, where the predominant form has $n = 2$, followed by $n = 3$, etc. The trimeric form of RRE could react with one molecule of MNIC to produce RBS and three molecules of thioether. Such chemistry may seem improbable, but iron persulfide complexes can be prepared by insertion of a thiolate into an iron-sulfur bond[85] and sulfur can be extruded from iron persulfide complexes.[86,87] Conversion of RRE into RBS could occur by insertion of a thiolate into an iron-sulfur bond followed by alkyl- or aryl-transfer within the coordinated disulfide and dissociation of the resultant thioether.

The exploration of the nitric oxide reactivity of homoleptic nickel(II) and cobalt(II) thiolate complexes has yielded interesting coordination compounds and suggests undiscovered reactivity for the analogous iron(II) complexes. Syntheses of alkyl variants of **2**, **3**, **5** and **6** will be interesting to pursue for comparison, as will iron analogs of **3**, together with attempts to convert RRE-type complexes to RBS.

4.5. References

(1)   Calabrese, V.; Mancuso, C.; Calvani, M.; Rizzarelli, E.; Butterfield, D. A.; Stella, A. M. G. "Nitric oxide in the central nervous system: neuroprotection versus neurotoxicity" *Nature Rev. Neurosci.* **2007,** *8,* 766–775.

(2)   Turchi, J. J. "Nitric oxide and cisplatin resistance: NO easy answers" *Proc. Natl. Acad. Sci. USA* **2006,** *103,* 4337–4338.

(3)   Bronte, V.; Zanovello, P. "Regulation of Immune Responses by L-Arginine Metabolism" *Nature Rev. Immunol.* **2005,** *5,* 641–654.

(4)   Robbins, A. H.; Stout, C. D. "Structure of activated aconitase: Formation of the [4Fe–4S] cluster in the crystal" *Proc. Natl. Acad. Sci. USA* **1989,** *86,* 3639–3643.

(5)   Kennedy, M. C.; Antholine, W. E.; Beinert, H. "An EPR Investigation of the Products of the Reaction of Cytosolic and Mitochondrial Aconitases with Nitric Oxide" *J. Biol. Chem.* **1997,** *272,* 20340–20347.

(6)   Ding, H.; Demple, B. "Direct nitric oxide signal transduction via nitrosylation of iron-sulfur centers in the SoxR transcription activator" *Proc. Natl. Acad. Sci. USA* **2000,** *97,* 5146–5150.

(7)   Harrop, T. C.; Song, D.; Lippard, S. J. "Interaction of Nitric Oxide with Tetrathiolato Iron(II) Complexes: Relevance to the Reaction Pathways of Iron Nitrosyls in Sulfur-Rich Biological Coordination Environments" *J. Am. Chem. Soc.* **2006,** *128,* 3528–3529.

(8)   Harrop, T. C.; Song, D.; Lippard, S. J. "Reactivity pathways for nitric oxide and nitrosonium with iron complexes in biologically relevant sulfur coordination spheres" *J. Inorg. Biochem.* **2007,** *101,* 1730–1738.

(9)   Lu, T.-T.; Chiou, S.-J.; Chen, C.-Y.; Liaw, W.-F. "Mononitrosyl Tris(Thiolate) Iron Complex [Fe(NO)(SPh)$_3$]$^-$ and Dinitrosyl Iron Complex [(EtS)$_2$Fe(NO)$_2$]$^-$: Formation Pathway of Dinitrosyl Iron Complexes (DNICs) from Nitrosylation of Biomimetic Rubredoxin [Fe(SR)$_4$]$^{2-/1-}$ (R = Ph, Et)" *Inorg. Chem.* **2006,** *45,* 8799–8806.

(10)   Chen, V. J.; Orville, A. M.; Harpel, M. R.; Frolik, C. A.; Surerus, K. K.; Münck, E.; Lipscomb, J. D. "Spectroscopic Studies of Isopenicillin N Synthase" *J. Biol. Chem.* **1989,** *264,* 21677–21681.

(11)   Arciero, D. M.; Lipscomb, J. D.; Huynh, B. H.; Kent, T. A.; Münck, E. "EPR and Mossbauer Studies of Protocatechuate 4,5-Dioxygenase: Characterization of a New Fe^{2+} Environment" *J. Biol. Chem.* **1983,** *258,* 14981–14991.

(12)   Rich, P. R.; Salerno, J. C.; Leigh, J. S.; Bonner Jr ., W. D. "A Spin 3/2 Ferrous-Nitric Oxide Derivative of an Iron-Containing Moiety Associated with *Neurospora Crassa* and Higher Plant Mitochondria" *FEBS Lett.* **1978,** *93,* 323–326.

(13)   Ermler, U.; Grabarse, W.; Shima, S.; Goubeaud, M.; Thauer, R. K. "Crystal Structure of Methyl-Coenzyme M Reductase: The Key Enzyme of Biological Methane Formation" *Science* **1997,** *278,* 1457–1462.

(14)   Singh, K.; Horng, Y.-C.; Ragsdale, S. W. "Rapid Ligand Exchange in the MCR_{red1} Form of Methyl-coenzyme M Reductase" *J. Am. Chem. Soc.* **2003,** *125,* 2436–2443.

(15)   Wolak, M.; Zahl, A.; Schneppensieper, T.; Stochel, G.; van Eldik, R. "Kinetics and Mechanism of the Reversible Binding of Nitric Oxide to Reduced Cobalamin B_{12r} (Cob(II)alamin)" *J. Am. Chem. Soc.* **2001,** *123,* 9780–9791.

(16)   Danishpajooh, I. O.; Gudi, T.; Chen, Y.; Kharitonov, V. G.; Sharma, V. S.; Boss, G. R. "Nitric Oxide Inhibits Methionine Synthase Activity *in Vivo* and Disrupts Carbon Flow through the Folate Pathway" *J. Biol. Chem.* **2001,** *276,* 27296–27303.

(17)   Yamamura, T.; Miyamae, H.; Katayama, Y.; Sasaki, Y. "Nickel Thiolates. Simple Synthesis, the Behavior upon Protolysis and Oxidation Potentials" *Chem. Lett.* **1985,** 269–272.

(18)   Dance, I. G. "Synthesis, Crystal Structure, and Properties of the Hexa(μ-benzenethiolato)tetra(benzenethiolatocobaltate(II)) Dianion, the Prototype Cobalt(II)–Thiolate Molecular Cluster" *J. Am. Chem. Soc.* **1979,** *101,* 6264–6273.

(19)   Arulsamy, N.; Bohle, D. S.; Butt, J. A.; Irvine, G. J.; Jordan, P. A.; Sagan, E. "Interrelationships between Conformational Dynamics and the Redox Chemistry of *S*-Nitrosothiols" *J. Am. Chem. Soc.* **1999,** *121,* 7115–7123.

(20)   Tran, D.; Skelton, B. W.; White, A. H.; Laverman, L. E.; Ford, P. C. "Investigation of the Nitric Oxide Reduction of the Bis(2,9-Dimethyl-1,10-phenanthroline) Complex of Copper(II) and the Structure of $[Cu(dmp)_2(H_2O)](CF_3SO_3)_2$" *Inorg. Chem.* **1998,** *37,* 2505–2511.

(21)   Sheldrick, G. M. *SHELXTL00: Program for Refinement of Crystal Structures,* University of Göttingen: Göttingen, Germany, 2000.

(22)   Sheldrick, G. M. *SHELXTL, Program Library for Structure Solution and Molecular Graphics,* v6.10; Bruker AXS: Madison, WI, 2001.

(23) Sheldrick, G. M. *SADABS: Area-Detector Absorption Correction*, University of Göttingen: Göttingen, Germany, 2001.

(24) Spek, A. L. *PLATON, A Multipurpose Crystallographic Tool*, Utrecht University: Utrecht, The Netherlands, 2000.

(25) Wayland, B. B.; Olson, L. W. "Spectroscopic Studies and Bonding Model for Nitric Oxide Complexes of Iron Porphyrins" *J. Am. Chem. Soc.* **1974,** *96*, 6037–6041.

(26) Scheidt, W. R.; Frisse, M. E. "Nitrosylmetalloporphyrins. II. Synthesis and Molecular Stereochemistry of Nitrosyl-α,β,γ,δ-tetraphenylporphinatoiron(II)" *J. Am. Chem. Soc.* **1975,** *97*, 17–21.

(27) Cruz, F. D.; Driaf, K.; Berthier, C.; Lameille, J.-M.; Armand, F. "Study of a self-assembled porphyrin monomolecular layer obtained by metal complexation" *Thin Solid Films* **1999,** *349*, 155–161.

(28) Richter-Addo, G. B.; Hodge, S. J.; Yi, G.-B.; Khan, M. A.; Ma, T.; Van Caemelbecke, E.; Guo, N.; Kadish, K. M. "Synthesis, Characterization, and Spectroelectrochemistry of Cobalt Porphyrins Containing Axially Bound Nitric Oxide" *Inorg. Chem.* **1996,** *35*, 6530–6538.

(29) Dierks, E. A.; Hu, S.; Vogel, K. M.; Yu, A. E.; Spiro, T. G.; Burstyn, J. N. "Demonstration of the Role of Scission of the Proximal Histidine-Iron Bond in the Activation of Soluble Guanylyl Cyclase through Metalloporphyrin Substitution Studies" *J. Am. Chem. Soc.* **1997,** *119*, 7316–7323.

(30) Darensbourg, D. J.; Decuir, T. J.; Stafford, N. W.; Robertson, J. B.; Draper, J. D.; Reibenspies, J. H.; Kathó, A.; Joó, F. "Water-Soluble Organometallic Compounds. 6. Synthesis, Spectral Properties, and Crystal Structures of Complexes of 1,3,5-Triaza-7-phosphaadamantane with Group 10 Metals" *Inorg. Chem.* **1997,** *36*, 4218–4226.

(31) Hunter, A. D.; Legzdins, P. "Reductive Synthesis and Characterization of the Complexes CpM(NO)L$_2$ (Cp = η^5-C$_5$H$_5$; M = Cr, Mo, or W; L = Lewis Base)" *Organometallics* **1986,** *5*, 1001–1009.

(32) Enemark, J. H.; Feltham, R. D. "Stereochemical Control of Valence. II. Behavior of the {MNO}^{n} Group in Ligand Fields" *J. Am. Chem. Soc.* **1974,** *96*, 5002–5004.

(33) Schebler, P. J.; Riordan, C. G.; Guzei, I. A.; Rheingold, A. L. "Phenyltris((*tert*-butylthio)methyl)borate: A Second Generation S$_3^-$ Ligand That Enforces Tetrahedral Coordination" *Inorg. Chem.* **1998,** *37*, 4754–4755.

(34) Fullmer, B. C.; Pink, M.; Fan, H.; Yang, X.; Baik, M.-H.; Caulton, K. G. "The Effect of One Valence Electron: Contrasting (PNP)Ni(CO) with (PNP)Ni(NO) to Understand the Half-Bent NiNO Unit" *Inorg. Chem.* **2008**, *47*, 3888–3892.

(35) Landry, V. K.; Pang, K.; Quan, S. M.; Parkin, G. "Tetrahedral nickel nitrosyl complexes with tripodal [N₃] and [Se₃] donor ancillary ligands: structural and computational evidence that a linear nitrosyl is a trivalent ligand" *Dalton Trans.* **2007**, 820–824.

(36) Landry, V. K.; Parkin, G. "Synthesis and structural characterization of [Bse^Me]Ni(PPh₃)(NO), a nickel complex with a bent nitrosyl ligand" *Polyhedron* **2007**, *26*, 4751–4757.

(37) Maffett, L. S.; Gunter, K. L.; Kreisel, K. A.; Yap, G. P. A.; Rabinovich, D. "Nickel nitrosyl complexes in a sulfur-rich environment: The first poly(mercaptoimidazolyl)borate derivatives" *Polyhedron* **2007**, *26*, 4758–4764.

(38) MacBeth, C. E.; Thomas, J. C.; Betley, T. A.; Peters, J. C. "The Coordination Chemistry of "[BP₃]NiX" Platforms: Targeting Low-Valent Nickel Sources as Promising Candidates to L3Ni=E and L3Ni≡E Linkages" *Inorg. Chem.* **2004**, *43*, 4645–4662.

(39) Rahman, A. F. M. M.; Salem, G.; Stephens, F. S.; Wild, S. B. "Stability and Stereochemistry of Tetrahedral Nickel Nitrosyl Complexes: Crystal and Molecular Structures of (*R**,*S**)-*anti*-[NiNCS(NO){1,2-C₆H₄(PMePh)₂}] and (*R**,*S**)-*anti*-[NiNO{P(OMe)₃}{1,2-C₆H₄(PMePh)₂}]PF₆" *Inorg. Chem.* **1990**, *29*, 5225–5230.

(40) Kriege-Simondsen, J.; Elbaze, G.; Dartiguenave, M.; Feltham, R. D.; Dartiguenave, Y. "Oxygen Atom Transfer Reactions. 2. Reaction of Carbon Monoxide with Ni(NO₂)₂(PMe₃)₂: Structure of Nitronitrosylbis(trimethylphosphine)nickel, Ni(NO₂)(NO)(PMe₃)₂" *Inorg. Chem.* **1982**, *21*, 230–236.

(41) Chong, K. S.; Rettig, S. J.; Storr, A.; Trotter, J. "Reactions of Ni(NO)I with pyrazolyl gallate ligands: crystal and molecular structure of [Me₂Ga(N₂C₅H₇)(OCH₂CH₂NMe₂)]Ni(NO)" *Can. J. Chem.* **1979**, *57*, 3107–3112.

(42) Di Vaira, M.; Ghilardi, C. A.; Sacconi, L. "Synthesis and Structural Characterization of Some Nitrosyl Complexes of Iron, Cobalt, and Nickel with Poly(tertiary phosphines and arsines)" *Inorg. Chem.* **1976**, *15*, 1555–1561.

(43) Meiners, J. H.; Rix, C. J.; Clardy, J. C.; Verkade, J. G. "Preparation, Properties, and Crystal Structure of a Cationic Nickel Nitrosyl Bicyclic Phosphite Complex" *Inorg. Chem.* **1975**, *14*, 705–710.

(44) Enemark, J. H. "Four-Coordinate Metal Nitrosyls. I. The Structure of Azidonitrosylbis(triphenylphosphine)nickel, $Ni(N_3)(NO)(P(C_6H_5)_3)_2$ " *Inorg. Chem.* **1971,** *10*, 1952–1957.

(45) Chen, Y.; Irie, Y.; Keung, W. M.; Maret, W. "*S*-Nitrosothiols React Preferentially with Zinc Thiolate Clusters of Metallothionein III through Transnitrosation" *Biochemistry* **2002,** *41*, 8360–8367.

(46) Dicks, A. P.; Williams, D. L. H. "Generation of nitric oxide from *S*-nitrosothiols using protein-bound Cu^{2+} sources " *Chem. & Biol.* **1996,** *3*, 655–659.

(47) Kelm, M. "Nitric oxide metabolism and breakdown" *Biochim. Biophys. Acta* **1999,** *1411*, 273–289.

(48) Singh, S. P.; Wishnok, J. S.; Keshive, M.; Deen, W. M.; Tannenbaum, S. R. "The chemistry of the *S*-nitrosoglutathione/glutathione system" *Proc. Natl. Acad. Sci. USA* **1996,** *93*, 14428–14433.

(49) Tsikas, D.; Frölich, J. C. "Trouble with the analysis of nitrite, nitrate, *S*-nitrosothiols and 3-nitrotyrosine: freezing-induced artifacts?" *Nitric Oxide* **2004,** *11*, 209–213.

(50) Vanin, A. F.; Papina, A. A.; Serezhenkov, V. A.; Koppenol, W. H. "The mechanisms of *S*-nitrosothiol decomposition catalyzed by iron" *Nitric Oxide* **2004,** *10*, 60–73.

(51) Bonner, L.; Stedman, G., The chemistry of nitric oxide and redox-related species. In *Methods in Nitric Oxide Research*, Feelisch, M.; Stamler, J. S., Eds. Wiley: London, 1996; pp 4–18.

(52) Ghosh, K.; Eroy-Reveles, A. A.; Avila, B.; Holman, T. R.; Olmstead, M. M.; Mascharak, P. K. "Reactions of NO with Mn(II) and Mn(III) Centers Coordinated to Carboxamido Nitrogen: Synthesis of a Manganese Nitrosyl with Photolabile NO" *Inorg. Chem.* **2004,** *43*, 2988–2997.

(53) Fujisawa, K.; Tateda, A.; Miyashita, Y.; Okamoto, K.-i.; Paulat, F.; Praneeth, V. K. K.; Merkle, A.; Lehnert, N. "Structural and Spectroscopic Characterization of Mononuclear Copper(I) Nitrosyl Complexes: End-on versus Side-on Coordination of NO to Copper(I)" *J. Am. Chem. Soc.* **2008,** 1205–1213.

(54) Ruggiero, C. E.; Carrier, S. M.; Antholine, W. E.; Whittaker, J. W.; Cramer, C. J.; Tolman, W. B. "Synthesis and Structural and Spectroscopic Characterization of Mononuclear Copper Nitrosyl Complexes: Models for Nitric Oxide Adducts of Copper Proteins and Copper-Exchanged Zeolites" *J. Am. Chem. Soc.* **1993,** *115*, 11285–11298.

(55) Heinemann, F. W.; Pritzkow, H.; Zeller, M.; Zenneck, U. "1,2,4-Triphospholyl Nickel Complexes: Evidence for a Dimerization Equilibrium That Includes a $\sigma-\pi$ Rearrangement of the Triphospholyl Ligand" *Organometallics* **2000**, *19*, 4283–4288.

(56) Chong, K. S.; Rettig, S. J.; Storr, A.; Trotter, J. "Anionic pyrazolyl-bridged nickel nitrosyl complexes. Synthesis, structure, and reactivity" *Can. J. Chem.* **1979**, *57*, 3099–3106.

(57) Chong, K. S.; Rettig, S. J.; Storr, A.; Trotter, J. "Neutral pyrazolyl-bridged nickel nitrosyl complexes. Synthesis, structure, and reactivity" *Can. J. Chem.* **1979**, *57*, 3090–3098.

(58) Del Zotto, A.; Mezzetti, A.; Novelli, V.; Rigo, P.; Lanfranchi, M.; Tiripicchio, A. "Nickel Nitrosyl Complexes with Diphosphines. The Crystal and Molecular Structure of [(dppe)(ON)Ni(μ-dppe)Ni(NO)(dppe)][BF$_4$]$_2$ (dppe = Ph$_2$PCH$_2$CH$_2$PPh$_2$) " *J. Chem. Soc., Dalton Trans.* **1990**, 1035–1042.

(59) Harrop, T. C.; Lippard, S. J. " unpublished results.

(60) Thomas, J. T.; Robertson, J. H.; Cox, E. G. "The Crystal Structure of Roussin's Red Ethyl Ester" *Acta Cryst.* **1958**, *11*, 599–604.

(61) Lim, M. H.; Kuang, C.; Lippard, S. J. "Nitric Oxide-Induced Fluorescence Enhancement by Displacement of Dansylated Ligands from Cobalt" *ChemBioChem* **2006**, *7*, 1571–1576.

(62) Franz, K. J.; Singh, N.; Spingler, B.; Lippard, S. J. "Aminotroponiminates as Ligands for Potential Metal-Based Nitric Oxide Sensors" *Inorg. Chem.* **2000**, *39*, 4081–4092.

(63) Gerbase, A. E.; Vichi, E. J. S.; Stein, E.; Amaral, L.; Vasquez, A.; Hörner, M.; Maichle-Mössmer, C. "Preparation, characterization and electrochemical studies of 1,1'-bis(diphenylphosphino)ferrocene (dppf) derivatives. Crystal structure of [dppfCo(NO)$_2$][SbF$_6$]" *Inorg. Chim. Acta* **1997**, *266*, 19–27.

(64) Roustan, J.-L.; Ansari, N.; Le Page, Y.; Charland, J.-P. "Molecular geometry of M(NO)$_2$ complexes: single crystal X-ray structure of Co(NO)$_2$(C$_5$H$_5$N)$^+$BF$_4$$^-$, lability of the pyridine ligands of Co(NO)$_2$(C$_5$H$_5$N)$_2$$^+$, and its relevance to the formation of the Co$_2$(NO)$_3$$^+$ bimetallic core" *Can. J. Chem.* **1992**, *70*, 1650–1657.

(65) Aresta, M.; Ballivet-Tkatchenko, D.; Bonnet, M. C.; Faure, R.; Loiseleur, H. "Synthesis and Structural Characterization of Co(NO)$_2$[PhP(OCH$_2$CH$_2$)$_2$NH]Cl: A Novel Carbon Dioxide Carrier" *J. Am. Chem. Soc.* **1985**, *107*, 2994–2995.

(66) Haymore, B. L.; Huffman, J. C.; Butler, N. E. "Linear vs. Bent Nitrosyl Ligands in Pseudotetrahedral Nitrosyl Complexes. Low-Temperature Structure of $CoI(NO)_2(P(C_6H_5)_3)$" *Inorg. Chem.* **1983,** *22,* 168–170.

(67) Kaduk, J. A.; Ibers, J. A. "Structure of Dinitrosyl (1,2-bis(diphenylphosphino)ethane)cobalt Hexafluorophosphate, $[Co(NO)_2((C_6H_5)_2PC_2H_4P(C_6H_5)_2)][PF_6]$ " *Inorg. Chem.* **1977,** *16,* 3283–3287.

(68) Del Zotto, A.; Mezzetti, A.; Rigo, P. "Five-coordinate diphosphine complexes of the $\{CoNO\}^8$ group, and their disproportionation reactions to cobalt(III) and $\{Co(NO)_2\}^{10}$ derivatives" *Inorg. Chim. Acta* **1990,** *171,* 61–69.

(69) Hendrickson, A. R.; Ho, R. K. Y.; Martin, R. L. "Four- and Five-Coordinated Nitrosyls of Cobalt Dithioacetylacetonate" *Inorg. Chem.* **1974,** *13,* 1279–1281.

(70) Martin, R. L.; Taylor, D. "Bending of Linear Nitric Oxide Ligands in Four-Coordinate Transition Metal Complexes. Crystal and Molecular Structure of Dinitrosyldithioacetylacetonatocobalt(–I), $Co(NO)_2(SacSac)$" *Inorg. Chem.* **1976,** *15,* 2970–2976.

(71) Reginato, N.; McCrory, C. T. C.; Pervitsky, D.; Li, L. "Synthesis, X-ray Crystal Structure, and Solution Behavior of $Fe(NO)_2(1\text{-MeIm})_2$: Implications for Nitrosyl Non-Heme-Iron Complexes with $g = 2.03$" *J. Am. Chem. Soc.* **1999,** *121,* 10217–10218.

(72) Strasdeit, H.; Krebs, B.; Henkel, G. "Synthesis and Structure of $[Fe(SPh)_2(NO)_2]^-$, the "Monomer" of Roussin's Phenyl Ester" *Z. Naturforsch. B* **1986,** *41,* 1357–1362.

(73) Hilderbrand, S. A.; Lippard, S. J. "Nitric Oxide Reactivity of Fluorophore Coordinated Carboxylate-Bridged Diiron(II) and Dicobalt(II) Complexes" *Inorg. Chem.* **2004,** *43,* 5294–5301.

(74) Chong, K. S.; Rettig, S. J.; Storr, A.; Trotter, J. "Synthesis and structure of 3,5-dimethylpyrazolyl iron and cobalt dinitrosyl dimers" *Can. J. Chem.* **1979,** *57,* 3119–3125.

(75) Strouse, C. E.; Swanson, B. I. "Dinitrosylcobalt Nitrite: Synthesis and X-Ray Crystallographic Structural Studies of a Cobalt Nitrosyl with Bridging Nitrite Groups" *J. Chem. Soc., Chem. Commun.* **1971,** 55–56.

(76) Dahl, L. F.; de Gil, E. R.; Feltham, R. D. "The Solid-state Structures of Dinitrosyliron Iodide and Dinitrosylcobalt Iodide: The Stereochemical Consequences of Strong Metal-Metal Interactions in Ligand-Bridged Complexes" *J. Am. Chem. Soc.* **1969,** *91,* 1653–1664.

(77)   Bitterwolf, T. E.; Pal, P. "Synthesis of the cobalt analogues of Roussin's red salt esters" *Inorg. Chim. Acta* **2006,** *359,* 1501–1503.

(78)   Shearer, J.; Kaminsky, W.; Kovacs, J. A. "A chloride ion contained in a cobalt 'claw': [Co₃(DADIT)₃]Cl(PF₆)₂" *Acta Cryst. C* **2003,** *59,* m379–m380.

(79)   Maisonnat, A.; Devillers, J.; Poilblanc, R. "Assembling Potentialities of an Anionic Tripod Ligand: Trirhodium and Triiridium Complexes of 1,1,1-Tris(sulfidomethyl)ethane. Molecular Structure and Crystal Packing of Ir₃(CH₃C(CH₂S)₃)(CO)₆" *Inorg. Chem.* **1987,** *26,* 1502–1507.

(80)   Cotton, F. A.; Wilkinson, G.; Murillo, C. A.; Bochmann, M., *Advanced Inorganic Chemistry.* 6th ed.; John Wiley & Sons, Inc.: 1999.

(81)   Whitener, M. A.; Bashkin, J. K.; Hagen, K. S.; Girerd, J.-J.; Gamp, E.; Edelstein, N.; Holm, R. H. "A New Inorganic Ring System: Planar Fe₃(μ₂-SR)₃ in [Fe₃(μ₂-SR)₃X₆]$^{3-}$— Synthesis, Structures, and Solution Conformation and Equilibrium" *J. Am. Chem. Soc.* **1986,** *108,* 5607–5620.

(82)   D'Addario, S.; Demartin, F.; Grossi, L.; Iapalucci, M. C.; Laschi, F.; Longoni, G.; Zanello, P. "Redox Behavior of the Black Roussinate [Fe₄S₃(NO)₇]⁻ Monoanion. Synthesis and Spectroscopic Characterization of the [Fe₄S₃(NO)₇]$^{n-}$ (n = 2, 3) Anions and Crystal Structures of the Mono- and Dianions in Their [NE₄]⁻ Salts" *Inorg. Chem.* **1993,** *32,* 1153–1160.

(83)   Li, L.; Reginato, N.; Urschey, M.; Stradiotto, M.; Liarakos, J. D. "The synthesis and structural characterization of linear and macrocyclic bis(dinitrosyliron) complexes supported by bis(phosphine) bridging ligands" *Can. J. Chem.* **2003,** *81,* 468–475.

(84)   Praneeth, V. K. K.; Neese, F.; Lehnert, N. "Spin Density Distribution in Five- and Six-coordinate Iron(II)-Porphyrin NO Complexes evidenced by Magnetic Circular Dichroism Spectroscopy" *Inorg. Chem.* **2005,** *44,* 2570–2572.

(85)   Wu, X.; Bose, K. S.; Sinn, E.; Averill, B. A. "Isolation and X-ray Structure of an Intermediate In the Reaction of (μ-S)₂Fe₂(CO)₆ with Thiolates: The [(μ-S)(μ-S₂-t-Bu)Fe₂(CO)₆]⁻ Ion" *Organometallics* **1989,** *8,* 251–253.

(86)   Schweitzer, D.; Shearer, J.; Rittenberg, D. K.; Shoner, S. C.; Ellison, J. J.; Loloee, R.; Lovell, S.; Barnhart, D.; Kovacs, J. A. "Enhancing Reactivity via Structural Distortion" *Inorg. Chem.* **2002,** *41,* 3128–3136.

(87) Coucouvanis, D.; Lippard, S. J. "Preparation and Structural Characterization of Six-Coordinate Iron(III) Complexes Containing the Fe–S–S Linkage" *J. Am. Chem. Soc.* **1968,** *90*, 3281–3282.
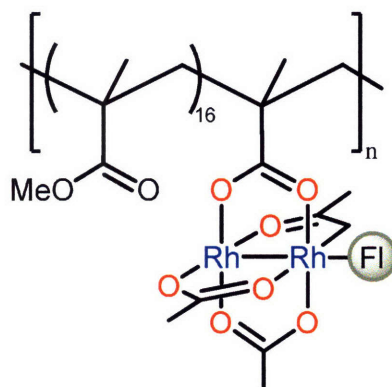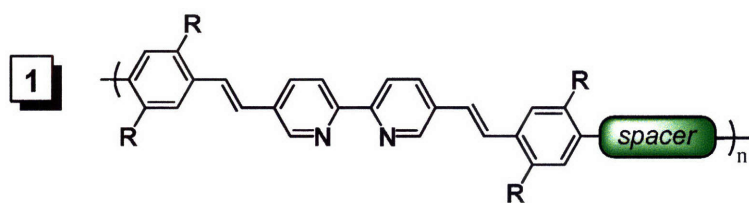
Chapter 2

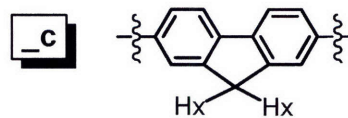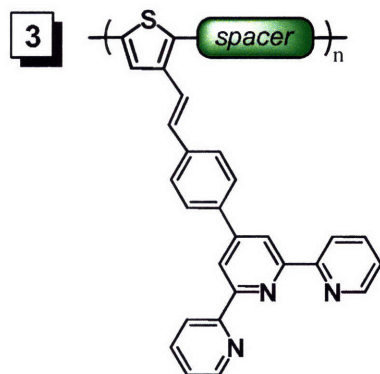Compound **1**. Fl = *N*-dansylpiperazine.

Chapter 3
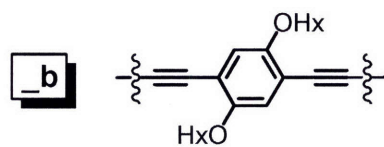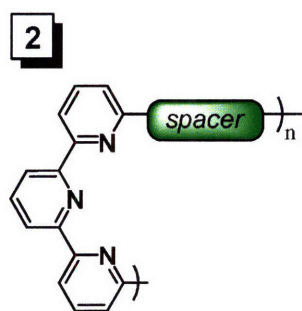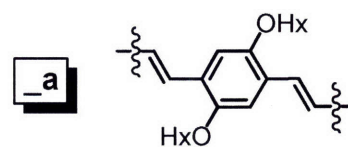
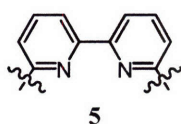Compounds **1–3**. For **1a**, R = OHx. For all other organic-soluble CPs, R = H.

Chapter 3 (cont)
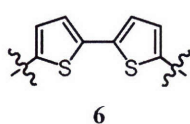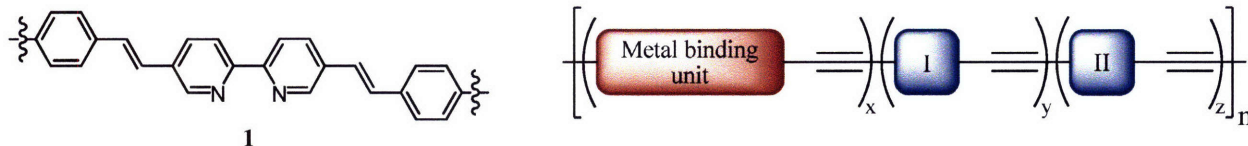
	MBU	x	y	z
4a	1	0.40	0.50	0.10
4b	1	0.20	0.50	0.30
5	5	0.25	0.50	0.25
6	6	0.25	0.50	0.25
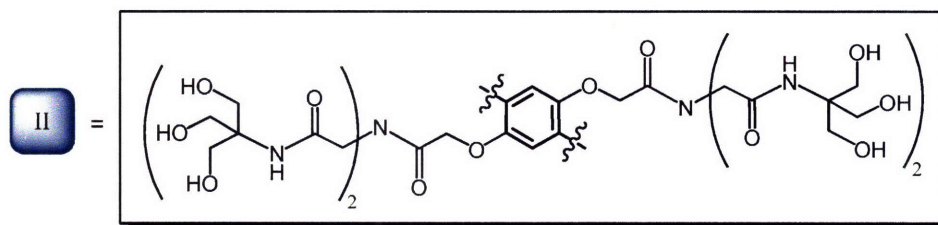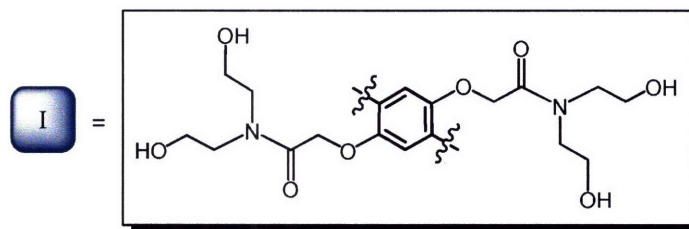
Compounds **4–6**. Table details monomer loading within each polymer.

Chapter 4

$(Et_4N)_2$ [PhS, PhS — Ni — SPh, NO]
Compound **2.**

(Et_4N) [PhS, PhS — Co — NO, NO]
Compound **5.**

$(Et_4N)_2$ [PhS, ON — Ni — S(Ph) — Ni — NO, SPh with Ph and S bridges]
Compound **3.**
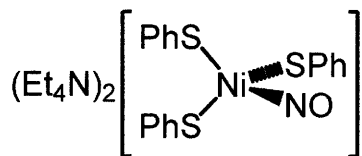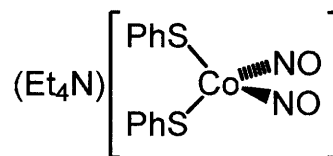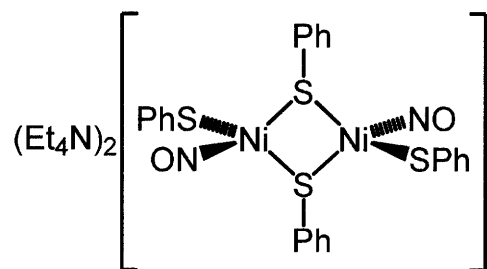
Compound **6.**
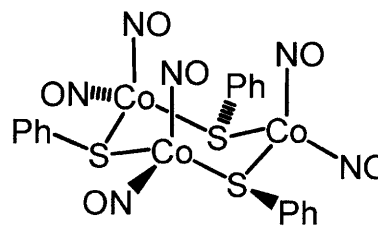
A. Education

2. **Massachusetts Institute of Technology**
   Ph.D. (Inorganic Chemistry); May 2008
   Advisor: Stephen J. Lippard
   Thesis: The Detection of Nitric Oxide and its Reactivity with Transition Metal Thiolate Complexes

1. **University of Chicago**
   S.B. Honors (Chemistry); May 2003
   S.M. (Inorganic Chemistry); May 2003
   Advisor: Gregory L. Hillhouse
   Thesis: Synthesis and Characterization of Three-Coordinate Nickel Chalcogenato Complexes

B. Peer-Reviewed Publications

5. Tennyson, Andrew G.; Smith, Rhett C.; Lippard, Stephen J.; "Selective Fluorescence Detection of Nitroxyl over Nitric Oxide in Buffered Aqueous Solution using a Conjugated Metallopolymer" *Polyhedron*, **2007**, *26*, 4625–4630.

4. Smith, Rhett C.; Tennyson, Andrew G.; Won, Annie C.; Lippard, Stephen J.; "Conjugated Metallopolymers for Fluorescent Turn-On Detection of Nitric Oxide" *Inorganic Chemistry*, **2006**, *45*, 9367–9373.

3. Do, Loi; Smith, Rhett C.; Tennyson, Andrew G.; Lippard, Stephen J.; "Luminescent Properties of Water-Soluble Conjugated Metallopolymers and Their Application to Fluorescent Nitric Oxide Detection" *Inorganic Chemistry*, **2006**, *45*, 8998–9005.

2. Smith, Rhett C.; Tennyson, Andrew G.; Lippard, Stephen J.; "Polymer-Bound Dirhodium Tetracarboxylate Films for Fluorescent Detection of Nitric Oxide" *Inorganic Chemistry*, **2006**, *45*, 6222–6226.

1. Smith, Rhett C.; Tennyson, Andrew G.; Lim, Mi Hee; Lippard, Stephen J.; "Conjugated Polymer-Based Fluorescence Turn-On Sensor for Nitric Oxide" *Organic Letters*, **2005**, *7*, 3573–3575.

C. Presentations at Scientific Meetings

1. Tennyson, Andrew G.; Melenkivitz, Rory P.; Mindiola, Daniel J.; Hillhouse, Gregory L.; "Redox properties of three-coordinate nickel complexes containing terminal alkoxide and thiolato ligands" Pew Midstates Science & Mathematics Consortium Undergraduate Research Symposium, Washington University at St. Louis, St. Louis, Missouri, USA, November, 2002. (Talk)